UNIVERSITY OF CALIFORNIA
RIVERSIDE

Development and Application of Functional Group Analysis for Secondary Organic Aerosol Studies

A Dissertation submitted in partial satisfaction
of the requirements for the degree of

Doctor of Philosophy

in

Environmental Toxicology

by

Sukon Aimanant

June 2012

Dissertation Committee:
Dr. Paul J. Ziemann
Dr. Janet Arey
Dr. Roger Atkinson

The Dissertation of Sukon Aimanant is approved:

_____

_____

_____

Committee Chairperson

University of California, Riverside

ACKNOWLEDGEMENTS

First of all, I would like to greatly thank to my advisor, Professor Paul J. Ziemann. He gave me an opportunity to learn so many new things about the principles of atmospheric chemistry and techniques which are used in atmospheric studies. I really appreciate his patient and his dedication to guide and help me until this thesis was completed. Without his support, the thesis would not be possible.

I also would like to express my thankfulness to Professor Janet Arey and Professor Roger Atkinson for being on my committee members. I truly thank to all people in Air Pollution Research Center who were always helpful when I needed help. And I needed to express my special thanks to Aiko Matsunaga, Christen Strollo, and Geoffrey Yeh for teaching me techniques and helping me on some special experiments, without them my study will not be completed. I would like to thank Thai government and US Department of Energy for being my sponsor over the course of my study in USA.

I also want to thank all my friends in ETOX program and Thai friends for their support and making my life enjoyable. Lastly, I would like to acknowledge my family. Their love and encouragement bring me success today.

ABSTRACT OF THE DISSERTATION

Development and Application of Functional Group Analysis
for Secondary Organic Aerosol Studies

by

Sukon Aimanant

Doctor of Philosophy, Graduate Program in Environmental Toxicology
University of California, Riverside, June 2012
Dr. Paul J. Ziemann, Chairperson

The objective of this dissertation was to develop spectrophotometric methods for functional group analysis of secondary organic aerosol (SOA) and to apply these in conjunction with other methods to studies of the aerosol products formed by oxidation of volatile organic compounds and oxidative aging in model reaction systems representative of the atmosphere.

In Chapter 2 spectrophotometric methods were developed to quantify carbonyl, hydroxyl, carboxyl, and ester groups in samples with compositions typical of oxidized atmospheric organic matter. The methods employ derivatizing agents to convert each functional group to a characteristic colored derivative that is then quantified by spectrophotometry. The effects of molecular structure on quantification were thoroughly evaluated by measuring calibration curves for a large variety of monofunctional and multifunctional compounds. In addition, potential interferences from other compounds containing non-target functional groups were determined and methods developed to eliminate these interferences. Detection limits were also determined.

In Chapters 3 and 4 the functional group analysis methods were used with methods for organic nitrate and peroxide analysis to investigate the chemical composition of SOA formed from OH radical-initiated reactions of *n*-pentadecane (a model alkane) in the presence of NO_x (Chapter 3) and in the absence of NO_x (Chapter 4), conditions typical of polluted and clean air. Real-time and offline thermal desorption particle beam mass spectrometry and SOA yield measurements were used in addition to functional group analysis to characterize the SOA. The results of functional group analysis were consistent with the complex array of products expected from the established reaction mechanisms and mass spectrometric data, lending support to the reaction mechanisms currently in use.

In summary, the developed functional group analysis methods are well suited for SOA studies. In the future they can be applied to further studies of complex SOA-forming reactions as well as the relationships between functional group composition and SOA properties such as cloud condensation nucleating activity and toxicity.

TABLE OF CONTENTS

LISTS OF FIGURES

LIST OF TABLES

CHAPTER 1

Introduction

1.1 Background

Atmospheric aerosols have in recent years attracted the interest of many researchers, due in large part to their effects on human health and the environment. Aerosols are complex systems with a wide range of physical-chemical properties and sources [Pöschl 2005]. The concentration, composition and size distribution of atmospheric aerosols are temporally and spatially highly variable. The particle number and mass concentrations typically range from about 10^2-10^5 cm^{-3} and 1-100 $\mu g\ m^{-3}$. Atmospheric aerosols come from a variety of natural and anthropogenic sources and can be classified into two categories depending on how they are introduced into the atmosphere. Primary aerosols are directly emitted into the atmosphere as condensed phases (liquid, solids, or a mixture) and include soil dust, biological material, and sea spray, as well as black carbon from sources such as natural and anthropogenic biomass burning and fossil-fuel combustion and the associated semi-volatile organic vapors which can condense under atmospheric conditions. Secondary aerosols are formed in the atmosphere by gas-to-particle conversion of volatile organic compounds (VOC), SO_2, and NO_x by homogeneous nucleation or by condensation onto pre-existing aerosols. Aerosols in the atmosphere are classified according to their diameter, with ultrafine particles being ≤ 0.1 μm, fine particles ≤ 2.5 μm ($PM_{2.5}$), and coarse particles > 2.5 μm. Fine particles have been shown to have deleterious effects on human health since they

can penetrate deep into the lung, and also to affect climate by efficiently scattering and absorbing light and acting as cloud condensation nuclei.

Organic material contributes ~20-50 % to the total fine aerosol mass at the continental mid-latitudes and increases to ~90 % in tropical forested areas [Kanakidou et. al. 2005]. Secondary organic aerosols (SOA), typically present in the fine particle size range, comprise ~60 % of organic mass in urban areas and up to ~95 % in remote areas [Zhang et al. 2007]. Therefore, the pathways leading to formation of SOA in the atmosphere are of interest due to their high potential to affect human health and the environment.

1.2 Effects of Atmospheric Aerosols

1.2.1 Environmental effects

Aerosols, especially those in the fine particle mode, can decrease visibility by efficiently scattering visible light. In addition, it is known that aerosols affect global climate directly by scattering and absorbing solar radiation and indirectly by acting as cloud condensation nuclei [Haywood and Boucher 2000; Andreae and Rosenfeld 2008].

For the direct effect, aerosols in the size range of 0.1 to 1.0 μm efficiently scatter incoming solar radiation back to space due to the similarity of particle size and the wavelength of light. Organic aerosols and sulphate aerosols are most effective at scattering short-wavelength solar radiation [Charlson et al. 1992]. They produce a negative radiative forcing resulting in cooling. However, some aerosols such as black carbon can absorb incoming and outgoing radiation causing warming effects.

For the indirect effect, aerosols can act as cloud condensation nuclei (CCN). CCN can affect cloud droplet number concentration affecting the reflectivity of clouds (Twomey first indirect effect) and cloud lifetime (second aerosol indirect effect) [Lohmann et al. 2005]. High concentrations of CCN cause an increase in cloud droplet number concentration, for constant liquid water content, and therefore reduce precipitation efficiency and increase cloud lifetime. SOA normally contains a large number and variety of oxygenated functional groups and therefore can have high polarity and water solubility. These properties can increase the potential of SOA to act as CCN, although the extent depends on the chemical and physical properties of the particles [Prenni et al. 2007]. Since the CCN activity of aerosols is still not well understood, the effect of aerosol indirect effects on climate forcing is still highly uncertain.

1.2.2 Adverse health effects

It is known that fine particles can penetrate deep into the lung and that ultrafine particles can penetrate the membrane of the respiratory tract and enter the blood circulation or be transported along the olfactory nerve into the brain [Elder et al. 2006]. But the properties of aerosols that determine their adverse effects, such as particle size, chemical composition, and solubility are still unclear, and a combination of properties might be responsible. Epidemiologic studies for both short-term and long-term effects indicated that increased levels of $PM_{2.5}$ increase cardiopulmonary morbidity and mortality [Klemm et al. 2004; Ostro et al. 2006; Mauderly et al. 2008; Simkhovich et al. 2008]. The proposed mechanisms of lung- and circulation-mediated cardiovascular toxicity of particulate matter include increasing production of reactive oxygen species

(ROS) in the airways and lung alveoli and activation of local inflammatory pathways. The ROS and pro-inflammatory cytokines released into the bloodstream affect heart rate, heart rate variability, blood pressure, vascular tone, blood coaguability and the progression of atherosclerosis. Ultrafine particles can be transported directly to the heart and can directly induce cardiac arrhythmias and decrease cardiac contractility and coronary flow. People with pre-existing cardiovascular disease and diabetic and elderly individuals are more susceptible to these effects [Simkhovich et al. 2008]. Recently, the cellular responses after exposure of lung cell culture to SOA at ambient-air concentration for 2 hr were investigated [Gaschen et al. 2010]. The results showed that there were only moderate responses including subtle changes in cellular function that are essential for lung homeostasis, decreasing phagocytic activity, increasing interleukin production. The responses depended on cell types and SOA originating from the anthropogenic and biogenic precursors 1,3,5-trimethylbenzene and α-pinene.

1.3 Formation of Secondary Organic Aerosols

1.3.1 Gas-phase reactions

In the atmosphere, SOA is formed from the reactions of VOC emitted from biogenic sources and anthropogenic sources with oxidants including the hydroxyl radical (OH), nitrate radical (NO_3), and ozone (O_3). The biogenic compounds are emitted mainly from vegetation and include isoprene, monoterpenes, sesquiterpenes and a number of oxygenated compounds [Atkinson and Arey 2003], and the major classes of anthropogenic compounds include alkanes, alkenes, aromatics, and oxygenated

compounds [Atkinson 2008]. The reactions of VOC with oxidants can lead to the addition of oxygenated functional groups to the parent compounds resulting in formation of low-volatility organic compounds that can undergo homogeneous nucleation or partition into pre-existing aerosol and hence form SOA.

1.3.1.1 Reaction with OH radicals

OH radicals are mainly formed in the troposphere during daytime from the photolysis of O_3 in the presence of water at wavelengths ≥290 nm, from the photolysis of nitrous acid (HONO) formed from heterogeneous hydrolysis of NO_2, and from the photolysis of formaldehyde and other carbonyls in the presence of NO [Atkinson 2000, 2008]. The OH radicals are also formed from the reactions of alkenes with ozone during both daytime and nighttime [Atkinson 2000]. The global tropospheric average OH radical concentration is 2.0 x 10^6 molecule cm^{-3} as a 12-hr daytime average [Atkinson 2008]. The OH radicals can react with all major classes of organic compounds including alkanes, alkenes, aromatics and oxygenated compounds such as carbonyls, alcohols, ethers, and esters. The only important chemical loss process for alkanes is reaction with the OH radical, and with Cl atom in Arctic during springtime, which is initiated by H-atom abstraction from C-H bonds. For alkenes and aromatics, the reaction is initiated dominantly by OH addition to C=C double bonds, and less so by H-atom abstraction [Atkinson 2008]. For oxygentated compounds, the OH radical reaction proceeds by H-atom abstraction from C-H bonds and less so from O-H bonds, by OH addition to the C=C double bonds and aromatic rings, and by H-atom abstraction from the CHO group of aldehydes to form acyl radicals [Atkinson and Arey 2003, Mellouki 2003]. The alkyl

or acyl radicals formed in these reactions subsequently react with O_2 to form alkyl or acyl peroxy radicals, which then react with each other, NO, NO_2, or HO_2 to form stable products as well as alkoxy or acyloxy radicals. These radicals then react with O_2, decompose, or isomerize, eventually forming stable products. The result of these reactions is a suite of products containing functional groups such as hydroxyl [CHOH], hydroperoxy [CHOOH], nitrate [$CHONO_2$], carboxyl [C(O)OH], carbonyl [CO], and ester [C(O)OR]. Similar products are formed from the alkyl and acyl peroxy radicals produced by the NO_3 and O_3 reactions discussed below.

1.3.1.2 Reaction with NO_3 radicals

NO_3 radicals are formed in the troposphere from the reaction of NO_2 with O_3. During daytime, NO_3 radicals photolyze rapidly and react with NO, therefore they are present in significant concentration only during nighttime, with a global 12-hr nighttime average concentration of 5×10^8 molecule cm^{-3} [Atkinson 2000]. NO_3 radical-initiated reactions are significant for alkenes, but not for other classes of compounds. [Atkinson and Arey 2003; Mellouki 2003]. The reaction is initiated by NO_3 addition to the C=C double bond followed by addition of O_2 to form β-nitrooxyperoxy radicals that react similarly to the alkyl peroxy radicals described in section 1.3.1.1.

1.3.1.3 Reaction with O_3

The presence of ozone in the troposphere is the result of transport downwards from the stratosphere, in situ formation and destruction, and dry deposition at the Earth's surface. In the troposphere, O_3 is formed solely by the photolysis of NO_2. The ozone reaction is an important chemical loss process for alkenes. The reaction proceeds by

addition of O_3 to the C=C double bond, forming an energy-rich primary ozonide that decomposes to form carbonyls plus Criegee intermediates that can subsequently react by a variety of pathways [Atkinson 2000, 2008].

1.3.2 Heterogeneous or multiphase reactions

SOA can also be formed by heterogeneous or multiphase reactions. A heterogeneous reaction refers to the reaction of volatile organic compounds or semi-volatile organic compounds at the particle surface, and a multiphase reaction occurs in the particle bulk [Pöschl 2005]. The reactions can be non-oxidative and oxidative. The most important non-oxidative reaction is oligomerization, which is often catalyzed by acids and involves the formation of covalent bonds between organic molecules to form high molecular weigh compounds with low volatility. The several classes of oligomer-forming reactions include the reaction of hydroperoxides with aldehydes to form peroxyhemiacetals, alcohols with aldeydes to form hemiacetals, carbonyls with carbonyls to form aldol products, and carboxylic acids with alcohols or carboxylic acids to form esters and acid anhydrides [Kroll and Seinfeld 2008]. The oxidative processes are the oxidation of particle-phase organics by the gas-phase oxidants OH, O_3, and NO_3. The mechanisms of particle-phase oxidation reactions are believed to be similar to those of gas-phase reactions.

1.4 Importance of Oxygenated Functional Group Composition in Atmospheric Organic Aerosols

Organic aerosols contribute approximately 20-50 % of the total fine atmospheric aerosol mass, and this organic fraction contains a large variety of compounds numbering in the thousands. In addition, the composition varies locally, regionally, and globally as well as diurnally and seasonally. This complexity and variability of composition makes identification and quantification at the molecular level complicated. To date, approximately <30% of total organic mass has been chemically identified [Desseari et al. 2006]. By contrast, analysis of functional group composition can quantify a large fraction of organic aerosol mass. The functional group composition gives valuable information on the average composition of organic compounds, oxidation state and reactivity of organic aerosol, surface-active character, and solubility [Tagliavini et al. 2005; Pang et al. 2006]. Among functional groups, oxygenated functional groups are usually characteristic of SOA and are more common in atmospheric aerosols [Gilardoni et al. 2007]. The presence of oxygenated functional groups in aerosol has important consequences for their hygroscopicity due to the impact on polarity and water solubility. Therefore, knowledge of the composition of oxygenated functional groups should provide valuable information for understanding the CCN activity of organic aerosols. In addition, functional group composition can be used to probe the products and chemical mechanisms of SOA formation and the chemical aging of aerosols due to prolonged oxidation. In terms of toxicity, it is thought that the increased polarity of aerosols can increase the uptake and retention of fine particles within the respiratory system leading to adverse health effects

for persons with asthma, children and individual with respiratory illness [Mazurek 2002]. Therefore, knowing the composition of oxygenated functional groups might lead to an improved understanding of the effect of aerosols on human health.

1.5 Objective and Overview of the Dissertation

The objective of this dissertation was to develop spectrophotometric methods for functional group analysis of secondary organic aerosol (Chapter 2) and to apply these functional group analysis methods and other methods to studies the products of VOC oxidation and oxidative aging in model system (Chapter 3, 4 and 5).

In Chapter 2 spectrophotometric methods were developed to quantify carbonyl, hydroxyl, carboxyl, and ester groups in samples with composition typical of oxidized atmospheric organic matter. The methods employ derivatizing agents to convert each functional group to a characteristic colored derivative that is then quantified by spectrophotometry. The effects of molecular structure on quantification have been thoroughly evaluated by measuring calibration curves for a large variety of monofunctional and multifunctional compounds. In addition, potential interferences from other compounds containing non-target functional groups have been determined and methods developed to eliminate these interferences. Detection limits were determined.

The functional group analysis methods described in Chapter 2 were used to investigate the chemical composition of secondary organic aerosol formed from the OH radical-initiated reaction of *n*-pentadecane in the presence of NO_x (Chapter 3), in the absence of NO_x (Chapter 4). Real-time and offline thermal desorption particle mass

spectrometry and SOA yield measurements were used in addition to functional group analysis to characterize the SOA.

1.6 References

Andreae, M. O., and Rosenfeld, D. Aerosol-Cloud-Precipitation Interactions. Part 1. The Nature and Sources of Cloud-Active Aerosols. *Earth-Sci. Rev*. 89, 13-41 (2008).

Atkinson, R. Atmospheric Chemistry of VOCs and NO_x. *Atmos. Environ*., 34, 2063-2101 (2000).

Atkinson, R., and Arey J. Gas-Phase Tropospheric Chemistry of Biogenic Volatile Organic Compounds: a Review. *Atmos. Environ.*, 37, Supplement No.2, S197-S219 (2003a).

Atkinson, R. and Arey, J. Atmospheric Degradation of Volatile Organic Compounds. *Chem. Rev*., 103, 4605-4638 (2003b).

Atkinson, R. Our Present Understanding of the Gas-Phase Atmospheric Degradation VOCs, *Simulation and Assessment of Chemical Processes in a Multphase Environment, Nato Science for Peace and Security Series C: Environmental Security*, 1-19 (2008).

Atkinson, R., Arey, J. and Aschmann, S. M. Atmospheric Chemistry of Alkanes: Review and Recent Developments. *Atmos. Environ*., 42, 5859-5871 (2008).

Charlson R. T., Schwartz S. E., Hales J. M., Cess R. D., Coakley J. A., and Jr, J. E. Climate Forcing by Anthropogenic Aerosols. *Science*., 255, 423-430 (1992).

Desseari, S., Fuzzi, S., Facchini, M. C., Mircea, M., Emblico, L., Cavalli, F., Maenhaut, W., Chi, X., Schkolnik, G., Falkovich, A., Rudich, Y., Claeys, M., Pashynska, V., Vas, G., Kourtchev, I., Vermeylen, R., Hoffer, A., Andreae, M. O., Tagliavini, E., Moretti, F., and Artaxo, P. Characterization of the Organic Composition of Aerosols from Rondônia, Brazil, during the LBA-SMOCC 2002 Experiment and its Representation through Model Compounds. *Atmos. Chem. Phys.*, 6, 375-402 (2006).

Elder, A., Gelrin, R., Silva, V., Feikert, T., Opanashuk, L., Carter, J., Potter, R., Maynard, A., Ito, Y., Finkelstein, J, and Oberdorster, G. Translocation of Inhaled Ultrafine Magnanese Oxide Particles to the Central Nervous System. *Environ. Health Perspect*., 114, 1172-1178 (2006).

Gaschen, A., Lang, D., Kalberer, M., Savi, M., Geiser, T., Gazdhar, A., Lehr, C. M., Bur, M., Dommen, J., Baltensperger, U., and Geiser, M. Celluar Responses after Exposure of Lung Cell Cultures to Secondary Organic Aerosol Particles. *Envion. Sci. Technol.*, 44, 1424-1430 (2010).

Gilardoni, S., Russell, L. M., Sorooshian, A., Flagan, R. C., Seinfeld, J. H., Bates, Quinn, P. K., Allan, Williams, B., Goldstein, A. H., Onasch, T. B., and Worsnop, D. R. Regional Variation of Organic Functional Groups in Aerosol Particles on Four U.S. East Coast Platforms During the International Consortium for Atmospheric Research on Transport and Transformation 2004 Campaign. *J. Geophys. Res.*, 112, D10S27, doi:10.1029/2006JD007737 (2007).

Haywood, J., and Boucher, O. Estimates of the Direct and Indirect Radiative Forcing due to Tropospheric Aerosols: A Review. *Rev. Geophys*., 38, 513-543 (2000).

Kanakidou, M., Seindeld, J. H., Pandis, S. N., Barnes, I., Dentner, F. J., Facchini, M. C., Dingenen, R. V., Ervens, B., Nenes, A., Swittlicki, E., Putaud, J. P., Putaud, J. P., Fuzzi, S., Horth, J., Moortgat, G. K., Winterhalter, R., Myhre, C. E. L., Tsigaridis, K., Vignati, E., Stephanou, E. G., and Wilson, J. Organic Aerosol and Global Climate modeling: a Review. *Atmos. Chem. Phys*., 5, 1053-1123 (2005).

Klemm, C. D., Lipfert, F. W., Wyzga, R. E., and Gust, C. Daily Mortality and Air Pollution in Atlanta: Two Years of Data from ARIES. *Inhal. Toxicol*., 16 (Supplement No. 1), 131-141 (2004).

Kroll, J. H., and Seinfeld, J. H. Chemistry of Secondary Organic Aerosol: Formation and Evolution of Low-Volatility Organics in the Atmosphere. *Atmos. Environ*., 42, 3593-3624 (2008).

Lohmann U., and Feichter J. Global Indirect Aerosol Effects: Review. *Atmos. Chem. Phys. Discuss*., 4, 7561-76149 (2004).

Mazurek, M. A. Molecular Identification of Organic Compounds in Atmospheric Complex Mixtures and Relationship to Atmospheric Chemistry and Sources. *Environ. Health Perspect*., 110, 995-1003 (2002).

Mellouki, A., Bras, G. L., and Sidebottom, H. Kinetics and Mechanisms of the Oxidation of Oxygenated Organic Compounds in the Gas Phase. *Chem. Rev*., 103, 5077-5096 (2003).

Pang, Y., Tupin, J., Gundel, L. A. On the Importance of Organic Oxygen for Understanding Organic Aerosol Particles. *Aerosol Sci. Technol.*, 40, 128-133 (2006).

Prenni, A. J., Petters, M. D., Kreidenweis, S. M., DeMott, P. J., and Ziemann, P. J. Cloud Droplet Activation of Secondary Organic Aerosol. *J. Geophys. Res.*, 112, D10223, doi:10.1029/2006JD007963 (2007).

Simkhovich, B. Z., Kleinmann, M. T., and Kloner, R. A. Air Pollution and Cardiovascular Injury: Epidemiology, Toxicolgy, and Mechanisms. *J. Am. Coll. Cardiol*., 52, 719-726 (2008).

Tagliavini, E., Moretti, F., Decesari, S., Facchini, M. C., Fuzzi, S., and Maenhaut, W. Functional Group Analysis by H NMR/Chemical Derivatization for the Characterization of Organic Aerosol from the SMOCC Field Campaign. *Atmos. Chem. Phys. Discuss.*, 5, 9447-9491 (2005).

Zhang, Q., Jimenez, J. L., Canagaratna, M. R., Allan, J. D., Coe, H., Ulbrich, I., Alfarra, M. R., Takami, A., Middlebrook, A. M., Sun, Y. L., Dzepina, K., Dunlea, E., Docherty, K., DeCarlo, P. F., Salcedo, D., Onasch, T., Jayne, J. T., Miyoshi, T., Shimono, A., Hatakeyama, S., Takegawa, N., Kondo, Y.,Schneider, J., Drewnick, F., Borrmann, S., Weimer, S., Demerjian, K., Williams, P., Bower, K., Bahreini, R., Cottrell, L., Griffin, R. J., Rautiainen, J., Sun, J. Y., Zhang, Y. M., and Worsnop, D. R. Ubiquity and Dominance of Oxygenated Species in Organic Aerosols in Anthropogenically-Influenced Northern Hemisphere midlatitudes, *Geophys. Res. Lett*., 34, L13801, doi:10.1029/2007GL029979, (2007).

CHAPTER 2

Development of Spectrophotometric Methods for Functional Group Analysis of Secondary Organic Aerosol

Abstract

Spectrophotometric methods were developed to quantify carbonyl, hydroxyl, carboxyl, and ester groups in samples with composition typical of oxidized atmospheric organic matter. The methods employ derivatizing agents to convert each functional group to a characteristic colored derivative that is then quantified by spectrophotometry. The effects of molecular structure on quantification have been thoroughly evaluated by measuring calibration curves for a large variety of monofunctional and multifunctional compounds. In addition, potential interferences from other compounds containing non-target functional groups have been determined and methods developed to eliminate these interferences. Detection limits are approximately 0.01, 0.02, 0.03, and 0.1 μmoles for carbonyl, hydroxyl, carboxyl, and ester groups. The use of these methods for analysis of secondary organic aerosol comprised of a complex mixture of oxidized compounds is demonstrated, although the methods should also be applicable to analysis of organic gas samples.

2.1 Introduction

Organic matter is an important component of the atmosphere that consists of thousands of compounds present in both gas and particulate form [Jacobson et al. 2000; Hallquist et al. 2009]. Complex mixtures of organic compounds are emitted to the atmosphere from many different anthropogenic and biogenic sources and once there can undergo chemical reactions that lead to the formation of more highly oxidized compounds, some of which have sufficiently low volatility to partition to particles as secondary organic aerosol (SOA) [Kroll and Seinfeld 2008]. Although SOA comprises most of the fine particulate (diameter ≤ 2.5 μm; $PM_{2.5}$) organic matter present in the atmosphere [Zhang et al. 2007; deGouw and Jimenez 2009] and fine particles are of considerable interest due to their effects on visibility [Seinfeld and Pandis 1998], climate [Haywood and Boucher 2000; Lohmann and Feichter 2005; Andreae and Rosenfeld 2008], and human health [Davidson and Solomon 2005], the mechanisms of the reactions by which organic compounds are oxidized in the atmosphere and the major sources of SOA have not yet been established. Such information is necessary to achieve a better understanding of atmospheric organic chemistry and the environmental effects of organic aerosols at local, regional, and global scales, as well as to improve atmospheric models that are widely used for establishing air quality regulations.

The chemical composition of organic aerosol is most commonly characterized using offline methods such as gas or liquid chromatography coupled to mass spectrometry (GC-MS and LC-MS) [Rogge et al. 1993; Yu et al. 1999; Gao et al. 2010], or online aerosol mass spectrometry (AMS) [Canagaratna et al. 2008]. These methods span a range in

chemical specificity from individual molecules to classification according to the degree of oxidation (as indicated by O/C and H/C ratios) [Aiken et al. 2008] or as either hydrocarbon-like or oxidized organic aerosol, HOA and OOA [Zhang et al. 2005]. Each method has its strengths and weaknesses, in terms of chemical specificity, the fraction of organic aerosol mass that can be analyzed, real time or offline analysis, sample size, measurement time resolution, and the cost and difficulty of analysis [Hallquist et al. 2009]. Alternatively, a few groups have employed Fourier transform infrared (FTIR) spectroscopy [Allen et al. 1994; Blando et al. 2001; Coury and Dillner 2008; Russell et al. 2011] and nuclear magnetic resonance (NMR) spectroscopy [Decesari et al. 2000] to quantify specific oxygen-, nitrogen-, and sulfur-containing functional groups in organic aerosol including carbonyl, hydroxyl, carboxyl, nitrate, amine, and sulfate, as well as saturated, unsaturated, and aromatic hydrocarbon groups. This approach is generally intermediate to those mentioned above in terms of chemical specificity and also with regards to other analytical strengths and weaknesses [Hallquist et al 2009]. In spite of the value of functional group analysis for characterizing organic aerosol in cases where molecular identification is not necessary, but more chemical detail is sought than what can be obtained by AMS methods, FTIR and NMR spectroscopy have seen relatively little use, especially in laboratory studies. The reasons for this are not entirely clear, but may be due in part to the considerable skill and experience needed to interpret FTIR and NMR spectra. Identification and quantification can be difficult because of overlapping peaks, the potential for matrix effects, and the requirement for functional group standards appropriate for the mix of organic compounds being analyzed [Blando et al. 2001].

Prior to the development of sophisticated FTIR, NMR, and mass spectrometer instrumentation, organic mixtures of interest in many research fields and in industrial applications were often routinely characterized using methods that involved reactions with derivatizing reagents to yield products that were characteristic of specific functional groups and were also colored, so that they could be quantified by measuring their absorbance. Although derivatization is still commonly used in atmospheric chemistry research to improve the properties of organic compounds for GC-MS analysis [Yu et al. 1998], because of the time consuming chemical processing and the generally poorer sensitivity of spectrophotometry compared to other methods, derivatization-spectrophotometric methods have mostly fallen out of favor. Nevertheless, over the past few years we have attempted to revive this approach for analysis of mixtures of atmospheric organic compounds, believing that if a suite of simple, reliable methods were available for routine analysis of the major functional groups that they would be valued and used. This is certainly the case in our own SOA research, where information on the composition of functional groups complements molecular information and can be critical to identifying reaction products and developing mechanisms for complex reaction systems. The approach used in our study was to identify the most promising methods for quantifying carbonyl, hydroxyl, carboxyl, and ester groups, from among the many that are available in the literature on organic analysis, and then evaluate these for specificity, interferences, and detection limits, modifying the methods when necessary or identifying better ones. The recommended methods and the results of the evaluations made using a large variety of monofunctional and multifunctional compounds are described in detail

below. An example of their application (together with methods we have used previously for peroxide [Docherty et al. 2005] and nitrate [Matsunaga and Ziemann 2009] analysis) to the analysis of SOA formed in an environmental chamber reaction is also presented.

2.2 Experimental Section

2.2.1 Spectrophotometric methods of functional group analysis

Chemical abbreviations. The following chemical abbreviations are used below: 2-nitrophenylhydrazine (2-NPH), 2-nitrophenylhydrazine hydrochloride (2-NPH.HCl), 2-nitrophenyl hydrazide (2-NP hydrazide), N,N′-dicyclohexylcarbodiimide (DCC), 2,4-dinitrophenylhydrazine (2,4-DNPH), 2,4-dinitrophenyl hydrazone (2,4-DNP hydrazone) triphenylphosphine (TPP), 4-nitrobenzoyl chloride (4-NBC), 4-dimethylaminopyridine (4-DMAP), and trimethylsilyldiazomethane (TMSDM).

Reagent solutions. Most of the reagent solutions described below were freshly prepared for each set of analyses, except for the 2-NPH.HCl, DCC, pyridine, and 2,4-DNPH solutions since contamination of these would be apparent from the reagent blank analyses. It is quite possible that the many of the other solutions do not need to be freshly prepared, but we did not evaluate this. The amounts of each of the freshly prepared reagent solutions listed below are those required for analysis of the following solutions: (1) two reagent blanks (analysis conducted with all reagents but without sample), (2) one sample (duplicate analysis), and (3) three standard solutions.

Instrumentation. The absorbance measurements were made using an USB4000-UV-Vis Miniature Fiber Optic spectrophotometer from Ocean Optics with a 1-cm quartz cell.

2.2.1.1 Carboxyl groups

Chemicals. The following chemicals, with purities or grades and suppliers, were used: 2-NPH.HCl (98%) [TCI]; DCC (99%), TPP (99%), cumene hydroperoxide (80%), benzoyl peroxide (97%), tridecanoic acid (98%), decanedioic acid (99%), 2-ketopentanedioic acid (98%), 2-ketohexanedioic acid (98%), (9Z)-octadec-9-enoic acid (99%), and 11-hydroxyundecanoic acid (96%) [Sigma-Aldrich]; thiourea (99%), extra dry pyridine (99.5%), KOH ("for analysis"; ≥85% with remainder water and <1% K_2CO_3 and trace metals), and absolute ethanol (99.5%) [Acros Organics]; and water (Optima) [Fisher Chemicals].

Reagents. The following reagent solutions were used in the analysis. (1) 2-NPH.HCl solution: 25 mL of 0.02 M 2-NPH.HCl in ethanol (requires gentle warming (~40 ^{o}C) to achieve complete dissolution). (2) DCC solution: 25 mL of 0.25 M DCC in ethanol. (3) Pyridine solution: 25 mL of 6% v/v pyridine in ethanol. (4) TPP solution: 5 mL of 0.01 M TPP in ethanol. (5) Thiourea solution: 10 mL of 10 g L^{-1} thiourea in ethanol. (6) KOH solution: 5 mL of 100 g L^{-1} KOH in 10% v/v water in ethanol.

Procedure. A sample or carboxylic acid standard containing at least ~0.03 μmole of carboxyl groups dissolved in 0.2 mL of ethanol is added to a 5 mL volumetric flask with 0.2 mL of TPP solution. This solution is kept at room temperature for 30 min to decompose peroxide compounds. In order, 0.5 mL each of the 2-NPH.HCl, pyridine, and

DCC solutions are added to the flask and the solution is kept at room temperature for 24 hr. Then, 1 mL of thiourea solution and 0.25 mL of KOH solution are added to the flask, whereupon a turbid brown-violet solution is formed. The solution is warmed in a water bath at 60 ^{o}C for 15 min to reduce the brown color, which masks the violet color and interferes with the absorbance measurement. After allowing the solution to cool to room temperature the volume is made up to the 5 mL mark with water. The absorbance of the solution is measured at 550 nm.

2.2.1.2 Carbonyl groups

Chemicals. The following chemicals, with purities or grades and supplier, were used: 2,4-DNPH (97%), TPP (99%), 3,4-hexanedione (95%), 2-ketopentanedioic acid (98%), 2-ketohexanedioic acid (98%), and pentane-1,5-dial in water (50%) [Sigma-Aldrich]; KOH ("for analysis"; ≥85% with remainder water and <1% K_2CO_3 and trace metals), concentrated HCl (ACS Plus), and absolute ethanol (99.5%) [Acros Organics]; hexane (Optima) [Fisher Chemicals]; nonanal (95%), undec-10-enal (95%), and 3-hexadecanone (99%) [Alfa Aesar]; 6-hydroxy-5-decanone (97%) and 5-hydroxy-2-pentanone (96%) [TCI]; and distilled water. A mixture of 9,10-ketonitrate octadecanoic acid isomers were synthesized by reacting (9Z)-octadec-9-enoic acid (oleic acid) particles with nitrate radicals in the environmental chamber [Docherty and Ziemann 2006], and then collecting the aerosol on a filter and purifying by HPLC-UV [Matsunaga and Ziemann 2009].

Reagents. The following reagent solutions were used in the analysis. (1) Hexane/ethanol solution: 30 mL of 30% v/v hexane in ethanol. (2) 2,4-DNPH solution:

25 mL of 0.005 M 2,4-DNPH in 4% v/v concentrated HCl in ethanol. (3) TPP solution: 5 mL of 0.01 M TPP in ethanol. (4) KOH solution: 50 mL of 100 g L^{-1} KOH in 20% v/v water in ethanol.

Procedure. A sample or carbonyl standard containing at least ~0.01 µmole of carbonyl groups dissolved in 1 mL of hexane/ethanol solution is added to a 5 mL volumetric flask along with 0.2 mL of TPP solution. This solution is kept at room temperature for 30 min to decompose peroxide compounds. Then 0.4 mL of 2,4-DNPH solution is added to the flask and the solution is kept at room temperature for 24 hr. Upon adding 3.0 mL of KOH solution a precipitate forms, which is dissolved by adding water up to the 5 mL mark. The absorbance of the solution is immediately measured at 480 nm.

2.2.1.3 Ester groups

Chemicals. The following chemicals, with purities or grades and suppliers, were used: hydroxylamine hydrochloride (99%), KOH ("for analysis"; ≥85% with remainder water and <1% K_2CO_3 and trace metals), $FeCl_3 \bullet 6H_2O$ (99%), concentrated HCl (Certified ACS Plus) and absolute ethanol (99%) [Acros Organics]; water (Optima) and bis(2-ethylhexyl)-decanedioate (97%) [Fisher Chemical]; methyl tridecanoate (98%), bis(2-ethylhexyl) phthalate (99%), methyl (Z)-octadec-9-enoate (99%), and dimethyl-3-oxopentanedioate (96%) [Sigma-Aldrich].

Reagents. The following reagent solutions were used in the analysis. (1) Ethanol/water solution: 100 mL of 50% v/v ethanol in water. (2) Hydroxylamine hydrochloride solution: 10 mL of 2.0 M hydroxylamine hydrochloride in 50% v/v ethanol in water. (3) KOH solution: 10 mL of 2.4 M KOH in 50% ethanol in water. (4) HCl

solution: 5 mL of 50% v/v concentrated HCl in 50% v/v ethanol in water. (5) $FeCl_3$ solution: 5 mL of 0.44 M $FeCl_3 \bullet 6H_2O$ in 6% v/v HCl solution in ethanol.

Procedure. A sample or ester standard containing at least ~0.1 µmole of ester groups dissolved in 1 mL of ethanol is added to a 5 mL volumetric flask. The hydroxylamine hydrochloride solution and KOH solution are then mixed, and 2 mL of that solution are added to the flask followed by 0.6 mL of water to dissolve the precipitate of hydroxylamine hydrochloride which forms. This solution is kept at room temperature for 1 hr. Successively, 0.5 mL each of HCl solution and $FeCl_3$ solution are added, followed by water up to the 5 mL mark. The absorbance of the solution is immediately measured at 540 nm.

2.2.1.4 Hydroxyl groups

Chemicals. The following chemicals, with purities or grades and supplier were used: 4-NBC (97%), 2 M TMSDM in diethyl ether, toluene (Certified ACS), 2-hexadecanone (99%), 1,10-decanediol (98%), 1,2-tetradecanediol (90%), 12-hydroxyoctadecanoic acid (99%), and 16-hydroxyhexadecanoic acid (98%) [Sigma-Aldrich]; 5-hydroxy-2-pentanone (96%) and 6-hydroxy-5-decanone (97%) [TCI]; 4-DMAP (99%) and extra dry pyridine (99.5%) [Acros Organics]; Na_2CO_3 (99%) [Baker & Adamson]; $NaHCO_3$ (99.7%) [Mallinickrodt]; NaCl (UPC/FCC); concentrated HCl (Certified ACS Plus), hexane (Optima), dichloromethane (Optima), and methanol (Optima) [Fisher Scientific]; and distilled water. A mixture of 9,10-hydroxynitrate octadecanoic acid isomers were synthesized by reacting (9Z)-octadec-9-enoic acid (oleic acid) particles with nitrate radicals in the environmental chamber [Docherty and Ziemann

2006], and then collecting the aerosol on a filter and purifying by HPLC-UV [Matsunaga and Ziemann 2009].

Reagents. The following reagent solutions were used in the analysis. (1) Methanol/toluene solution: 30 mL of 40% v/v methanol in toluene. (2) TMSDM solution: 5 mL of 0.04 M TMSDM (in diethyl ether) in methanol/toluene solution. (3) 4-NBC solution: 2 mL of 100 g L^{-1} 4-NBC in pyridine. (4) 4-DMAP solution: 25 mL of 0.02 M 4-DMAP and 50 g L^{-1} Na_2CO_3 in water. (5) $NaHCO_3$ solution: 25 mL of 50 g L^{-1} $NaHCO_3$ in water. (6) HCl solution: 200 mL of 0.24 N HCl and 25 g L^{-1} NaCl in water. (7) Dichloromethane/hexane solution: 50 mL of 9% v/v hexane in dichloromethane.

Procedure. A sample or alcohol standard containing at least ~0.02 μmole of hydroxyl groups dissolved in 100 μL of pyridine is added to a 5 mL reaction vial with 150 μL of 4-NBC solution. The solution is kept at room temperature for 1 hr. The pyridine is then evaporated in ~10 min using a stream of nitrogen and 2 mL of 4-DMAP solution is added to hydrolyze the excess 4-NBC. The vial is treated in an ultrasonic bath for 2 min and then left for 30 min to complete dissolution of the reagent. Because the derivatives are poorly soluble in water and give a turbid solution, they are extracted into 5 mL of the dichloromethane/hexane solution in a separatory funnel and the organic phase is washed once with 2 ml of $NaHCO_3$ solution and three times with 5 ml of HCl solution. The absorbance of the dichloromethane/hexane layer, which contains the derivatives, is measured at 253 nm.

Additional processing of a sample containing carboxylic acids. Prior to hydroxyl group analysis 100 μL of sample dissolved in the methanol/toluene solution is added to a

5 mL reaction vial with 200 μL of TMSDM solution. The mixture is kept at room temperature for 1 hr. The methanol and toluene are then evaporated in ~10 min using a stream of nitrogen and the residue is dissolved in 100 μl pyridine.

2.2.2 Functional group composition of secondary organic aerosol formed from the reaction of α-pinene with O_3.

Chemicals. (1S)-(-)-α-pinene (99%) and cyclohexane (HPLC) were obtained from Sigma-Aldrich. Ozone was generated using a Welsbach T-408 ozone generator.

Environmental chamber method. Replicate experiments were performed of reactions conducted in the dark in a 8300 L FEP Teflon environmental chamber filled with clean, dry air (< 5ppbv hydrocarbons and < 1% RH) at room temperature and atmospheric pressure. Cyclohexane and ozone were added to achieve chamber concentrations of 1200 and 2 ppmv, respectively, and then α-pinene (equivalent to a 1 ppmv concentration in the chamber in the absence of reaction) was added to initiate the reaction, which consumed all the α-pinene. The amount of cyclohexane present was sufficient to scavenge >99% of the OH radicals formed in the reaction [Docherty et al. 2005].

Filter sampling and sample preparation. Duplicate particle samples were collected after each experiment on previously weighed Millipore filters (0.45 μm pore size, Fluoropore FHLP, 47 mm). Sample air volumes were ~1 m^3 collected over ~1 hr through stainless steel tubing. Immediately after sampling, each filter was weighed to calculate the mass of sample collected, and then extracted twice in 4 ml of ethyl acetate at room temperature for >10 min. For each filter, extracts were combined into a 4-ml brown

vial that was previously weighed, and then dried in a stream of N_2. The vial was weighed again to determine the mass of sample. The dried sample was dissolved in an appropriate volume of ethyl acetate to achieve a sample concentration of ~1 mg mL^{-1}. Separate aliquots were taken for analysis of each functional group and dried in a stream of N_2 to remove ethyl acetate, and then dissolved in an appropriate solvent for each analysis as noted in the procedures described above. A clean blank filter was also prepared and analyzed similarly. The methods used for nitrate and peroxide analysis were described previously [Matsunaga and Ziemann 2009, Docherty and Ziemann 2005].

Elemental analysis. Dried filter extracts were also analyzed for C and N using a high temperature combustion elemental analyzer (Costech ECS 4010 CHNSO) and for O and H using a temperature conversion elemental analyzer (Thermo TC/EA) interfaced to an isotope ratio mass spectrometer (Thermo Delta V).

2.3 Results and Discussion

The chemical abbreviations used in the following discussion are given in Section 2.2.1.

2.3.1 Analysis of carboxyl groups

The use of 2-NPH for spectrophotometric analysis of carboxylic acids in aqueous and non-aqueous solutions has been reported [Munson and Bilous 1977; Horikawa and Tanimura 1982; Miwa et al. 1980, 1985; Karany et al. 1989, Adel-Hay et al. 1990]. Munson and Bilous (1977) first reported a method for quantifying carboxylic acids in a non-aqueous mixed solvent by direct coupling with 2-NPH using DCC as a coupling agent in the presence of pyridine. The method was only applied to aliphatic acids, not to

aromatic acids. Later, Miwa et al. (1980) used 2-NPH.HCl instead of the free base and found that 2-NPH.HCl reacted with both aliphatic and aromatic acids in aqueous ethanol in the presence of DCC and a small amount of pyridine. The basis of the method is that carboxylic acids are reacted with 2-NPH.HCl by using DCC as a coupling agent in the presence of pyridine, forming 2-NP hydrazide derivatives that give an intense violet color in an alkaline medium. The absorbance is measured at 550 nm. The violet color of 2-NP hydrazides developed in strongly alkaline medium (pH>12) could be attributed to the resonance form having a quinoidal structure [Miwa et al. 1985]. The chemistry of carboxyl group analysis is shown in Figure 2.1.

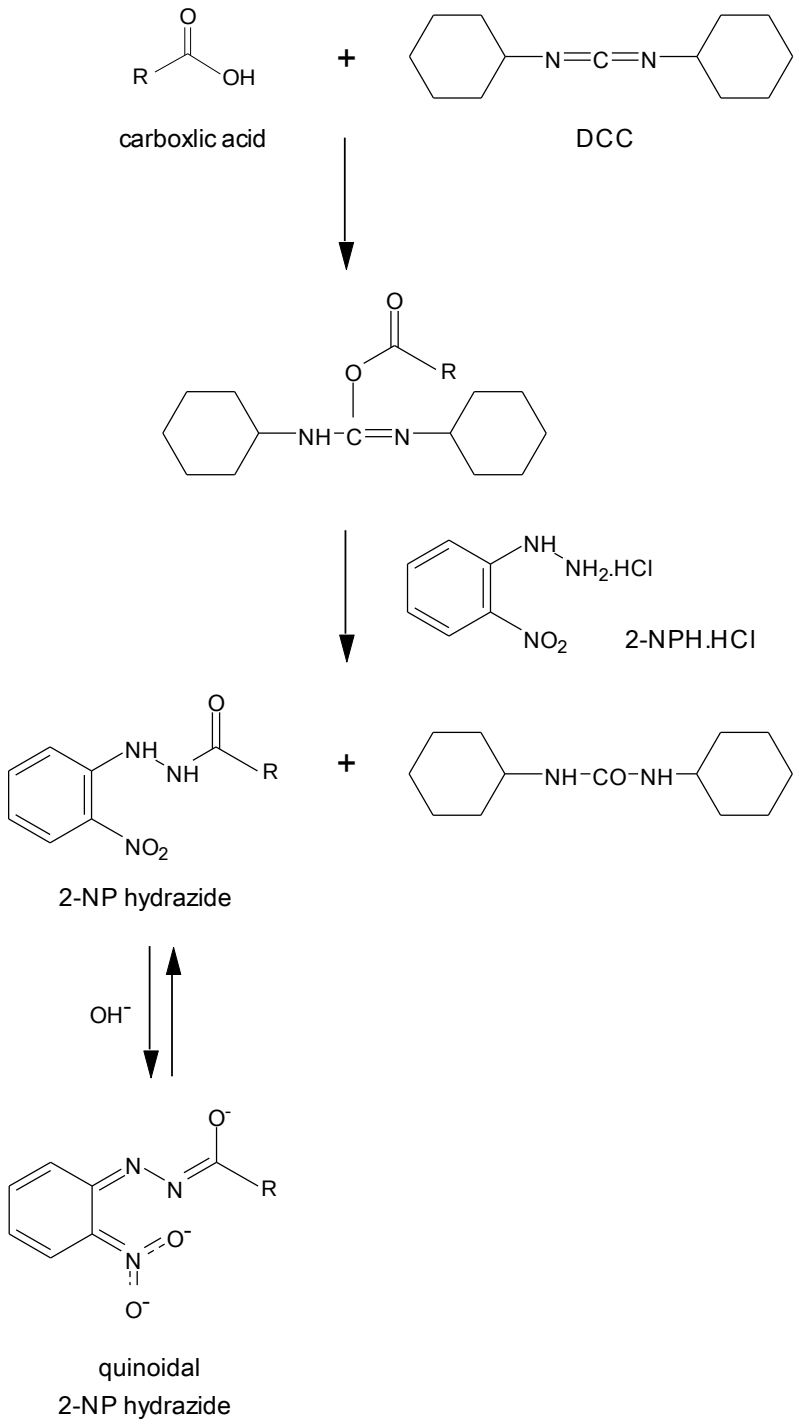

Figure 2.1. Chemistry of carboxyl group analysis.

The procedure used here (Section 2.2.1.1) was modified from that of Miwa et al. (1980) for a variety of reasons. The reaction mixture is kept at room temperature for 24 hr instead of at 25 ^{o}C for 2 hr because the absorbance of the 2-NP hydrazides of carboxylic acids increased when kept for 24 hr. They also suggested that the reaction mixture can alternatively be heated at 37 ^{o}C for 1 hr or at 60 ^{o}C for 20 min, but the absorbance decreases with increasing temperature because of partial conversion of carboxylic acids to unreactive ethyl esters in the coupling reaction. According to Miwa et al. (1980), on making the 2-NP hydrazide solution alkaline, a brownish insoluble substance formed, similar to that observed in this study. They suggested adding thiourea solution to dissolve the insoluble substance, but we observed that this prevented color formation, similar to Adbel-Hay et al. (1990). We also observed turbidity after making the 2-NP hydrazide solution alkaline, which they did not observe. We then determined that adding thiourea to the 2-NP hydrazide solution prior to making the solution alkaline successfully dissolved the insoluble substances. Upon making this solution strongly alkaline, an intense brown color appeared, which was decolorized by heating at 60 ^{o}C for 15 min. As was suggested by Horikawa and Tanimura (1982), the compound responsible for this brown color is probably an aminoguanidine derivative produced by addition of 2-NPH to DCC in the reaction solution, and decolorization due to decomposition of this derivative to 1-hydroxy-1, 2, 3-benzotriazole and a urea derivative. They also observed that increasing the temperature of the alkaline solution from 60 ^{o}C to 80 ^{o}C caused partial decomposition of the 2-NP hydrazides, resulting in about a 10 % decrease in the color intensity obtained from benzoic acid. We also observed that making up the final volume

with ethanol, as in the procedure of Miwa and co-workers, resulted in an unstable absorbance, but that by using water instead of ethanol a stable absorbance was achieved.

The absorbance maxima of a variety of 2-NP hydrazide derivatives of carboxylic acids were measured in a number of previous studies [Munson and Bilous 1972; Miwa et al. 1980, 1985; Horikawa and Tanimura 1982; Karany et al. 1989; Adel-Hay et al. 1990]. The absorbance maxima for most carboxylic acids were in the range of 530-570 nm, with the exception of 2-ketopentanedioic acid, which had a maximum at 442 nm [Miwa et al. 1980]. Since our major interest is in quantifying total carboxylic acids in SOA that typically contains a mixture of carboxylic acids, often with unknown structures, the average wavelength of 550 nm is used in our method.

The effect of molecular structure on the method results were evaluated by preparing calibration curves for a selection of monocarboxylic and dicarboxylic acids, some of which also contained carbonyl or hydroxyl groups or C=C double bonds. The results are shown in Figure 2.2. Linearity was excellent over the range of concentrations measured. Values of ε (M^{-1} cm^{-1})for the compounds tested were in the range 4200–6800, with the exception of 2-ketopentanedioic acid, for which ε ~ 1300. Most had values of ε ~ 5100, similar to those reported previously [Horikawa and Tanimura 1982]. The presence of a functional group adjacent to the chromophore is known to affect UV-Vis absorbance through electronic interactions (Pavia et. al 2007), as is observed here. In the case of 2-hydroxyhexadecanoic acid, the hydroxyl group increases ε by ~30%, whereas for 2-ketohexanedioic and 2-ketopentanedioc acid the carbonyl group decreases ε by ~20% and

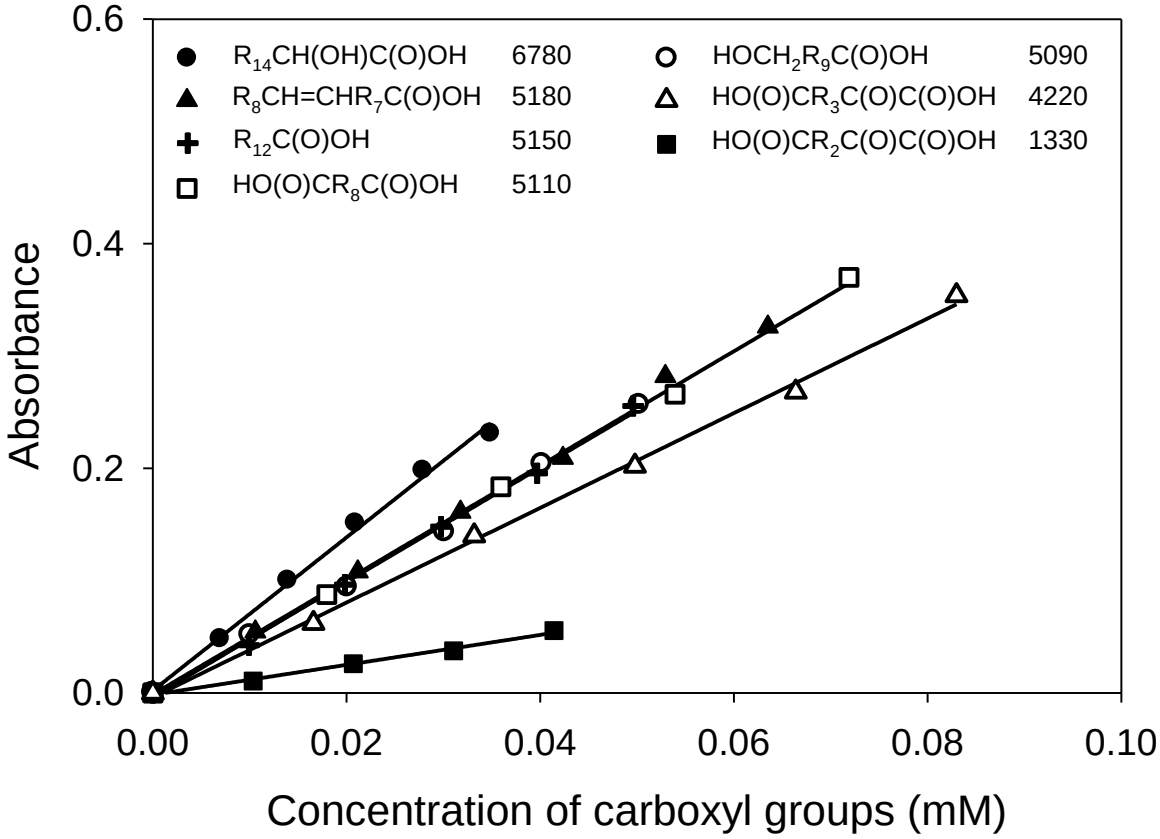

Figure 2.2. Calibration curves of carboxylic acids: 2-hydroxyhexadecanoic acid (●), (9Z)-octadec-9-enoic acid (▲), tridecanoic acid (✚), decanedioic acid (□), 11-hydroxyundecanoic acid (○), 2-ketohexanedioic acid (△), 2-ketopentanedioic acid (■). The corresponding structures and values of ε (M^{-1} cm^{-1}) are shown in the legend. R_n designates $(CH_2)_n$ or $H(CH_2)_n$ depending on whether the alkyl group is in the interior or on end of the molecule. The values of ε were calculated as $\varepsilon = 10^3 \times m$, where m is the slope of the least-squares line fit to the calibration curve A = m[C] + b, A = absorbance = absorbance (sample) – absorbance (blank), and [C] is the concentration of carboxyl groups (mM). For all lines $|b| \leq 0.005$ and $R^2 > 0.99$.

~75%. Functional groups that are not adjacent to the chromophore are expected to have much less effect on ε, as observed here where the hydroxyl group in 11-hydroxyundecanoic acid and the C=C double bond in (9Z)-octadec-9-enoic acid have negligible effects. For analysis of samples containing carboxylic acids with known structures, appropriate calibration curves can be prepared, whereas for samples containing unidentified compounds use of a simple monocarboxylic acid should give reasonably accurate results in most cases. Except for 2-ketopentanedioic acid, values ε for all the carboxylic acids analyzed here were within ~30 % of the value measured for tridecanoic acid.

The method was also tested for potential interferences from compounds containing other functional groups that are likely to be present in an SOA mixture. It was determined that nitrate, carbonyl, hydroxyl, ester, and peroxy groups other than hydroperoxy have no or little interference, but that hydroperoxides interfered by giving the same response as carboxylic acids. Therefore, in our method TPP solution is added to the sample prior to analysis to decompose peroxides, similar to the approach used by Chiba et al. (1989) to remove peroxides prior to carbonyl analysis. TPP is a common reducing agent for organic hydroperoxides, and is oxidized to TPP oxide while the hydroperoxides are reduced to alcohols that do not interfere with the carboxyl group analysis. The reaction is

$$(C_6H_5)_3P + ROOH \longrightarrow (C_6H_5)_3PO + ROH$$

The effects of cumene hydroperoxide and TPP on the analysis of carboxylic acids are shown in Figure 2.3. When cumene hydroperoxide was analyzed by the carboxyl group

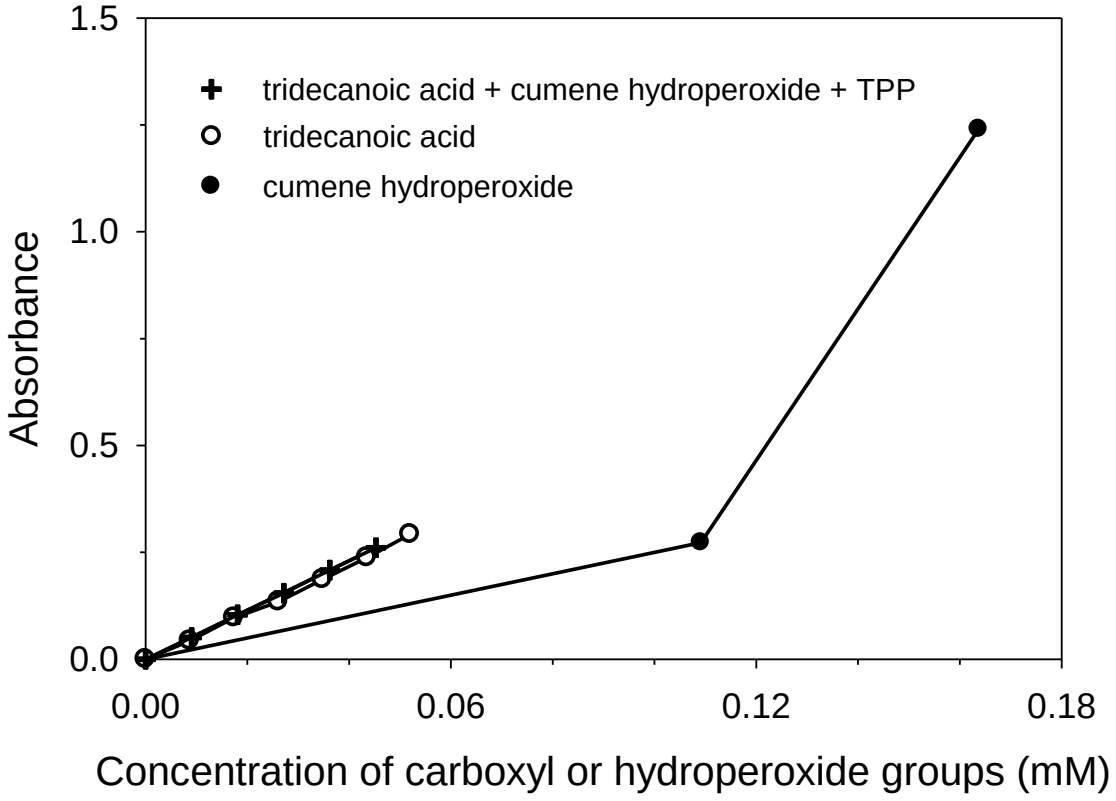

Figure 2.3. Analysis of carboxyl groups in solutions containing either cumene hydroperoxide, tridecanoic acid, or cumene hydroperoxide + tridecanoic acid + TPP.

method in the absence of carboxylic acid, significant (nonlinear) absorbance was observed, which would clearly interfere with the quantification of carboxyl groups. However, when TPP was first added to a mixture of cumene hydroperoxide and tridecanoic acid, the absorbance was identical to that observed for a pure tridecanoic solution.

Surprisingly, when benzoyl peroxide was used to test for removal of peroxides by TPP the result was different. Analysis of benzoyl peroxide after adding TPP resulted in an absorbance that was twice the absorbance of an equal concentration of tridecanoic acid, as shown in Figure 2.4. The likely reason is that TPP converts benzoyl peroxide to benzoic acid anhydride, as shown by Greenbaum et. al. (1956), the benzoic acid anhydride reacts with 2-NPH.HCl to give a 2-NP hydrazide derivative and benzoic acid [Munson 1974], and the benzoic acid then reacts with 2-NPH.HCl to give another 2-NP hydrazide derivative, as shown in Figure 2.5. Thus, acyl and diacyl peroxides will interfere with this method, as will the previously reported acid anhydrides and acid chlorides [Munson 1974].

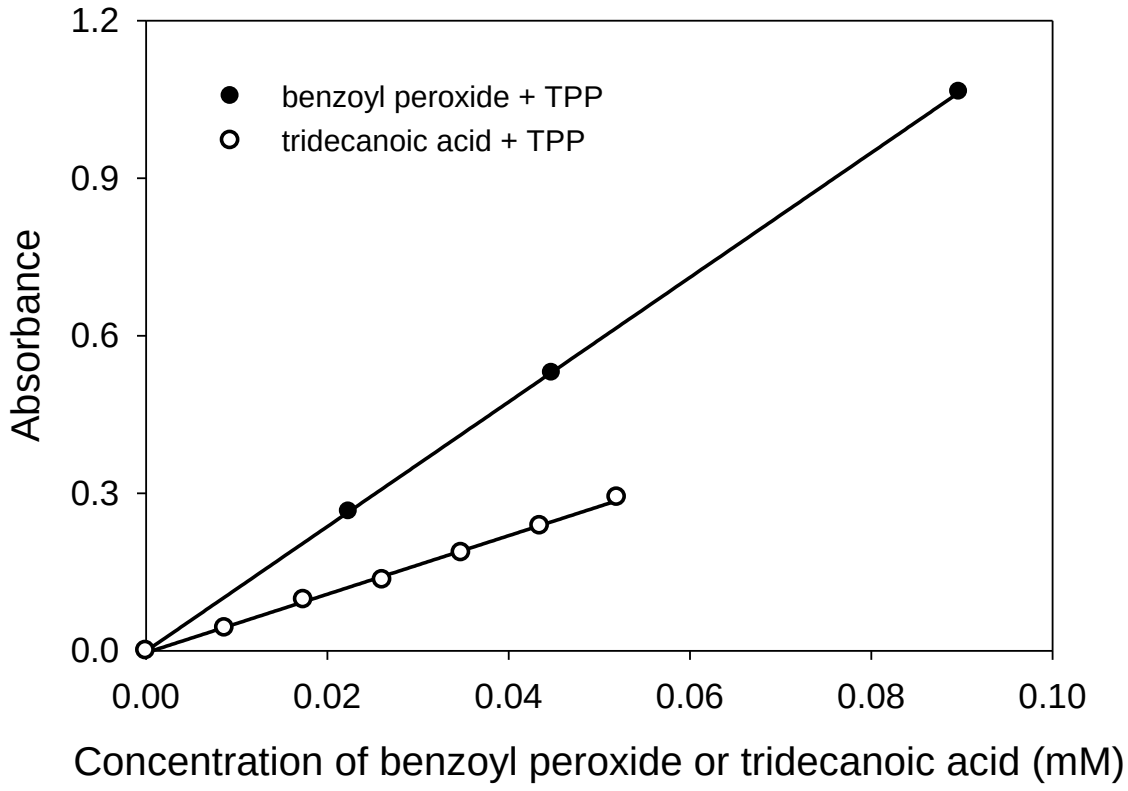

Figure 2.4. Analysis of carboxyl groups in solutions containing either benzoyl peroxide + TPP or tridecanoic acid + TPP.

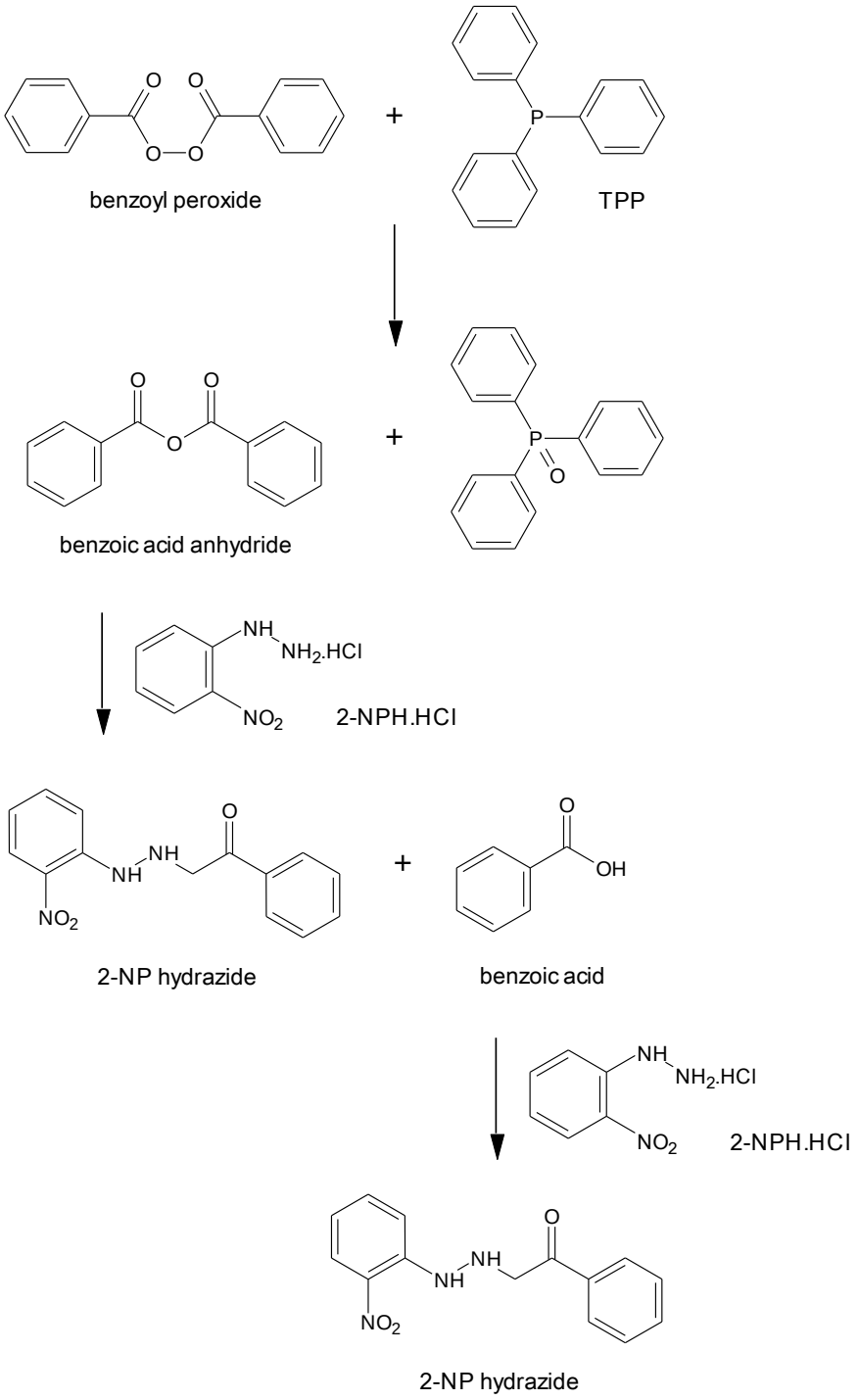

Figure 2.5. Formation of two 2-NP hydrazides from reaction of benzoyl peroxide with TPP and 2-NPH.HCl.

The detection limit for this method, calculated as 3× the standard deviation of blank measurements, was 0.03 μmoles of carboxyl groups for carboxylic acids with ε = 5100. The reproducibility determined from multiple analyses of tridecanoic acid was 6 % relative standard deviation.

2.3.2 Analysis of carbonyl groups

2,4-DNPH is a well-known derivatizing agent for carbonyl groups and is widely used for quantifying trace amounts of carbonyl compounds by spectrophotometry [Lappin 1951; Jordan an Veatch 1964; Yukawa 1993; Meyer and Rebrovic 1995]. The method used here was adapted from the American Society of Testing and Materials (ASTM) standard method and the methods of Lappin (1951) and Jordan and Veatch (1964).

The method is based on the reaction of aldehydes and ketones with 2,4-DNPH in acidic solution to form 2,4-DNP hydrazone derivatives. These derivatives are then reacted with base to produce a very intense wine-red color due to the formation of the quinoidal ion and the absorbance is measured at 480 nm. The chemistry of carbonyl group analysis is shown in Figure 2.6.

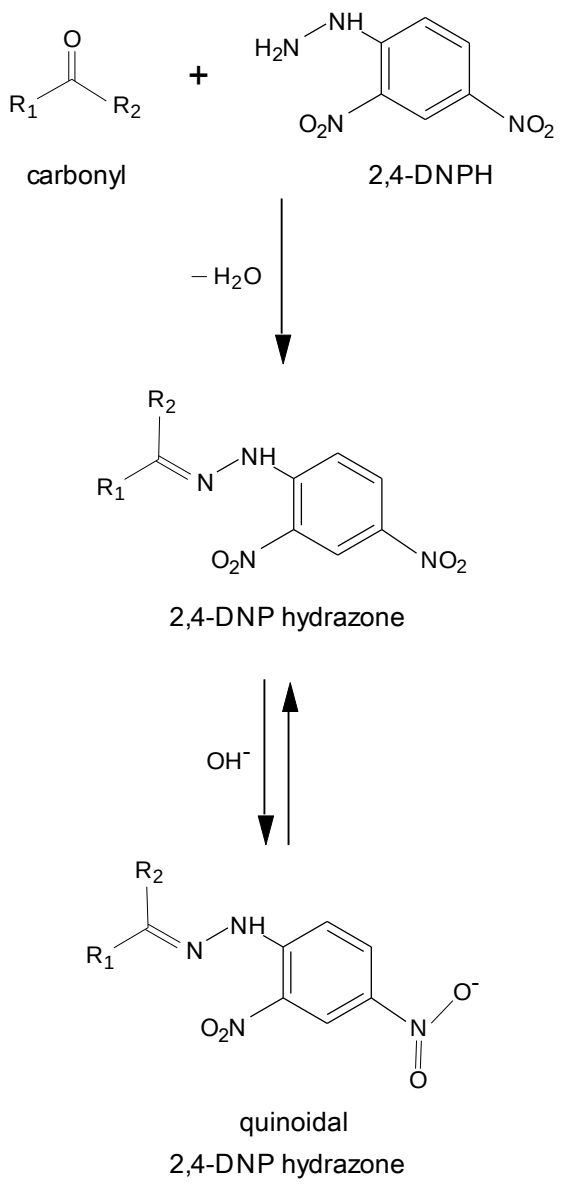

Figure 2.6. Chemistry of carbonyl group analysis.

Although the absorbance maxima for most derivatized aliphatic aldehydes and ketones is 430 nm [Lappin 1951; Jordan an Veatch 1964; Yukawa 1993], the wavelength used here was 480 nm as in the ASTM standard method and as was suggested by Lappin et al (1951). This is because at 480 nm the relationship between absorbance and concentration is more linear. Moreover, in our method the reaction mixture is kept at room temperature for 24 hr instead of at room temperature or 50 ^{o}C for 30 min [Lappin 1951; Jordan an Veatch 1964]. This is easier and guarantees that the reaction is complete.

There are two critical points regarding this analysis that need to be emphasized. Firstly, after adding the KOH solution to the reaction mixture, a KCl precipitate will form. Sufficient water must be added to completely dissolve the precipitate. Secondly, because the absorbing quinoidal ion that forms upon making the solution alkaline is unstable, for accurate results the absorbance needs to be measured within 10 min of adding the KOH solution [Lappin 1951; Jordan and Veatch 1964; Yukawa 1993; Meyer and Rebrovic 1995].

The effect of molecular structure on the method results were evaluated by preparing calibration curves for a selection of ketones, diketones, aldehydes, and dialdehydes, some of which also contained hydroxyl, carboxyl, or nitrate groups or C=C double bonds. The results are shown in Figure 2.7. Linearity was excellent over the range of concentrations measured. Values of ε (M^{-1} cm^{-1}) were the same for ketones and aldehydes, and for all the compounds tested were in the range 6600–15600, although except for 6-hydroxy-5-decanone and 9,10-ketonitrate octadecanoic acid isomers, which have hydroxyl and nitrate groups adjacent to the carbonyl groups, the range was 8900–11300. The hydroxyl

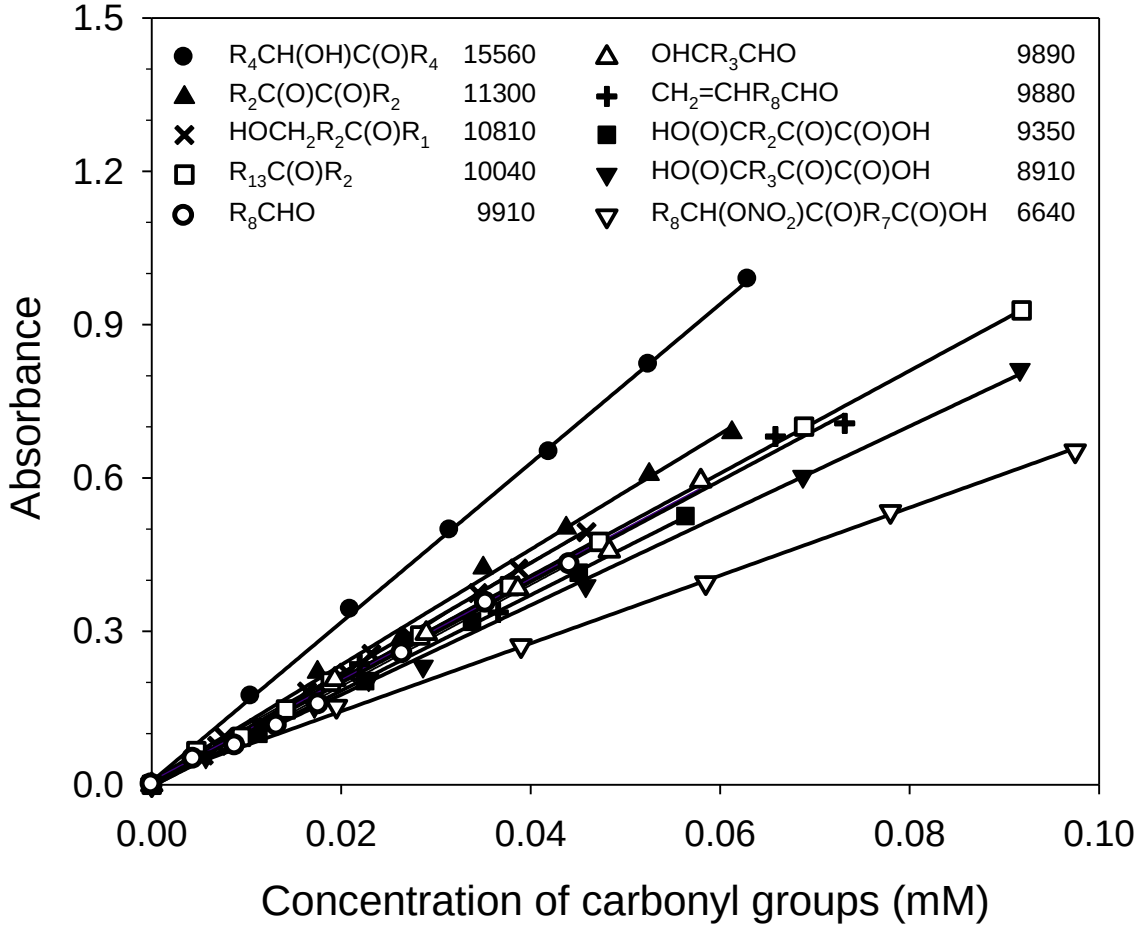

Figure 2.7. Calibration curves of carbonyl compounds: 6-hydroxy-5-decanone (●), 3,4-hexadecadione (▲), 5-hydroxy-2-pentanone (✕), 3-hexadecanone (□), nonanal (○), pentane-1,5-dial (△), undec-10-enal (✚), 2-ketopentanedioic acid (■), 2-ketohexanedioic acid (▼), 9,10-ketonitrate octadecanoic acid isomers (▽). The corresponding structures and values of ε (M^{-1} cm^{-1}) are shown in the legend. R_n designates $(CH_2)_n$ or $H(CH_2)_n$ depending on whether the alkyl group is in the interior or on end of the molecule. The values of ε were calculated as $\varepsilon = 10^3 \times m$, where m is the slope of the least-squares line fit to the calibration curve A = m[C] + b, A = absorbance = absorbance (sample) – absorbance (blank), and [C] is the concentration of carbonyl groups (mM). For all lines $|b| \leq 0.011$ and $R^2 > 0.99$.

group increased ε, as was the case in the carboxyl group analysis, whereas the nitrate group decreased ε. Vicinal carboxyl or carbonyl groups or non-vicinal functional groups had little effect on the values of ε. For analysis of samples containing carbonyls with known structures, appropriate calibration curves can be prepared, whereas for samples containing unidentified compounds use of a simple ketone or aldehyde should give reasonably accurate results in most cases. Except for 6-hydroxy-5-decanone and the 9,10-ketonitrate octadecanoic acid isomers, values of ε for all the carbonyls analyzed here were within ~10 % of the values measured for 3-hexadecanone and nonanal, whereas for the other two compounds values were within ~50 %.

The method was also tested for potential interferences from other compounds containing nitrate, carboxyl, hydroxyl, ester, peroxy, and hydroperoxy groups. Only hydroperoxides interfered with the analysis by giving the same response as carbonyls. Hydroperoxides are thus decomposed prior to analysis by adding TPP, as was suggested by Chiba et al. (1989) and was done for the carboxyl group analysis. This had no or little other effect on carbonyl analysis. It is worth noting that ketones and aldehydes present in the form of hemiacetals and peroxyhemiacetals are measured by this method, since peroxyhemiacetals are converted to hemiacetals by reaction with TPP and hemiacetals reversibly dissociate to carbonyls and alcohols under the conditions of the analysis.

The detection limit for this method, calculated as 3× the standard deviation of blank measurements, was 0.01 μmoles of carbonyl groups for carbonyl compounds with ε = 10000, the average value for the compounds tested. The reproducibility determined by multiple analyses of 3-hexadecanone was 4 % relative standard deviation.

2.3.3 Analysis of Ester groups

The hydroxamic acid method has been used for spectrophotometric analysis of esterified fatty acids in plasma [Stern and Shapiro 1953; Morgan and Kingsbury 1959], in serum [Verheyden and Nys 1962], and in oil [Hill 1946], as well as compounds already containing ester groups, such as surfactants [Feldmann et al. 1971], drugs [Feldmann et al. 1970], acetylcholine, and a neurotransmitter [Hestrin 1950]. The method is based on the conversion of esters to their hydroxamic acids by the use of hydroxylamine hydrochloride in alkaline medium. After adding an acidified solution of alcoholic $FeCl_3$, a red-colored complex of ferric hydroxamate is formed and the absorbance is measured at 540 nm. The chemistry of ester group analysis is shown in Figure 2.8.

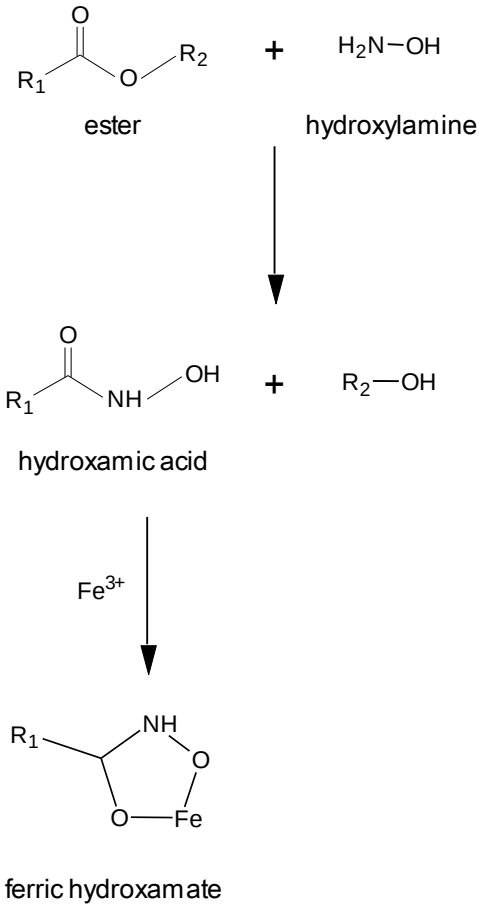

Figure 2.8. Chemistry of ester group analysis.

The method used here for ester analysis is a modified version of the method of Goldenberg (1958), which was developed for spectrophotometric analysis of carboxylic acids and their corresponding esters. In general, the method consists of two steps: the formation of hydroxamic acids by reaction of esters with hydroxylamine in alkaline medium and the color developing step involving the reaction of ferric ion with the hydroxamic acids in acidic medium. In the hydroxamic acid formation step, the rate of reaction depends on the concentration of hydroxylamine, pH, temperature, and reaction time. The reaction rate increases with increasing concentration of hydroxylamine [Hestrin 1949; Stern and Shapiro 1953; Goddu et al. 1955]. A low concentration of hydroxylamine gave a low molar absorptivity; however, too high of a concentration decreased the color intensity in the color-developing step [Stern and Shapiro 1953; Goddu et al. 1955]. This might be because the remaining hydroxylamine competes with hydroxamic acids for ferric ions in the color-developing step [Goddu et al. 1955]. Although increasing the pH seems to increase the rate of the reaction, the base-catalyzed hydrolysis of esters might compete with the formation of hydroxamic acids, resulting in decreased color intensity [Verheyden and Nys 1962; Feldmann et al. 1970]. By using a higher temperature, the time for conversion to the hydroxamic acid can be shortened, but prolonged heating can cause the decomposition of hydroxamic acids [Goddu et al. 1955; Verheyden and Nys 1962; Feldmann et al. 1970]. Therefore, a study was conducted here to determine the optimal heating procedure for analysis of a mixture of esters. For simplicity and to avoid decomposition of products, the reaction was allowed to proceed at room temperature. On the basis of previous studies that determined reaction times

ranging from 2–120 min for maximum hydroxamic acid formation for esters of monocarboxylic acids, alkyl and phenylalkyl carboxylic acids, and dicarboxylic and tricarboxylic acids [Hestrin 1949; Goldenberg 1958; Verheyden and Nys 1962; Thompson 1950], an average value of 60 min was used for the reaction time. When the reaction was allowed to proceed for 24 hr, a loss of linearity was observed, as shown in Figure 2.9.

The color intensity produced from the reaction of ferric ion with hydroxamic acids depends on the concentration of ferric iron and pH [Hestrin 1949; Goddu et al. 1955; Verheyden and Nys 1962]. The concentration of ferric iron needs to be high enough to complete the conversion of the hydroxamic acid to the hydroxamate to obtain maximum color [Goddu et al. 1955]. Hestrin (1949) suggested using a considerable molar excess of iron for full color development. Goddu et al. (1955) observed that optimum color was obtained for a ferric ion concentration of 2 mM. Higher concentrations of ferric ion were not useful because they increased the color intensity of the blank. The HCl needs to be added to neutralize the NaOH added in the first step and to acidify the reaction solution in the color-developing step. HCl needs to be added prior to addition of $FeCl_3$ to avoid the reaction of ferric ion with hydroxylamine in alkaline medium. Hestrin (1949) observed that the color is independent of pH for pH between 1.0–1.4, but lower for pH between 0.6–1.0. He also observed that the stability of color depends on pH. In 10 min, the color decreased by ~5 % at pH 1.0 and ~12 % at pH 1.4. Loss of color upon standing appears to be inevitable, however [Thompson 1950; Stern and Shapiro 1953; Goddu et al. 1955; Goldenberg 1958; Morgan and Kingsbury 1959; Verheyden and Nys 1962; Feldmann

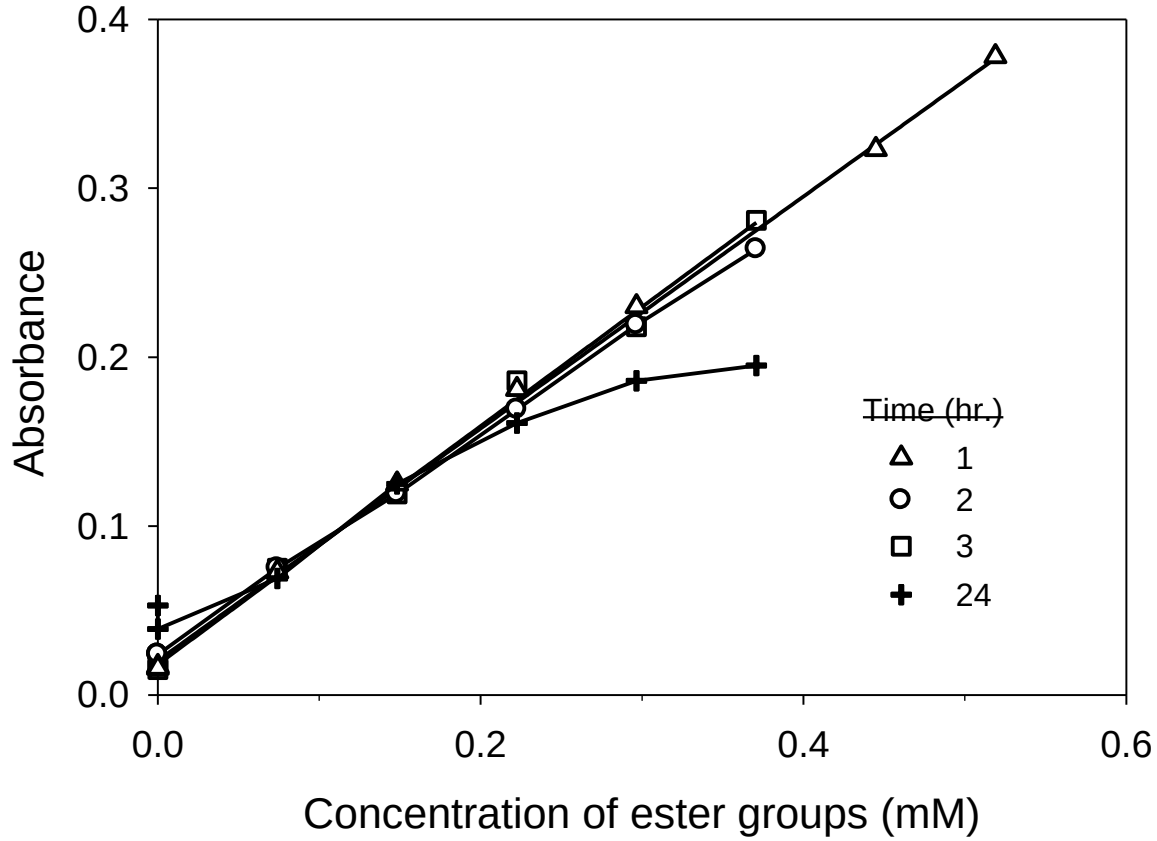

Figure 2.9. Effect of reaction time on absorbance of the ferric hydroxamate of methyl tridecanoate.

et al. 1970, 1971], including for our method, so the absorbance was measured immediately after adding HCl and $FeCl_3$.

The solvent used in this method was found to affect the sensitivity. Ethanol was a suitable solvent in many experiments [Hill 1946; Hestrin 1949; Thompson 1950; Stern and Shapiro 1953; Goddu et al. 1955; Goldenberg 1958; Morgan and Kingsbury 1959; Verheyden and Nys 1962; Feldmann et al. 1970],], since ethanol can dissolve the reagents including hydroxylamine, NaOH or KOH, HCl, and $FeCl_3$, which hardly dissolve in most organic solvents, and can also dissolve the hydroxamic acid and ferric hydroxamate products. But because the NaCl by-product does not dissolve in absolute ethanol, water needs to be added. Some studies have observed that adding water can cause a slight loss in sensitivity, however, perhaps because of competition between water and hydroxamic acids for ferric ions [Goddu 1955]. Hill (1946) observed that for long-chain esters water interfered with color development, whereas Stern and Shapiro (1953) observed that for long-chain esters such as triolein, at an optimum concentration of hydroxylamine at room temperature color intensity increased with increasing water content to a maximum at 15 % water and then slightly decreased at higher water content. Goldenberg (1955), Stern and Shapiro (1953), and Hristen (1949) have all used water as a major solvent along with ethanol for analysis of a variety of esters.

The absorbance maxima of ferric hydroxamates formed from a variety of esters were also investigated [Hill 1946; Hestrin 1949; Thompson 1950; Stern and Shapiro 1953; Goddu et al. 1955; Goldenberg 1958; Morgan and Kingsbury 1959; Verheyden and Nys 1962; Feldmann et al. 1970, 1971], with results showing absorption maxima in the

range 515–560 nm. Therefore, in our method we use the average wavelength of 540 nm for analysis of a mixture of esters, as suggested by Goddu (1955), where there is also a little absorption by ferric ion.

Calibration curves were prepared for a selection of esters with different structures, although no compounds were available with functional groups adjacent to an ester group. Nonetheless, there were considerable differences in measured values of ε (M^{-1} cm^{-1}). The results are shown in Figure 2.10. Linearity was excellent over the range of concentrations measured, and values of ε ranged from 300–900. The range for esters without an additional functional group was 530–690, with the values for the unsaturated ester and ketoester being 300 and 900. The value of ε measured for methyl (Z)-octadec-9-enoate (methyl oleate) was similar to that reported by Goddu (1955). In addition to possible electronic effects of the ketone group and C=C double bond on ε, the differences observed among esters might be due to the differences in the rates of hydroxamic acid formation, hydrolysis of esters in alkaline medium, and decomposition of ferric hydroxamates. For analysis of samples containing esters with known structures, appropriate calibration curves can be prepared, whereas for samples containing unidentified compounds use of a simple ester such as methyl tridecanoate or bis(2-ethylhexyl)decanedioate (also referred to as dioctyl sebacate) should give reasonably accurate results in most cases. Values of ε for all the esters analyzed here were within ~50 % of the values measured for these compounds.

The method was also tested for potential interferences from other compounds containing nitrate, carboxyl, hydroxyl, peroxy, and hydroperoxy groups. None of these

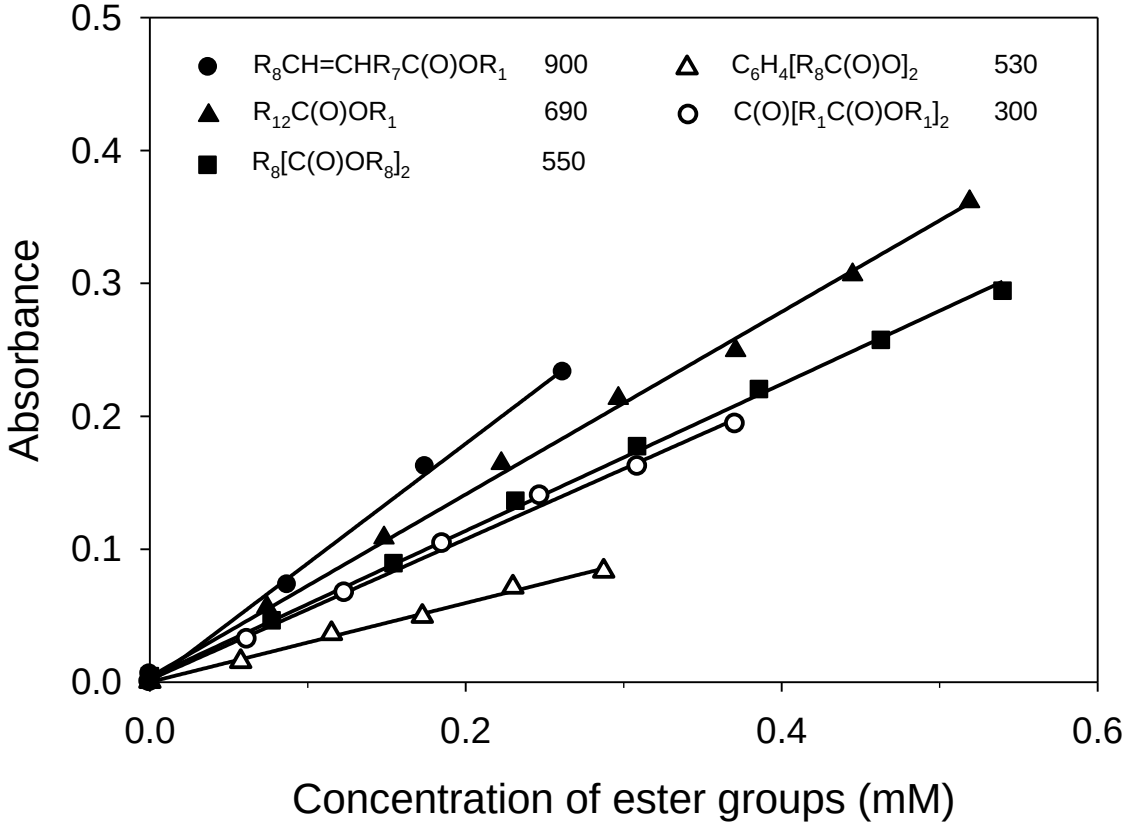

Figure 2.10. Calibration curves of esters: methyl (Z)-octadec-9-enoate (●), methyl tridecanoate (▲), bis(2-ethylhexyl)decanedioate (■), bis(2-ethylhexyl)phthalate (○),dimethyl-3-oxopentanedioate (△). The corresponding structures and values of ε (M^{-1} cm^{-1}) are shown in the legend. R_n designates $(CH_2)_n$ or $H(CH_2)_n$ depending on whether the alkyl group is in the interior or on end of the molecule. The values of ε were calculated as $\varepsilon = 10^3 \times m$, where m is the slope of the least-squares line fit to the calibration curve A = m[C] + b, A = absorbance = absorbance (sample) – absorbance (blank), and [C] is the concentration of ester groups (mM). For all lines $|b| \leq 0.004$ and $R^2 > 0.99$.

groups interfered with the ester analysis, but because the hydroxamic acid method is used to analyze acid anhydrides [Morgan 1958], amides [Bergmann 1952], and acyl phosphates [Lipmann and Critchfield 1960] under similar conditions, these compounds would interfere with the analysis.

The detection limit for this method, calculated as 3× the standard deviation of blank measurements, was 0.1 μmoles of ester groups for ester compounds with ε = 550, the average value for the compounds tested. The reproducibility determined by multiple analyses of bis(2-ethylhexyl)decanedioate was 5 % relative standard deviation.

2.3.4 Analysis of hydroxyl groups

Spectrophotometric analysis of hydroxyl groups by using 4-NBC as a derivatizing agent was first proposed by Scoggins (1964). Hydroxyl groups are esterified using 4-NBC, and the 4-NB esters are then extracted, washed, and the absorbance measured at 253 nm. Unfortunately, in this study we determined that his method is not suitable for diols or for compounds containing functional groups adjacent to a hydroxyl group, such as 6-hydroxy-5-decanone and 2-hydroxyhexadecanoic acid.

Nachtmann (1976), however, used 4-NBC as a derivatizing agent for analysis of polyols such as sugars and glycosides by HPLC with UV detection. He observed that ε was proportional to the number of hydroxyl groups in a molecule, with a value of 14800 for a monoalcohol and 162000 for the polyol raffinose, which contains 11 hydroxyl groups. This suggested that 4-NBC reacted with all the hydroxyl groups in a molecule. The difference between the methods of Nachtmann (1976) and Scoggins (1964) is the extraction step. After derivatization, Nachtmann removed the pyridine by evaporation

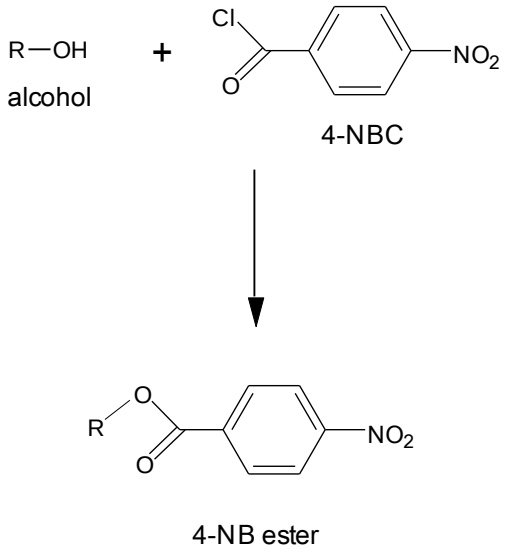

Figure 2.11. Chemistry of hydroxyl group analysis.

and hydrolyzed the excess reagent with 5 % $NaCO_3$ solution containing 4-DMAP. The 4-NB esters were then extracted into chloroform and washed with 5 % $NaHCO_3$ and 0.05 N HCl solution containing 5 % NaCl. Our method is a modified version of the one used by Nachtmann (1976). The chemistry of hydroxyl group analysis is shown in Figure 2.11.

The effect of molecular structure on the method results were evaluated by preparing calibration curves for a selection of monoalcohols and diols, some of which also contained carboxyl, carbonyl, or nitrate groups. The results are shown in Figure 2.12. Linearity was excellent over the range of concentrations measured. Values of ε for all the compounds tested were in the range 9100–15900, although except for 6-hydroxy-5-decanone and 5-hydroxy-2-pentanone the range was 13400–15900. The presence of a carbonyl group decreases ε by ~30%, similar to the effect on carboxyl group analysis. For analysis of samples containing alcohols with known structures, appropriate calibration curves can be prepared, whereas for samples containing unidentified compounds use of a simple alcohol such as 2-hexadecanol should give reasonably accurate results in most cases. Values of ε for all the alcohols analyzed here were within ~30 % of the value measured for 2-hexadecanol.

The method was also tested for potential interferences from other compounds containing nitrate, carboxyl, hydroxyl, ester, peroxy, and hydroperoxy groups. No interference was observed for nitrates, ketones, or esters, or from peroxides other than hydroperoxides, and only a small interference was observed for aldehydes. Conversely, interferences from carboxylic acids and hydroperoxides groups were significant, as shown in Figure 2.13. The effect of carboxylic acids is surprising, since values of

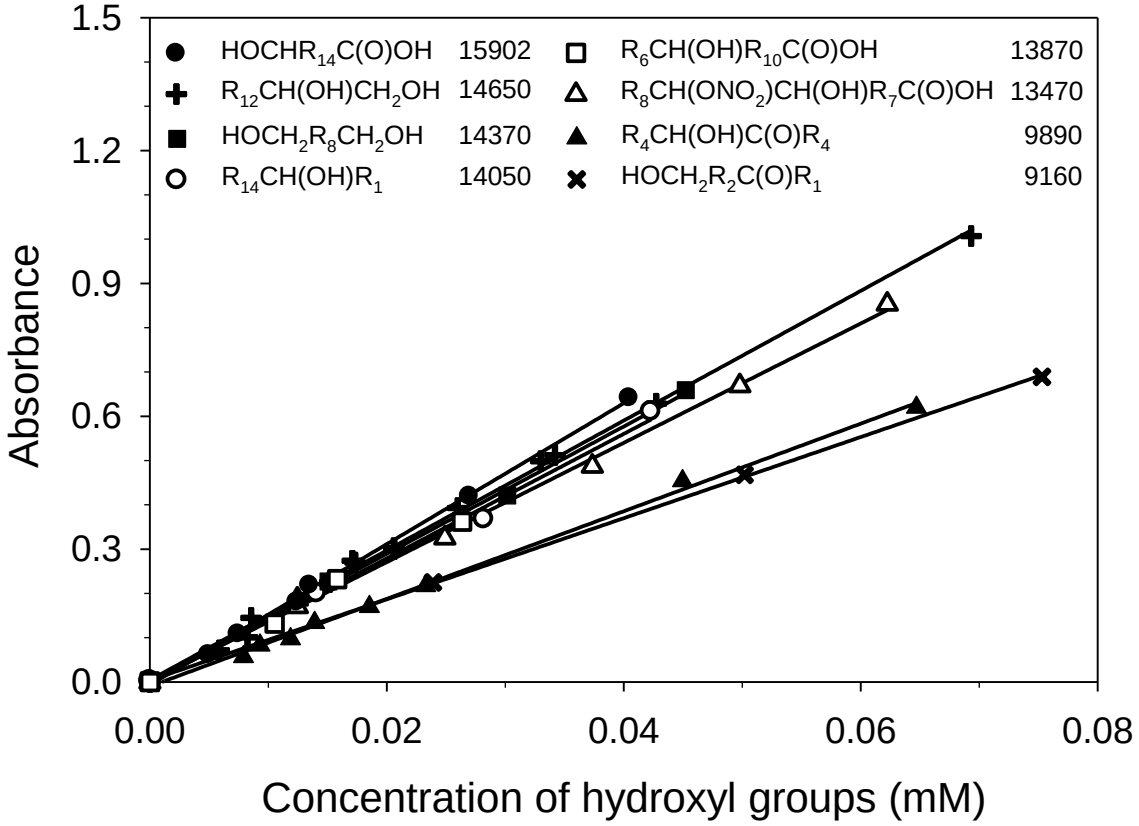

Figure 2.12. Calibration curves of alcohols: 16-hydroxyhexadecanoic acid (●), 1,2-tetradecanediol (✚), 1,10-decanediol (■), 2-hexadecanol (○), 12-hydroxyoctadecanoic acid (□), 9,10-hydroxynitrate octadecanoic acid isomers (△), 6-hydroxy-5-decanone (▲), 5-hydroxy-2-pentanone (✖). The corresponding structures and values of ε (M^{-1} cm^{-1}) are shown in the legend. R_n designates $(CH_2)_n$ or $H(CH_2)_n$ depending on whether the alkyl group is in the interior or on end of the molecule. The values of ε were calculated as $\varepsilon = 10^3 \times m$, where m is the slope of the least-squares line fit to the calibration curve A = m[C] + b, A = absorbance = absorbance (sample) – absorbance (blank), and [C] is the concentration of hydroxyl groups (mM). For all lines $|b| \leq 0.004$ and $R^2 > 0.99$.

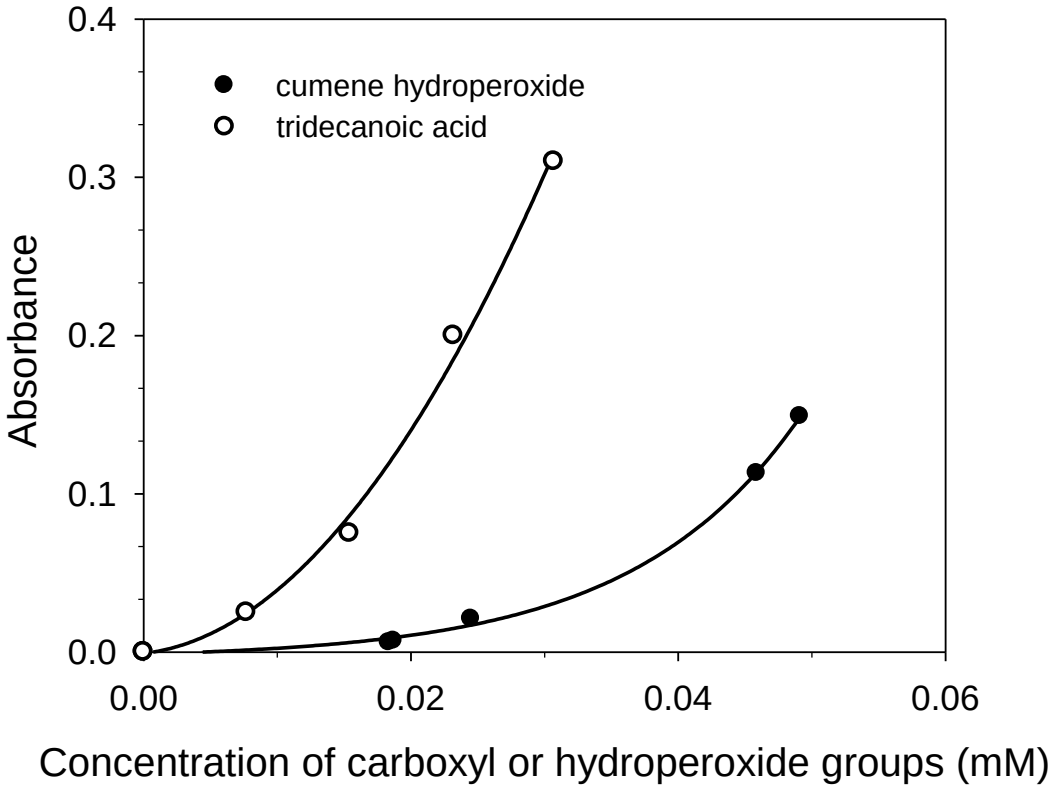

Figure 2.13. Analysis of hydroxyl groups in solutions containing either cumene hydroperoxide or tridecanoic acid.

ε measured for 16-hydroxyhexadecanoic acid and 12-hydroxyoctadecanoic acid were similar to those of monoalcohols and diols. Nonetheless, carboxyl groups are removed by converting them to their corresponding methyl esters by reaction with TMSDM prior to derivatization of hydroxyl groups with 4-NBC. Hydroperoxides could not be removed by reaction with TPP, as is done in some of our other methods, because alcohols are formed in the process. Instead, because hydroperoxides only interfere at concentrations greater than ~0.02 mM, the sample is diluted to achieve a concentration of peroxides ≤ 0.02 mM prior to hydroxyl group analysis. The peroxide concentration is measured using the method of Docherty et al. 2005, which measures total peroxides and thus gives an upper limit to the hydroperoxide concentration. With this procedure, monoalcohols, diols and alcohols containing vicinal functional groups can be analyzed.

The detection limit for this method, calculated as 3× the standard deviation of blank measurements, was 0.02 μmoles of hydroxyl groups for alcohols with ε = 14400 (on a per hydroxyl group basis), the average value for the compounds tested. The reproducibility determined by multiple analyses of 1,2-tetradecanediol was 7 % relative standard deviation.

2.3.5 Method for calculating functional group composition

The functional group composition of a sample, including methylene groups (CH_2), is obtained by assuming that the only functional groups possibly present in the sample are carboxyl, carbonyl, ester, hydroxyl, peroxide, nitrate, and methylene. The most likely groups omitted by this assumption are ether and epoxides, but these are expected to be absent or minor in most cases. The approach is to first sum the masses of measured

functional groups, calculated as the measured moles × molecular weight using the following molecular weights: carboxyl [C(O)OH] = 45, carbonyl [C(O)] = 28, hydroxyl [CHOH] = 30, nitrate [$CHONO_2$] = 75, ester [C(O)O] = 44, and peroxide [CHOOH] = 46. This value is then subtracted from the measured sample mass to obtain the mass due to methylene groups, which is then divided by 14 (molecular weight of CH_2) to obtain the moles of CH_2 groups. This information is then used to calculate the mole fraction of each functional group, equal to the moles of functional group/total moles of functional groups. A convenient way to represent the functional group composition is to then multiply these mole fractions by an assumed average carbon number for the reaction product molecules (usually that of the parent hydrocarbon), to obtain the average number of each functional group per molecule.

2.3.6 Functional group composition of secondary organic aerosol

The methods developed here were also used to analyze SOA formed from the reaction of α-pinene with O_3 in the presence of cyclohexane as an OH radical scavenger. α-Pinene is the largest contributor to monoterpene emissions to the atmosphere (primarily by coniferous trees), which account for ~10 % of the emissions of volatile organic compounds on a global scale [Guenther et al. 1995]. Its reaction with O_3 efficiently produces low-volatility products that can condense to form SOA. Molecular analysis of SOA formed from this reaction has identified and quantified a variety of multifunctional products containing carboxyl, carbonyl, ester, hydroxyl, and peroxy groups, many of which are thought to be present in the form of oligomers [Yu et al. 1999; Gao et al. 2010; Docherty et al. 2005]. Russell et al. (2011) has also used FTIR to analyze

Table 2.1. The composition of functional groups in SOA products from reaction of α-pinene with ozone in the presence of cyclohexane.

Functional Group (FG)	FG MW (g mole^{-1})	Experiment	FG/SOA[a] (μmole mg^{-1})	FG/SOA[b] (g g^{-1})	FG Mole Fraction[d]	FG/C_{10} molecule[e]
Carboxyl [C(O)OH]	45	1	6.813	0.3066	0.150	1.50
		2	7.679	0.3456	0.176	1.76
		Average±SD	7.246 ±0.613	0.3261± 0.0276	0.163±0.018	1.63±0.18
Carbonyl [C(O)]	28	1	4.324	0.1211	0.095	0.95
		2	4.502	0.1261	0.103	1.03
		Average±SD	4.413±0.126	0.1236±0.0035	0.099±0.006	0.99±0.06
Hydroperoxide [CHOOH]	46	1	0.622	0.0286	0.014	0.14
		2	0.710	0.0327	0.016	0.16
		Average±SD	0.666±0.062	0.0306±0.0029	0.015±0.002	0.15±0.02
Hydroxyl [CHOH]	30	1	0.726	0.0218	0.016	0.16
		2	1.009	0.0303	0.023	0.23
		Average±SD	0.868±0.200	0.0260±0.0060	0.020±0.005	0.20±0.05
Ester [C(O)O]-R	44	1	2.026	0.0891	0.045	0.45
		2	1.654	0.0728	0.038	0.38
		Average±SD	1.840±0.263	0.0810±0.0116	0.041±0.005	0.41±0.05
Methylene [CH_2]	14	1		0.4328[c]	0.681	6.81
		2		0.3927[c]	0.643	6.43
		Average±SD		0.4128±0.0284	0.662±0.026	6.62±0.26
Average MW[f]	220	1				
	229	2				
Elemental Analysis[g]						
O/C	0.54 (0.44)					
H/C	1.54 (1.65)					

[a] Results from functional group analysis

[b] FG/SOA (g g^{-1}) = FG/SOA (μmole mg^{-1}) x 10^{-3} x FG MW (g mole^{-1})

[c] CH_2/SOA (g g^{-1}) = 1- sum of measured FG (g g^{-1})

[d] FG Mole Fraction = FG (mole)/sum of FG (mole); where FG (mole) = [FG/SOA (g g^{-1})]/MW (g mole^{-1}) of FG

[e] FG/C_{10} molecule = FG Mole Fraction x carbon number of α-pinene (10)

[f] Average MW = sum of (FG/ C_{10} molecule x FG MW (g mole^{-1})

[g] The values were calculated from functional group composition analysis and the values in parentheses were calculated from elemental analysis.

the functional group composition of organic aerosol collected in a coniferous forest in Whistler, Canada, where monoterpenes dominate organic emissions and SOA is expected to derive largely from the oxidation of these compounds. The results of our analyses are shown in Table 2.1 along with the O/C and H/C ratios calculated from the functional group composition and measured by standard combustion methods. Assuming that all products contain 10 carbon atoms (the same as α-pinene), the average number of carboxyl, carbonyl, ester, hydroxyl, hydroperoxide, and methylene groups, per molecule, were 1.63, 0.99, 0.41, 0.20, 0.15, and 6.62. Average O/C and H/C ratios calculated from the functional group composition were 0.54 and 1.56, which compare well with average values of 0.48 and 1.72 measured using standard combustion methods. For comparison, the average number of carboxyl, carbonyl (including esters), hydroxyl, and methylene groups per C_{10} molecule in the organic aerosol in Whistler (calculated by multiplying FTIR-measured mole fractions by 10) were 1.0, 1.6, 2.5, and 4.4, and the reported average O/C ratio was 0.72 (Russell et al. 2011). This composition is reasonably similar to that measured here for SOA formed in the chamber, although the Whistler aerosol had a much higher concentration of hydroxyl groups, fewer carboxyl groups, and overall was more highly oxidized. This may reflect a significant contribution to the Whistler aerosol of products formed from reactions of OH radicals with monoterpenes, which are expected to contain more hydroxyl and less carboxyl groups than the products of O_3 reactions (Capouet et al. 2008). In the clean remote atmosphere, the ratio of OH:O_3 reaction for α-pinene is ~0.6:0.4 (Atkinson and Arey and 2003).

2.4 Conclusions

The spectrophotometric methods developed here can be used to quantify the concentrations of carbonyl, hydroxyl, carboxyl, and ester groups in collected samples of atmospheric organic matter. The methods employ derivatizing agents to convert each functional group to a characteristic colored derivative that is then quantified by measuring the absorbance using spectrophotometry. The effects of molecular structure on quantification have been evaluated by measuring calibration curves for a large variety of monofunctional and multifunctional compounds, and potential interferences from other compounds containing non-target functional groups have been determined and methods developed to eliminate these interferences. This means, for example, that under the conditions of these analyses carboxylic acids and alcohols do not form esters and esters do not hydrolyze to carboxylic acids and alcohols. Furthermore, formation of hemiacetals and peroxyhemiacetals by the reversible reactions of alcohols and hydroperoxides with carbonyls does not effect the quantification of any of these functional groups. For analysis of samples containing compounds with known structures, appropriate calibration curves can be prepared, whereas for samples containing unidentified compounds use of a simple monofunctional carboxylic acid, ketone or aldehyde, ester, and alcohol should give results that are within ~30 % (and often much less) of the correct value, and at worst ~50%. Detection limits are approximately 0.01, 0.02, 0.03, and 0.1 μmoles for carbonyl, hydroxyl, carboxyl, and ester groups. A complete set of duplicate analyses (including peroxide [Docherty et al. 2005] and nitrate [Matsunaga and Ziemann 2009]) requires ~1 mg of sample and takes ~3 days, although additional samples can be analyzed in parallel.

Unfortunately, it is unlikely that detection limits could be substantially improved by using longer cell path lengths, because the reagent blanks already have sufficiently high absorbance with a 1 cm cell (carbonyl and carboxyl ~ 0.1, ester ~ 0.2, and hydroxyl ~ 0.3) that use of, for example, a 50 cm waveguide fully saturates the blank absorbance. We did not attempt to determine the source of this absorbance, but since the chemicals we used were of very high purity it was probably not due to impurities. Although these methods were demonstrated here by analyzing SOA samples, they should also be applicable to analysis of organic gas samples, although care must be taken to avoid evaporation of the more volatile compounds during sample processing. To analyze organic compounds present in ambient air, one would need to first determine the amount of background visible absorbance in the sample (due to species such as brown carbon and humic-like substances) and then correct for this in absorption measurements on derivatized samples. These methods should complement the use of FTIR and NMR for functional group analysis, since although those methods have lower detection limits they are less specific for some functional groups.

2.5 References

Adel-Hay, M. H., Kotany, M. A., Bedair, M. M., and Gazy, A. A. Colorimetric Determination of Seven Nonsteroidal Anti-Inflammatory Drugs Using 2-Nitrophenylhydrazine Hydrochloride. *Anal. Lett*., 23, 281-294 (1990).

ASTM International, Standard Test Method for Trace Quantities of Carbonyl Compounds with 2,4-Dinitrophenylhydrazine, Designation: E411-05, 502-505 (2005).

Bergmann, F., Colorimetric Determination of Amides as Hydroxamic Acids, *Anal. Chem.*, 24, 1367-1369 (1952).

Capouet, M., Müller, J. F., Ceulemans, K., Compernolle, S., Vereecken, L., and Peeters, J.,. Modeling Aerosol Formation in Alpha-Pinene Photo-Oxidation Experiments. *J. Geophys. Res*., 113, D02308 (2008).

Chiba, T., Takazawa, M., and Fujimoto, K. A Simple Method for Estimating Carbonyl Content in Peroxide-Containing Oils. *J. Am. Oil. Chem.*, 66, 1588-1592 (1989).

Feldmann, J. A., and Robb, B. J. Colorimetric Determination of Atropine, Homatropine, Scopolamine and their Derivatives by the Ferric Hydroxamate Method. *J. Pharm. Sci*., 59, 1646-1647 (1970).

Feldman, J. A., Frank, S. G., and Holmes, J. H. Determination of Di-(2-ethylexyl) Sodium Sulfonsuccinate and Related Dialkyl Esters in Aqueous Solutions by the Ferric Hydroxamate Procedure. *J. Pharm. Sci*., 60, 920-921 (1971).

Greenbaum M. A., Denney D. B., and Hoffmann A. K. A Study of the Mechanism of the Conversion of Benzoyl Peroxide to Benzoic Anhydride by Triphenylphosphine. *J. Am. Chem. Soc.*, 78, 2563-2565 (1956).

Goddu, R. F., LeBlanc, N. F., and Wright, C. M. Spectrophotometric Determination of Esters and Anhydrides by Hydroxamic Acid Reaction. *Anal. Chem*., 27, 1251-1255 (1955).

Goldenberg, V., Colorimetric Determination of Carboxylic Acid Derivatives as Hydroxamic Acids. *Anal. Chem*., 30, 1327-1330 (1958).

Hestrin, S. The Reaction of Acetylcholine and other Carboxylic Acid Derivates with Hydorxylamine and its Analytical Application. *J. Biol. Chem*., 180, 249-260 (1949).

Hill, U. T. Colorimatric Determination of Fatty Acids and Esters. *Ind. Eng. Chem*., 18, 317-319 (1946).

Horikawa, R., and Tanimura, T. Spectrophotometric Determination of Carboxylic Acids with 2-Nitrophenylhydrazine in Aqueous Solution. *Anal. Chim. Acta*., 63, 1629-1642 (1982).

Johnson, D. P., and Critchfield, F. E. Colorimetric Determination of Low Concentration of Primary and Secondary Alcohols. *Anal. Chem*., 32, 865-867 (1960).

Jordan, D. E., and Veatch, F. C. Spectrophotometric Determination of Trace Concentrations of Carbonyl Compounds. *Anal. Chem*., 36, 120-124 (1964).

Jordan, D. E. Simultaneous Determination of Trace Concentrations of Saturated and α,β-Unsaturated Carbonyl Compounds in Organic Systems. *Anal. Chim. Acta*., 37, 379-390 (1966).

Korany, M. A., Abdel-Hay, M. H., Bedair, M. M., and Gazy, A. A. Colorimetric Determination of Some Penicillins and Cephalosporins with 2-Nitrophenylhydrazine Hydrochloride. *Talanta*., 36, 1253-1257 (1989).

Lappin, G., Colorimetric Method for Determination of Traces of Carbonyl Compounds. *Anal. Chem*., 23,541-542 (1951).

Lipmann, F., and Tuttle, L. C. A Specific Micromethod for the Determination of Acyl Phosphates. *J. Biol. Chem*., 159, 21-28 (1945).

Meyer, S., and Rebrovic, L. The Spectroscopic Ouinoidal Ion Method for the Analysis of Carbonyl Compounds. *J. Am. Oil. Chem*., 72, 385-387 (1995).

Miwa, H., Yamamoto, M., and Momose, T. Colorimetric Detection and Determination of Carboxylic Acids with 2-Nitrophenylhydrazine Hydrochloride. *Chem. Pharm. Bull*., 28, 599-605 (1980).

Umbreit, G. R., and Houtman, R. L. Colorimetric Analysis of Organic Hydroxyl Groups. *J. Pharm. Sci*., 56, 349-351 (1967).

Morgan, K. J. The Ferric Hydroxamate Colour Reaction II. The Spectrophotometric Determination of Acetic Anhydride. *Anal. Chem. Acta*., 19, 27-31 (1958).

Morgan, D. M., and Kingsbury, K. J. A Modified Hydroxamic Acid Method for Determinating Total Esterified Fatty Acids in Plasma. *The Analyst*, 84, 409-414 (1959).

Munson, J. W., and Bilous, R. Colorimetric Determination of Aliphatic Acids. *J. Pharm. Sci*., 66, 1403-1405 (1972).

Munson, J. W. 2-Nitrophenylhydrazine: A Selective Reagent for Colorimetric Determination of Carboxylic Acid Anhydrides and Chlorides. *J. Pharm. Sci*., 63, 252-257 (1975).

Nachtmann, F. Some Properties of 4-Nitrobenzoates of Saccharides and Glycosides; Application to High-Pressure Liquid Chromatography. *Z. Anal. Chem*., 282, 209-213 (1976).

Norio, H., Toyohiko, A., and Takayuki, S. New Methods and Reagents inorganic Synthesis. 14 A Simple Efficient Preparation of Methyl Esters with Trimethylsilyl-diazomethane ($TMSCHN_2$) and Its Application to Gas Chromatographic Analysis of Fatty Acids. *Chem. Pharm. Bull*., 29, 1475-1478 (1981).

Pavia, D. L., Lampman, G. M., Kriz, G. S., and Vyvyan J. R. *Introduction to Spectroscopy*, Fourth edition, Brooks/Cole Cengage Learning, Belmont, CA (2007).

Presser, A., and Hüfner, A. Trimethylsilyldiazomethane - A Mild and Efficient Reagent for the Methylation of Carboxylic Acids and Alcohols in Natural Products, *Monatshefte für Chemie*, 135, 1015-1022 (2004).

Scoggins, M. W. Determination of Trace Quantities of Alcohols by Ultraviolet Spectrophotometry of Akyl Nitrobenzoates. *Anal. Chem*., 36, 1152-1153 (1964).

Stern I., and Shapiro B. A Rapid and Simple Method for the Determination of Esterified Fatty Acids and for Total Fatty Acid in Blood. *J. Clin. Path*., 6, 158-159 (1953).

Thompson, A. R. A Colorimetric Method for the Determination of Esters. *Australian J. Sci. Research.*, 3A, 128-135 (1950).

Verheyden, J., and Nys, J. The Estimation of Fatty Acid Esters in Serum by the Hydroxamate Method. *Clin. Chim. Acta*, 7, 262-269 (1962).

Yukawa, N., Takamura, H., and Matoba, T. Determination of Total Carbonyl Compounds in Aqueous Media. *J. Am. Oil. Chem*., 70, 881-884 (1993).

CHAPTER 3

Composition in Secondary Organic Aerosol Formed from the Environmental Chamber Reaction of *n*-Pentadecane with OH Radicals in the Presence of NO_x

Abstract

In this chapter the functional group analysis methods described in Chapter 2 were used to investigate the chemical composition of secondary organic aerosol formed from the OH radical-initiated reaction of *n*-pentadecane in the presence of NO_x. Experiments were conducted in an environmental chamber under low and high UV irradiation to vary OH radical exposure and thus evaluate the effects of the extent of oxidation on the reaction products. Real-time and offline thermal desorption particle mass spectrometry and SOA yield measurements were used in addition to functional group analysis to characterize the SOA. Results of functional group analysis indicate the presence of carbonyl, hydroxyl, and nitrate groups in SOA formed from 1 min of irradiation, consistent with expectations based on the well-established reaction mechanism and product vapor pressures, with the major SOA products appearing to be first-generation 1,4-hydroxynitrates, cyclic hemiacetals, and their dimers, and second-generation cyclic hydroxynitrates. SOA formed from 60 min of irradiation contained carbonyl, hydroxyl, and nitrate groups as well as ester and peroxide groups associated with second- and third-generation carbonylesters and acyl peroxynitrate esters, and possibly hemiacetals. The cyclic hydroxynitrates, carbonylesters, and acyl peroxynitrate esters were formed via

heterogeneous/multiphase cyclization and dehydration of 1,4-hydroxycarbonyls to form dihydrofurans, followed by further OH radical reactions. The results demonstrate the value of these functional group analysis methods for SOA studies and lend additional support for the currently accepted mechanism of SOA formation from reactions of alkanes under these conditions, including the role of heterogeneous/multiphase reactions.

3.1 Introduction

Three classes of organic compounds: alkanes, alkenes, and aromatics, constitute the majority of volatile organic compound (VOC) emissions to the atmosphere [Calvert et al., 2000; Guenther et al. 1995]. Once in the atmosphere, VOCs react primarily with OH radicals, O_3, and NO_3 radicals to form oxidized products [Atkinson and Arey 2003]. Some of these products have sufficiently low vapor pressures to partition into aerosol particles and form secondary organic aerosol (SOA) [Kroll and Seinfeld 2008], which can contribute significantly to the mass of atmospheric fine particulate matter (diameter $\leq$ 2.5 μm) and thus affect atmospheric processes such as light scattering and absorption [Seinfeld and Pandis 1998; Haywood and Boucher 2000], cloud formation [Andreae and Rosenfeld 2008; Lohmann and Feichter 2005], the hydrologic cycle [Ramanathan et al. 2001], and atmospheric chemistry [Ravishankara 1997], as well as human health [Davidson et al. 2005]. Alkanes and aromatic hydrocarbons tend to be most abundant in urban areas [Calvert et al. 2000], whereas alkenes dominate biogenic emissions and represent ~90% of global VOC emissions [Guenther et al. 1995]. The chemical composition of the products of VOC oxidation and thus SOA depends on the identity of

the VOC and oxidant, NO_x concentrations, and also particle properties such as acidity and water content that can affect heterogeneous/multiphase reactions that can occur on/in particles and potentially lead to the formation of oligomers [Atkinson and Arey 2003; Kroll and Seinfeld 2008]. In urban areas where alkane and NO_x concentrations are high, OH radical-initiated reactions of alkanes lead to the formation of first-generation products containing primarily carbonyl, hydroxyl, and nitrate groups, and with further reaction can form higher-generation multifunctional products that contain more of these functional groups as well as ester and acyl peroxynitrate groups [Arey et al. 2001; Martin et al. 2002; Atkinson and Arey 2003; Atkinson et al. 2008; Lim and Ziemann 2009a; Ziemann 2011]. The kinetics, products, and mechanisms of these reactions are reasonably well understood, and the yields of most of the first- and some second-generation gas-phase products of the reactions of *n*-alkanes have been quantified [Arey et al. 2001; Martin et al. 2002; Reisen et al. 2005]. Some of the first- and higher-generation products of alkane reactions that form SOA have also been identified, and the importance of heterogeneous/multiphase reactions in SOA formation demonstrated [Lim and Ziemann 2009a,b]. And although the yields of SOA formed from a large variety of linear, branched, and cyclic alkanes have been measured [Lim and Ziemann 2009c; Presto et al. 2010], the SOA products of these reactions have not been quantified. Because of the relatively few number of products expected to be formed from the OH radical-initiated reactions of alkanes in the presence of NO_x, and the lack of prior quantitative SOA analyses, SOA formed from these reactions provides a good system for applying the functional group analysis methods described in Chapter 2. This chapter describes the

results of environmental chamber experiments conducted on the reaction of OH radicals with *n*-pentadecane, the linear C_{15} alkane, in the presence of NO_x. The study employs functional group analysis, elemental analysis, particle mass spectrometry, and measurements of SOA yields to investigate the chemistry of SOA formation, including the effects of oxidative aging on SOA composition.

3.2 Experimental Section

Chemicals. The following chemicals, with purities or grades and suppliers, were used: *n*-pentadecane (99%), 2-ethylhexyl nitrate (97%), tridecanoic acid (98%), benzoyl peroxide (97%) [Sigma-Aldrich]; bis(2-ethylhexyl)-decanedioate (DOS) (97%) [Fisher Chemicals]; 5-hydroxy-2-pentanone (96%) [TCI]. NO and NH_3 [Matheson Gas]. Methyl nitrite was synthesized [Taylor et al. 1980] and stored in liquid nitrogen. See Chapter 2 for a description of the chemical used for functional group analysis.

Environmental chamber method. Reaction were conducted in a 8300 L FEP Teflon environmental chamber filled with clean, dry air (< 5 ppbv hydrocarbon and < 1% RH) at about 20^{o}C and atmospheric pressure. UV lamps cover two walls outside the chamber and act as a light source for photolysis. All chemicals were added to the chamber in a flow of N_2. Measured amounts of *n*-pentadecane, methyl nitrite (CH_3ONO), NO, NH_3, and water were added separately from a glass bulb, and dioctyl sebacate (DOS) seed particles were generated using an evaporation-condensation apparatus.

The reaction was initiated by turning on the UV lights to generate OH radicals via photolysis of methyl nitrite [Atkinson et al. 1981]. The NO was added to enhance

Table 3.1. Experimental conditions of the reaction of *n*-pentadecane with OH radicals in the presence of NO_x.

Experiment	Lights (min/%)	*n*-Pentadecane (ppmv)	CH_3ONO (ppmv)	NO (ppmv)	NH_3 (ppmv)	RH (%)	OA[1] ($\mu g\ m^{-3}$)	SOA[2] corrected ($\mu g\ m^{-3}$)	SOA yield
1 Initial	1/100	0.976	9.9	9.1	-	≤ 0.1	0.1		
At 4 min		0.770		8.3			880	880	0.482
2 Initial	1/100	0.976	9.3	8.9	-	≤ 0.1	0.2		
At 4 min		0.699		8.0			920	920	0.378
3 Initial	1/100	0.976	9.5	8.2	5	≤ 0.1	0.2		
At 4 min		0.751		7.5			810	810	0.406
4 Initial	1/100	0.976	9.4	9.1	-	≤ 0.1	190		
At 4 min		0.797		8.5			860	670	0.424
5 Initial	60/50	0.976	10.7	13.9	-	≤ 0.1	140		
At 60 min		0.165		9.8			5390	5510	0.769
6 Initial	60/50	0.976	11.2	10.5	-	≤ 0.1	230		
At 60 min		0.105		9.2			5590	5740	0.746
7 Initial	60/50	0.976	10.9	11.5	-	75	200		
At 60 min		0.150		9.4			5870	6430	0.881

[1]In experiments 4-7 initial OA is DOS seed.

[2]Corrected for loss to walls using decay in DOS *m/z* 185 signal.

conversion of HO_2 to OH and to suppress the O_3 and NO_3 radical formation. The concentration of NO_2 increases during the experiment and eventually scavenges most OH radicals to form HNO_3. The lights were turned on for 1 min at 100% light intensity (corresponding to a NO_2 photolysis rate constant of 0.61 min^{-1}) in experiments 1-4 and for 60 min at 50% light intensity (corresponding to a NO_2 photolysis rate constant of 0.37 min^{-1}) in experiments 5-7. In experiment 3, 5 ppmv of NH_3 was added immediately after 1 min of irradiation.

Particle and gas analysis. A thermal desorption particle beam mass spectrometer (TDPBMS) was used to analyze particle composition in real-time [Tobias et al. 2000] and by temperature-programmed thermal desorption (TPTD) [Tobias and Ziemann 1999]. Air was sampled into the TDPBMS and particles were formed into a beam and impacted on a polymer-coated metal vaporizer [Chattopadhyay and Ziemann 2005]. For real-time analysis, the rod was resistively heated to 160^{o}C. Particles vaporized upon impact and the vapor was ionized by 70 eV electrons and analyzed in a quadrupole mass spectrometer. For TPTD analysis, the rod was cooled to -40^{o}C and particles were collected for 30 min. The rod was allowed to warm to -5^{o}C and then heated to 200^{o}C using a 2^{o}C min^{-1} ramp to desorb and separate compounds by volatility prior to mass analysis.

Aerosol volume concentrations were measured using a scanning mobility particle sizer (SMPS). SOA mass concentration was calculated by subtracting the initial particle volume concentration from the highest aerosol volume concentration for 1 min light exposure experiments and from the corrected aerosol volume concentration at 60 min for 60 min light exposure experiments and then multiplying by a particle density of 1.06

g cm^{-3} [Lim and Ziemann 2009c]. *n*-Pentadecane was collected on Tenax TA and analyzed by GC-FID [Docherty et al. 2005] to determine the mass of *n*-pentadecane reacted. SOA yields were calculated as SOA mass/reacted *n*-pentadecane mass. NO and NO_x were measured using a Thermo Environmental Instruments Inc. model 42 chemiluminescence NO-NO_2-NO_x analyzer.

Filter sampling and sample preparation for functional group analysis.

Duplicate particle samples were collected after each experiment on previously weighed Millipore filters (0.45 μm pore size, Fluoropore FHLP, 47 mm). Sample air volumes were ~ 2 m^3 collected over ~2 hr through stainless steel tubing for 1 min light exposure experiments and ~ 0.5 m^3 collected over ~ 40 min for 60 min light exposure experiments. Immediately after sampling, each filter was weighed to calculate the mass of sample collected, and then extracted twice in 4 ml of ethyl acetate at room temperature for >10 min. For each filter, extracts were combined into a 4-ml brown vial that was previously weighed, and then dried in a stream of N_2. The vial was weighed again to determine the mass of sample. Aerosol mass was collected ~ 1mg for 1 min light exposure experiments and ~ 5 mg for 60 min light exposure experiments. Dried samples were dissolved in an appropriate volume of ethyl acetate to achieve a sample concentration of at least ~1 mg mL^{-1}. Separate aliquots were taken for analysis of each functional group and dried in a stream of N_2 to remove ethyl acetate, and then dissolved in an appropriate solvent for each analysis as noted in the procedures described in Experimental section in Chapter 2. A clean blank filter was also prepared and analyzed similarly. The methods used for nitrate and peroxide analysis were described previously [Matsunaga and Ziemann 2009,

Docherty and Ziemann 2005]. The standard curves used for quantification of each functional group were prepared using 2-ethylhexyl nitrate for nitrate groups, 5-hydroxy-2-pentanone for carbonyl and hydroxyl groups, tridecanoic acid for carboxyl groups, benzoyl peroxide for peroxide groups and bis(2-ethylhexyl)-decanedioate for ester groups.

Elemental analysis. Dried filter extracts were also analyzed for C and N using a high temperature combustion elemental analyzer (Costech ECS 4010 CHNSO) and for O and H using a temperature conversion elemental analyzer (Thermo TC/EA) interfaced to an isotope ratio mass spectrometer (Thermo Delta V).

3.3 Results and Discussion

Reaction mechanism and products. The mechanism and products of the reaction of *n*-pentadecane with OH radicals in the presence of NO_x is shown in Figure 3.1 (Atkinson and Arey, 2003; Atkinson et al., 2008; Lim and Ziemann, 2009). The reaction is initiated by abstraction of an H atom to form H_2O and an alkyl radical. Structure-reactivity calculations [Kwok and Atkinson 1995] indicate that this abstraction occurs 98% at secondary H atoms (C_2–C_{14}) and 2% at primary H atoms (C_1 and C_{15}). In air, alkyl radicals immediately add O_2 to form alkylperoxy radicals, which in the presence of NO then react to form either alkyl nitrates [**1**] or alkoxy radicals and NO_2. Alkoxy radicals then isomerize through a 1,5-H-atom shift to form 1,4-hydroxyalkyl radicals, which then add O_2 and react with NO to form either 1,4-hydroxynitrates [**2**] or 1,4-

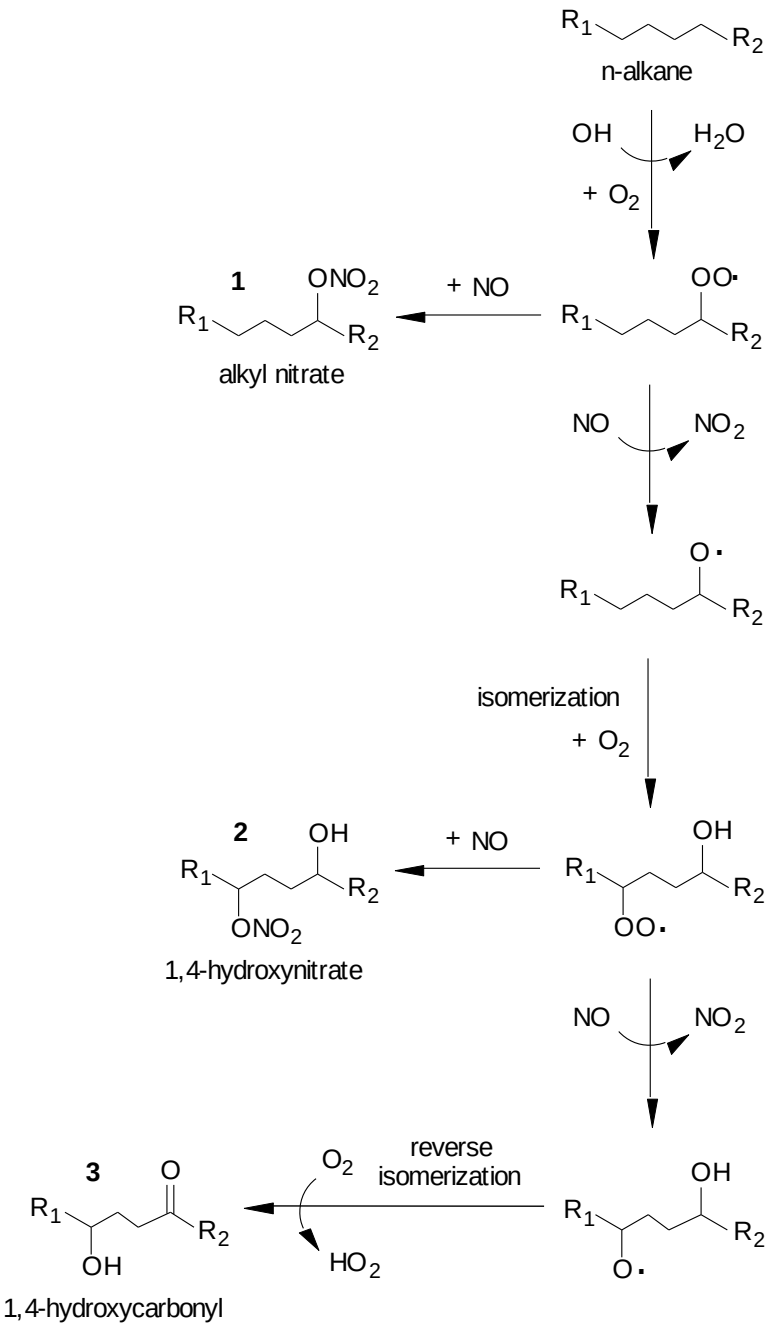

Figure 3.1. Mechanism of reaction of OH radicals with *n*-alkanes in the presence of NO_x.

hydroxyalkoxy radicals. The 1,4-hydroxyalkoxy radicals undergo a reverse isomerization and then react with O_2 to form a 1,4-hydroxycarbonyl [**3**] and HO_2. It is worth noting that although alkoxy radicals can also react with O_2 to form carbonyls and decompose to form pairs of carbonyls and alkyl radicals, for *n*-alkanes > C_6 these reactions are too slow to compete with isomerization and so are not shown in the mechanism figure. Recent measurements in our laboratory indicate that the yield of alkyl nitrate for the *n*-pentadecane reaction is 0.27, in good agreement with the value of 0.29 predicted by the model developed by Arey et al. (2001), and that the yield of 1,4-hydroxynitrate is 0.10. The expected yield of 1,4-hydroxycarbonyl is thus 0.63, in good agreement with an average value of 0.54 measured by Reisen et al. (2005) for reactions of the C_5–C_8 *n*-alkanes.

The 1,4-hydroxycarbonyls formed in this reaction can react on/in particles or the walls of the environmental chamber, as shown in Figure 3.2. The reactions are catalyzed by acid and involve first cyclization to form a cyclic hemiacetal [**4**] and then dehydration to form a dihydrofuran [**5**] (Martin et al. 2002; Atkinson et al. 2008; Lim and Ziemann, 2009). Measurements and modeling indicate that under conditions similar to these that the probability that a 1,4-hydroxycarbonyl will cyclize upon collision with a particle (i.e., the reactive uptake coefficient) is ≥ 0.5, and that the timescale for dehydration is ~ 15 min [Lim and Ziemann, 2009b]. The dihydrofurans formed via this process evaporate from the particles and react rapidly with OH radicals (or O_3 or NO_3 radicals if present) [Martin et al. 2002] to form primarily cyclic hydroxynitrates [**6,7**] and carbonylesters [**8**] (Figure 3.2). Reaction involves addition of an OH radical to the C=C bond to form a

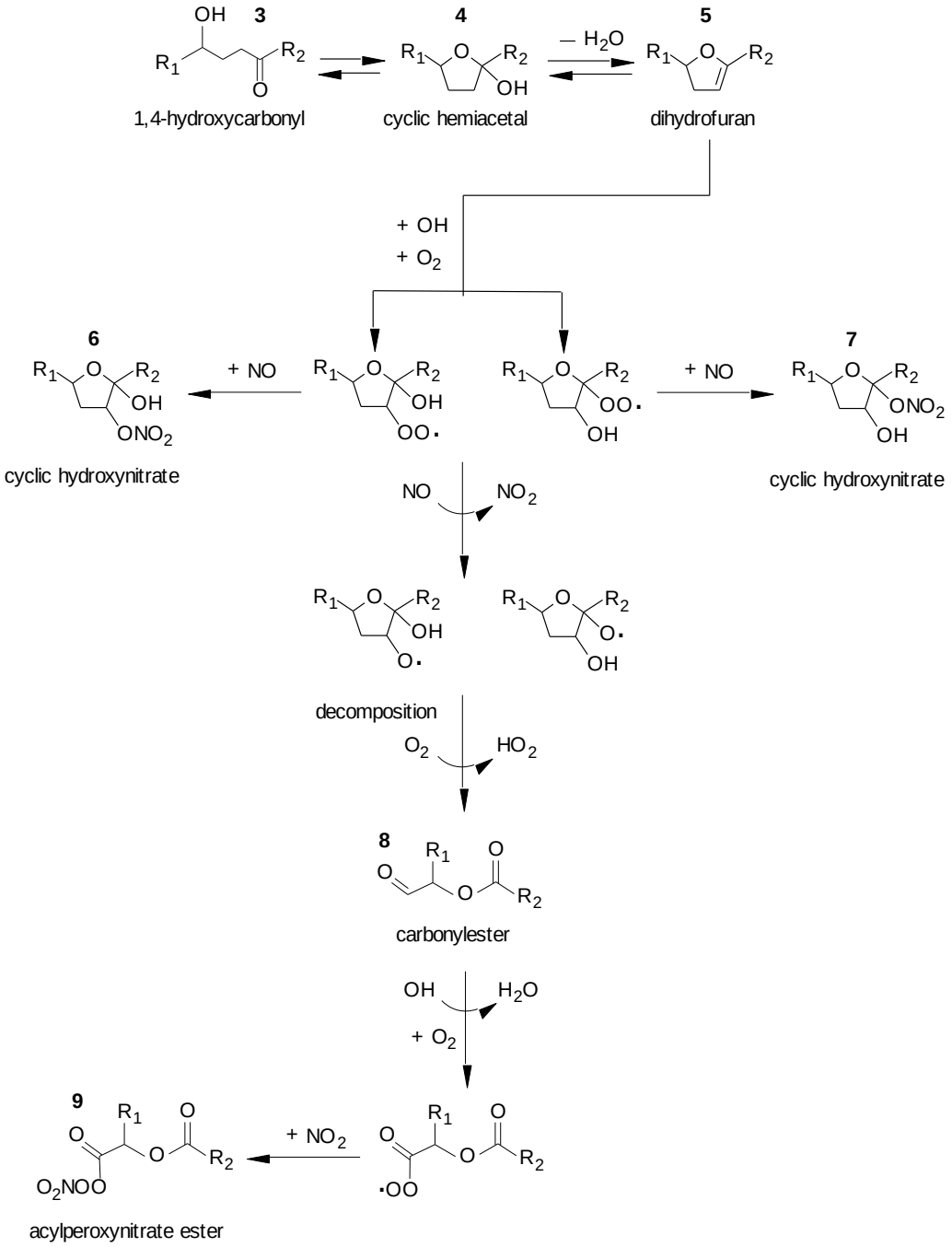

Figure 3.2. Mechanism of reaction of 1,4-hydroxycarbonyls to form cyclic hemiacetals and dihydrofurans, and subsequent reactions with OH radicals in the presence of NO_x.

β-hydroxyalkyl radical, which then adds O_2 and reacts with NO to form either a cyclic β-hydroxynitrate or cyclic β-hydroxyalkoxy radical. Cyclic β-hydroxyalkoxy radicals are expected to rapidly decompose via ring opening and then react with O_2 to form a carbonylester and HO_2. On the basis of β-hydroxynitrate yields measured for reactions of linear and branched C_{15} alkenes [Matsunaga and Ziemann 2010], the yields of cyclic β-hydroxynitrates formed here from reactions of NO with secondary and tertiary C_{15} β-hydroxyperoxy radicals should be approximately 0.15 and 0.25. If the sole other product is the carbonyl ester, then the expected yields of cyclic β-hydroxynitrates and carbonylesters should be approximately 0.2 and 0.8. Martin et al. (2002) measured a carbonylester yield of 0.72 from the reaction of the dihydrofuran formed from 2-hydroxy-5-pentanone and also observed smaller decomposition products. The yield of cyclic β-hydroxynitrates is expected to be < 5% for C_5 β-hydroxyperoxy radicals (O'Brien et al. 1998). Alkyl nitrates, 1,4-hydroxynitrates, 1,4-hydroxycarbonyls, and carbonylesters can also react with OH radicals to form higher generation products. Reactions that occur via H-atom abstraction should mostly be similar to those shown in Figure 1 and thus add nitrate, 1,4-hydroxynitrate, and 1-4-hydroxycarbonyl groups to the parent compound. In the case of carbonylesters, however, H-atom abstraction occurs preferentially from the aldehyde group to form an acyl radical that then adds O_2 to form an acylperoxy radical (Figure 3.2). Acylperoxy radicals either react with NO_2 to form acylperoxynitrates [**9**] or with NO to form NO_2 and acyloxy radicals that decompose to alkyl radicals and CO_2 (not shown).

1 minute irradiation. The SOA formed in environmental chamber reactions was analyzed as described above to obtain the following information: aerosol mass concentrations (SMPS), real-time (RTMS) and temperature-programmed thermal desorption (TPTD) mass spectra, and functional group composition (FG). In the experiments described here the lights were turned on for 1 min at 100% light intensity (corresponding to a NO_2 photolysis rate constant of 0.61 min^{-1}) and then turned off. Results for the four experiments conducted were similar, so representative results from one experiment are discussed.

SMPS analysis. The aerosol mass concentrations measured over the course of Experiment 4 are shown in Figure 3.3A. The concentrations have been corrected for loss of aerosol to the chamber walls by using the decay in the DOS mass spectral signal at *m/z* 185, which is possible because DOS is effectively non-volatile and essentially all the *m/z* 185 signal comes from DOS (shown from similar experiments conducted without DOS seed particles). The initial organic aerosol (OA) mass concentration was 190 μg m^{-3} from DOS seed particles, and in 1 min of irradiation increased to 860 μg m^{-3} due to the addition of 670 μg m^{-3} of SOA. The concentration of *n*-pentadecane reacted in this 1 min period was 1550 μg m^{-3} (0.179 ppmv), corresponding to an SOA yield of 0.42. For a liquid aerosol with this mass concentration gas-particle partitioning equilibrium should be achieved in < 1 s [Matsunaga and Ziemann 2010], and if the SOA was non-volatile and no further SOA was formed through heterogeneous-multiphase reactions, then the OA mass shown in Figure 3.3 should have stayed constant during the next 225 min of the

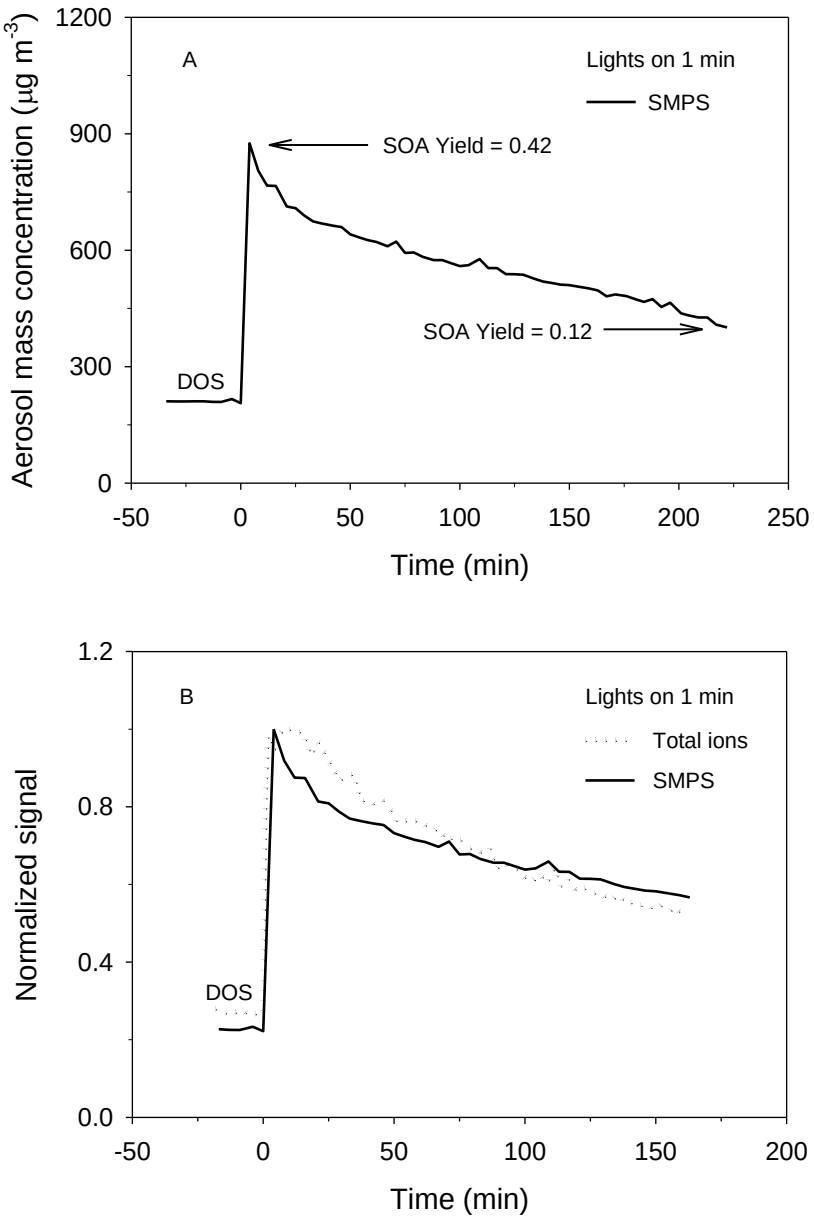

Figure 3.3. (A) Aerosol mass concentrations and SOA yields measured during the 1 min irradiation experiment using the SMPS, and (B) aerosol mass concentrations and total ion signals measured during the 1 min irradiation experiment using the SMPS and TDPBMS. SMPS and TDPBMS measurements were corrected for loss of aerosol to the chamber walls by using the decay in the DOS mass spectral signal, and in Figure (B) the profiles were normalized to the maximum values.

experiment. This was clearly not the case, as the results indicate that ~70% of the SOA evaporated during this period, resulting in a decrease in the SOA yield to 0.12.

RTMS and TPTD analysis. The total ion RTMS signal (*m/z* 40–500) measured during Experiment 4 and corrected for wall loss by dividing by the *m/z* 185 signal from DOS is shown in Figure 3.3B, where it is plotted normalized to the maximum value and compared with the similarly normalized OA mass concentrations. The two profiles track each other well, as expected if the total ion signal is proportional to the OA mass concentration and the proportionality factor does not change significantly during the experiment due to changes in composition that can potentially change compound ionization behavior. Changes tend to be small for compounds with large carbon numbers and similar structures [Harrison et al. 1966; Sauter et al. 1986; Allan et al. 2003], which is the case here.

Real-time mass spectra of SOA obtained 2 min after the start of the reaction (1 min after turning off the lights) and after 60 min are shown in Figure 3.4 with the signals from DOS removed and the mass spectrum at 60 min corrected for particle loss to the walls using the DOS signal. The spectra are similar, indicating no major change in composition, although the decrease in signals over 60 min due to SOA evaporation is apparent. A TPTD profile of the total ion signal with the contribution for DOS removed) for OA collected immediately after turning off the lights is shown in Figure 3.5. Because of the proportionality between total ion signal and OA mass this profile represents a quantitative distribution of SOA volatility. The SOA desorbs between ~0–125 ^{o}C, which by comparison with the desorption temperatures of compounds with known vapor

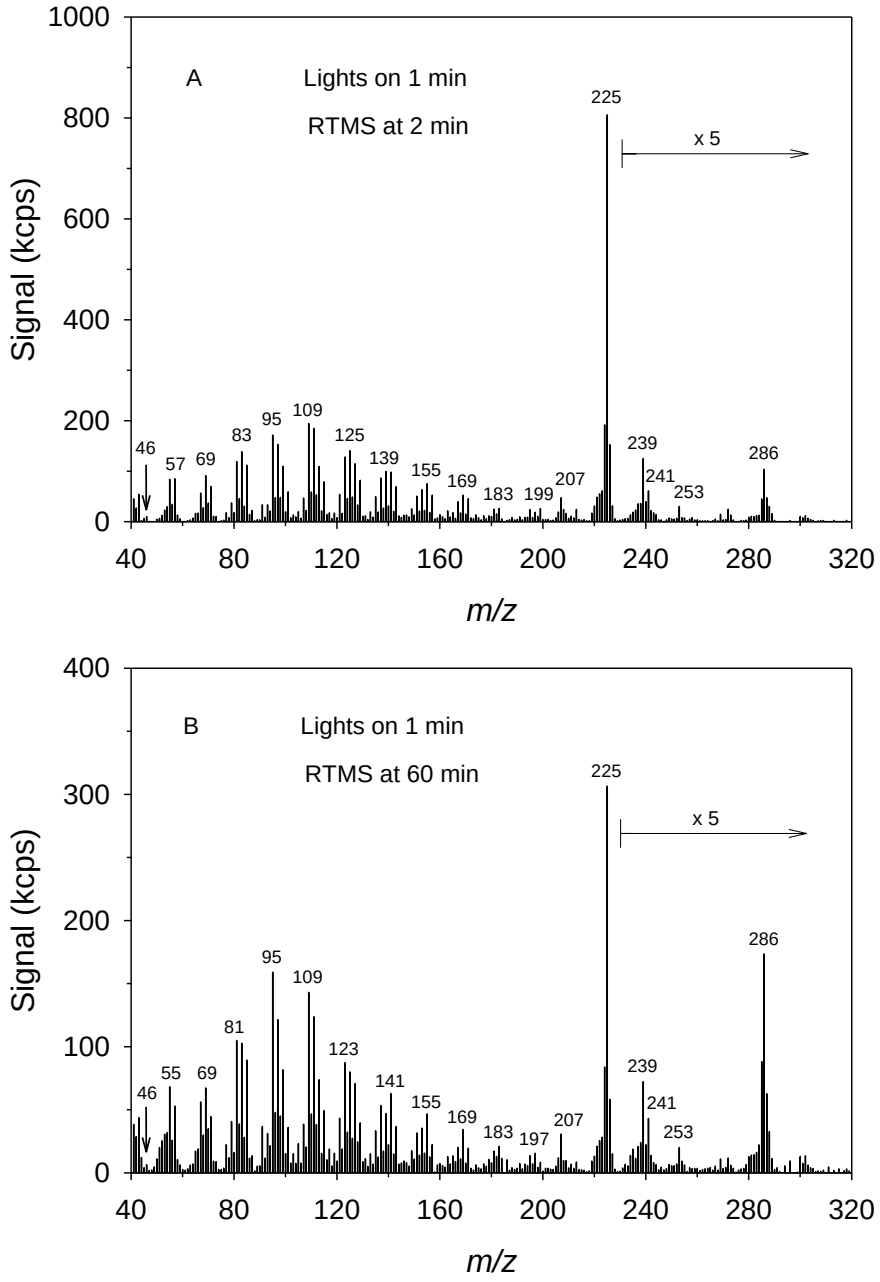

Figure 3.4. Real-time mass spectra of SOA formed during the 1 min irradiation experiment, measured (A) 2 min and (B) 60 min after turning on the lights. The signals from DOS were removed from the mass spectra and the mass spectrum at 60 min was corrected for particle loss to the walls using the decay in the DOS mass spectral signal.

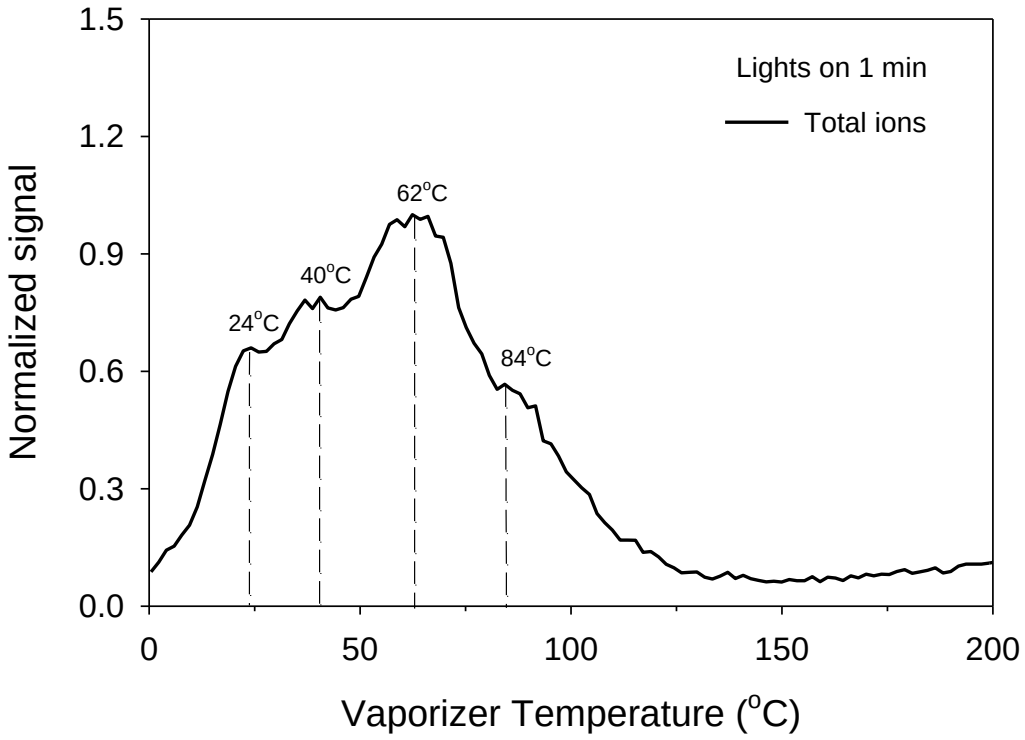

Figure 3.5. TPTD profile of the total ions for SOA formed during the 1 min irradiation experiment and collected immediately after turning off the lights. The signals from DOS were removed from the profile and the signal was normalized to the maximum value.

pressures [Lim and Ziemann 2009a] corresponds to a very large range of compound vapor pressures of ~ 10^{-1}–10^{-11} Pa. Explanations for the various distinctive, high mass peaks observed in the mass spectrum of SOA formed during 60 min of irradiation based on fragmentation of potential reaction product ions, TPTD profiles and mass spectra, and RTMS time profiles have been proposed previously [Lim and Ziemann 2009a]. Fewer products are formed in the 1 min reaction, so the SOA composition is simpler and easier to interpret.

The first two peaks in the total ion TPTD profile shown in Figure 3.5 occur at ~20–25 ^{o}C and ~35–40 ^{o}C, but are not well resolved. Nonetheless, the compounds responsible for these peaks are probably 1,4-hydroxynitrate [**2**] (M = 289) isomers. The TPTD profile of *m/z* 215, which exhibits clears peak at 21 ^{o}C and 35 ^{o}C, is shown in Figure 3.6 along with the mass spectra at these two temperatures. The mass spectra are essentially identical, except for the very small peak at *m/z* 241 in the 35 ^{o}C spectrum. The peak in the mass spectra at *m/z* 215 $(M–74)^+$ is probably due to fragmentation of 1,4-hydroxynitrate isomer ions by loss of NO_2 + CH_2=CH_2, the peak at *m/z* 225 $(M–64)^+$ by loss of NO_2 + H_2O, and the series of peaks at *m/z* 211, 197, 183… is consistent with loss of HNO_3 + an alkyl group (CH_3, C_2H_5, C_3H_7…) that depends on the particular isomer. Our group has recently verified these peak assignments through HPLC-TDPBMS analysis of the C_{15} 1,4-hydroxynitrate isomers. Based on this analysis, however, the source of the very small peak in the 35 ^{o}C mass spectrum does not appear to be 1,4-hydroxynitrate isomers. One possibility is that it is associated with dinitrates, which are second-generation products whose yield should be ~10% of the yield of 1,4-hydroxynitrates. These compounds

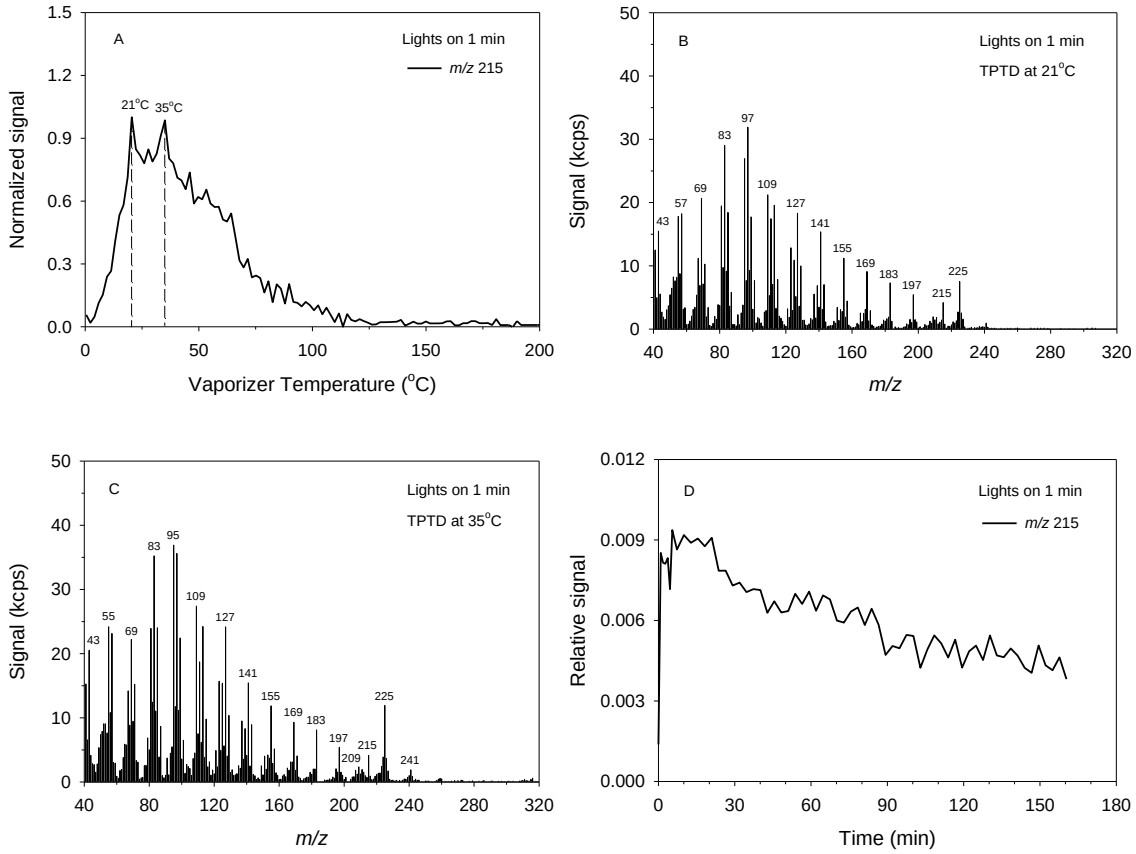

Figure 3.6. (A) TPTD profile of *m/z* 215, TPTD mass spectra at (B) 21 ^{o}C and (C) 35 ^{o}C, and (D) real-time profile of *m/z* 215 for SOA formed during the 1 min irradiation experiment and collected immediately after turning off the lights. The signals from DOS were removed from the mass spectra and profiles, the TPTD profile was normalized to the maximum signal, and the real-time *m/z* 215 signal was corrected for particle loss to the walls using the DOS signal and normalized to the signal at the end of the experiment.

should have similar vapor pressures to 1,4-hydroxynitrates [Pankow and Asher 2008] and so should desorb in this temperature range. The vapor pressures of compounds with desorption temperatures (T_{des}) between 20–40 ^{o}C can be estimated using the calibration curve, $\log P(Pa) = -0.55 - 0.079T_{des}(^{o}C)$, reported previously [Lim and Ziemann 2009a].The values are 7×10^{-3}–2×10^{-4} Pa, which is quite a large range for a series of isomers, but the position of functional groups on the carbon chain and intermolecular hydrogen bonding between functional groups can both have significant effects on vapor pressure. For comparison, the value calculated using the structure-activity relationship of Pankow and Asher (2008) is 6×10^{-5} Pa, slightly lower than minimum estimated value.

The partitioning of 1,4-hydroxynitrates between the gas and particle phases can be calculated using the theory developed by Pankow (1994), the range of vapor pressures estimated from TPTD analysis, the maximum OA mass concentration of 860 μg m^{-3}, and an assumed mean molecular weight of OA of 300 g mol^{-1} and activity coefficient of unity. The fraction of 1,4-hydroxynitrates in particles should then range from ~50%–100%, and for alkyl nitrates, whose vapor pressures are predicted to be ~170 × higher than those of 1,4-hydroxynitrates [Pankow and Asher 2008], the range would be ~0%–15%. It is thus reasonable that alkyl nitrates were not detected in the particles. A similar calculation for 1,4-hydroxynitrates at the end of the experiment, when the OA mass concentration was 200 μg m^{-3} (due to particle wall loss and evaporation of other products, as discussed below), indicates that the fraction of 1,4-hydroxynitrates in particles should then range from ~20%–90%, representing a significant loss of 1,4-hydroxynitrates from the particles. This is consistent with the time profile of *m/z* 215 (corrected for particle loss

to the walls using the DOS signal) shown in Figure 3.6D, in which the signal decreases by ~50% from the peak value over 225 min.

The third peak in the total ion TPTD profile occurs at ~55–70 ^{o}C (Figure 3.5). The mass spectrum at 61 ^{o}C and the mass spectrum extracted from the TPTD data by plotting only those *m/z* values that exhibit a peak in a narrow range of temperatures around 61 ^{o}C [Tobias and Ziemann 1999], which was possible because of the relatively smooth *m/z* profiles in the region, are shown in Figure 3.7. The mass spectra are similar, but the extracted spectrum has fewer peaks and is more representative of a single compound because of the constraint that all *m/z* exhibit a maximum. The extracted spectrum shown in Figure 7B is consistent with the cyclic hemiacetal [**4**] (M = 242), where *m/z* 225 $(M-17)^{+}$ is due to loss of OH, and the series of peaks *m/z* 195, 181, 167… is due to loss of H_2O + an alkyl group (CH_3, C_2H_5, C_3H_7…) that depends on the particular isomer. These fragmentation patterns are typical of cyclic ethers such as cyclic hemiacetals [McLafferty and Turecek 1993]. The *m/z* 225 TPTD profile is shown in Figure 3.7C, and is clearly dominated by the signal at ~60 ^{o}C, with small signal at lower temperatures due to 1,4-hydroxynitrates and also a significant shoulder between ~70–100 ^{o}C. The mass spectrum at 84 ^{o}C is shown in Figure 3.7D. This spectrum is very similar to that of the cyclic hemiacetal (Figure 3.7B), but with a few additional peaks due to other products. One possible explanation for this is that the spectrum is associated with a dimer formed by dehydration of a pair of cyclic hemiacetals (ROH) according to the reaction

$$2ROH \rightarrow ROR + H_2O$$

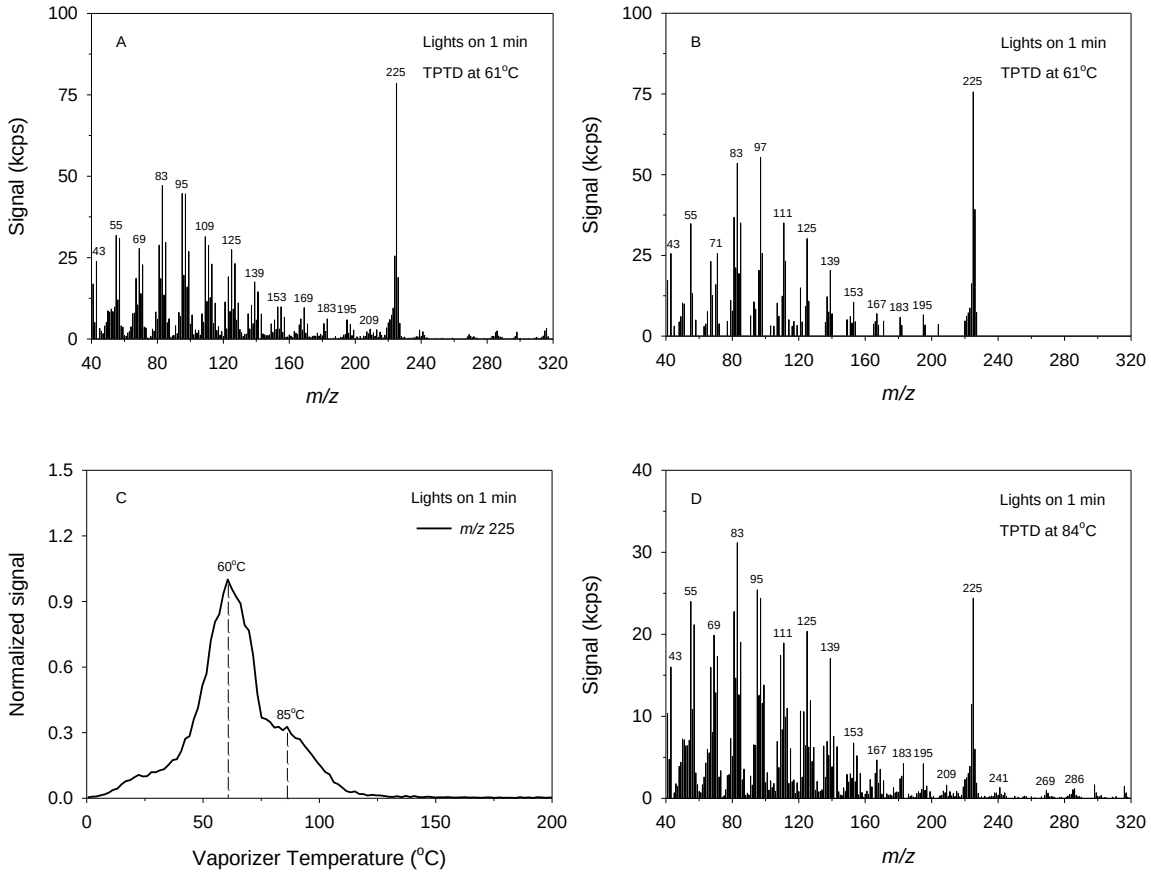

Figure 3.7. (A) TPTD mass spectrum at (A) 61 ^{o}C, (B) mass spectrum extracted from the TPTD data by plotting only those *m/z* values that exhibit a peak in a narrow range of temperatures around 61 ^{o}C, (C) TPTD profile of *m/z* 225, and (D) TPTD mass spectrum at 84 ^{o}C for SOA formed during the 1 min irradiation experiment and collected immediately after turning off the lights. The signals from DOS were removed from the mass spectra mass spectra and profile and the TPTD profile was normalized to the maximum signal.

Although the mass of this compound would be approximately twice that of a cyclic hemiacetal, thus leading to a much lower vapor pressure, loss of a hydrogen-bonding hydroxyl group will compensate for this to some extent. The mass spectrum of the dimer should be very similar to that of the cyclic hemiacetal since α-cleavage following ionization of the O atoms in either ring will generate the same ions. This reaction is similar to the acid-catalyzed reversion reaction that occurs with sugars such as glucose and fructose [van Dam et al. 1986].

Because the cyclic hemiacetals and dimers desorb above ~50 ^{o}C their vapor pressures should be less than ~3×10^{-5} Pa, and they should be present >99% in the particle phase. The time profile of *m/z* 225 (corrected for particle loss to the walls by using the DOS signal) that is shown in Figure 3.8A, however, indicates significant loss from the particles during the experiment. This loss is best explained as being due to dehydration of cyclic hemiacetals to dihydrofurans, which then evaporate because of their much higher vapor pressures (Figure 3.2). The first order rate constant for dehydration, k_d, can be obtained by fitting the *m/z* 225 time profile to an exponential curve as shown in Figure 3.8B. The result is $k_d = 0.021$ min^{-1}, which is equivalent to a timescale of ~45 min. This value of k_d is ~ 3× smaller than the value measured previously by using a more complex model to fit the time profiles of cyclic hemiacetals with a range of carbon numbers during 60 min irradiations [Lim and Ziemann 2009b]. The value determined here might be smaller because less HNO_3, which catalyzes the cyclization and dehydration reactions, is formed in 1 min than in 60 min of irradiation.

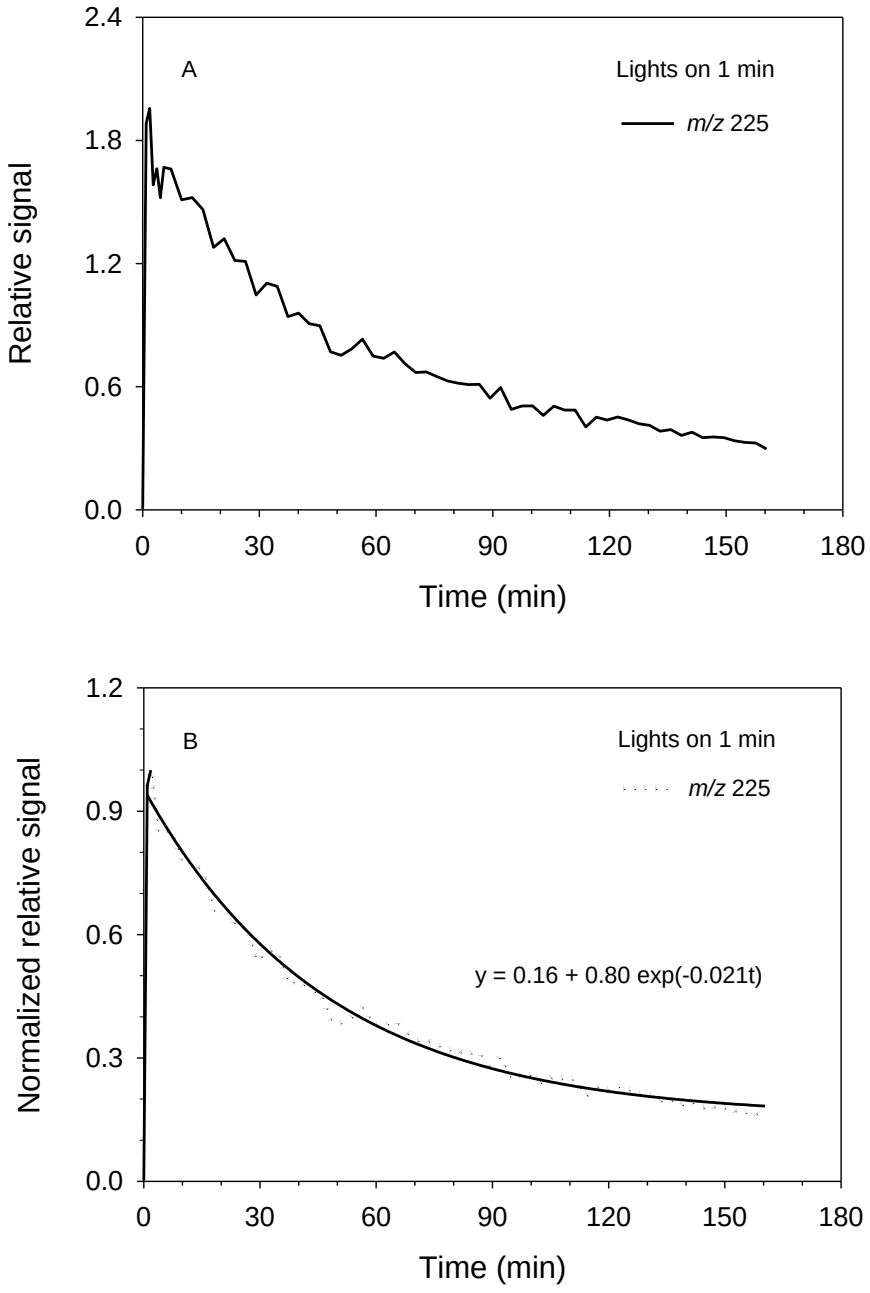

Figure 3.8. (A) Real-time profile of *m/z* 225 for SOA formed during the 1 min irradiation experiment and (B) a fit of an exponential curve to the profile to determine the rate constant for dehydration of the cyclic hemiacetal. The *m/z* 225 signal was corrected for particle loss to the walls using the decay in the DOS mass spectral signal and the signal was normalized to the maximum value.

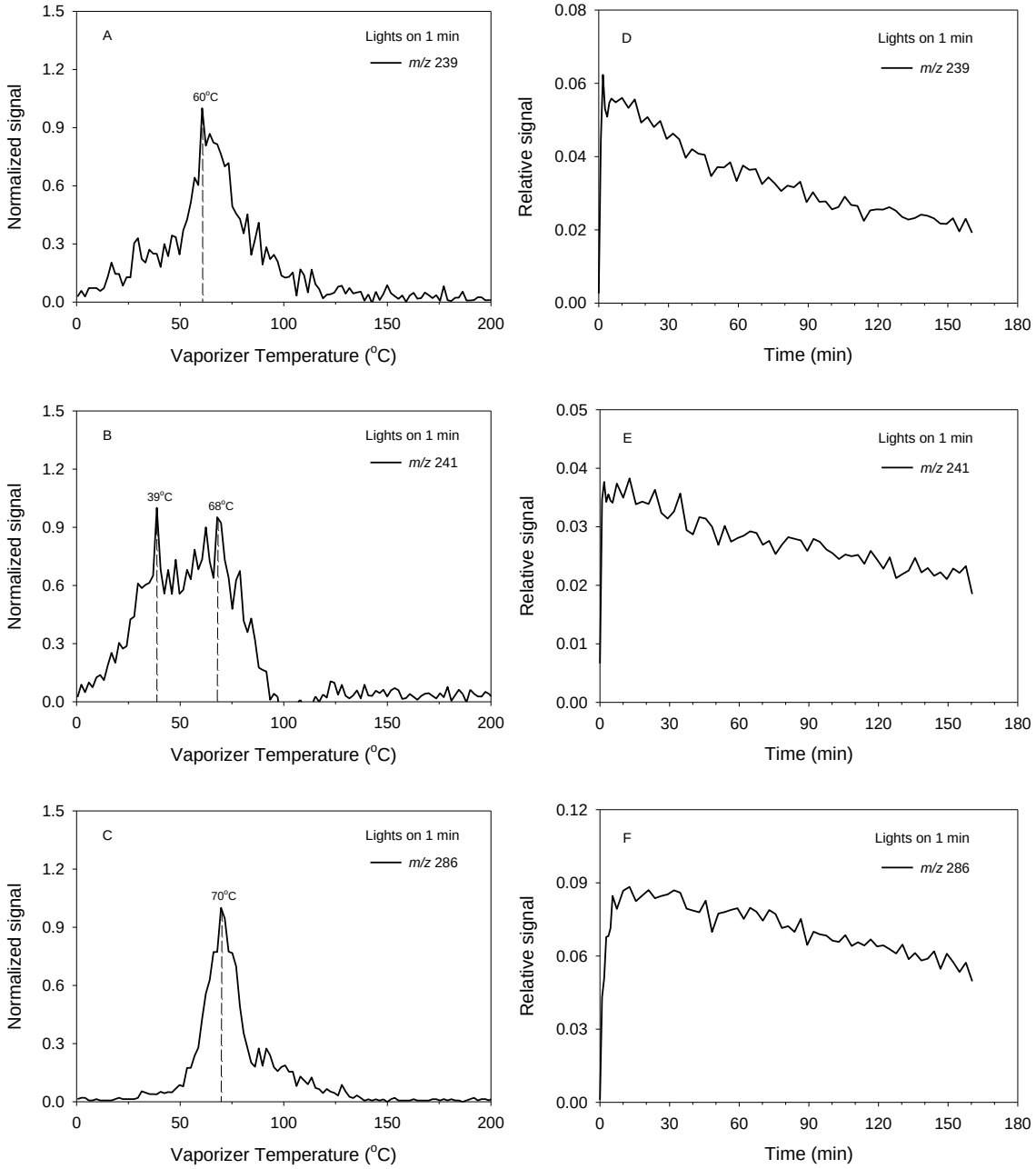

Figure 3.9. TPTD profiles for (A) *m/z* 239, (B) *m/z* 241, and (C) *m/z* 286, and real-time profiles for (D) *m/z* 239, (E) *m/z* 241, and (F) *m/z* 286 for SOA formed during the 1 min irradiation experiment. The signals from DOS were removed from the profiles and the signals were normalized to the maximum values.

Other characteristic ions appear in the SOA mass spectrum at *m/z* 239, 241, and 286. The TPTD and time profiles for these are shown in Figure 3.9. The TPTD profiles for these ions all have peaks in the range ~60–70 ^{o}C, and so appear to associated with products that are slightly less volatile than cyclic hemiacetals, which are responsible for the peak in the *m/z* 225 profile at ~60 ^{o}C. As was the case for cyclic hemiacetals, in spite of the low vapor pressures of these compounds (as indicated by their high desorption temperatures), the time profiles for all these ions (corrected for particle loss to the walls by using the DOS signal) indicate that significant evaporation occurs during the course of the experiment. These observations indicate that a significant fraction of the signal from these ions is associated with compounds that are similar in structure to cyclic hemiacetals and so can dehydrate, but have additional functional groups that are responsible for the slightly higher desorption temperatures. This is consistent with the following assignments: *m/z* 239 $(M–64)^+$ due to loss of H_2O and NO_2 from cyclic β-hydroxynitrates [**6**] (M = 303), *m/z* 241 $(M–62)^+$ due to loss of NO_3 from cyclic β-hydroxynitrates [**7**] (M = 303), and *m/z* 286 $(M–17)^+$ due to loss of OH from cyclic β-hydroxynitrates [**6**] (M = 303) and from a cyclic hemiacetal formed from a secondary reaction of OH radicals with an alkyl nitrate (M = 303). Differences in the rates of dehydration of the latter two compounds could explain the slight differences in the *m/z* 239 and *m/z* 286 TPTD and time profiles.

Functional group analysis. The results of the functional group analysis of the SOA are shown in Table 3.2. The only functional groups detected were carbonyl, hydroxyl,

Table 3.2 Functional group composition of SOA products formed from the reaction of *n*-pentadecane with OH radicals in the presence of NO_x for 1 min light exposure.

Functional group	Functional group/C_{15} molecule				
	exp. 1	exp. 2	exp. 3	exp. 4	average ± SD
nitrate [$CHONO_2$]	0.81	0.80	0.81	0.91	0.83 ± 0.04
hydroxyl [CH_2OH]	0.90	1.13	0.91	1.18	1.03 ± 0.13
carbonyl [C(O)]	0.26	0.26	0.29	0.22	0.26 ± 0.02
ester [C(O)O]-R	<LOD	<LOD	<LOD	<LOD	
carboxyl [C(O)OH]	<LOD	<LOD	<LOD	<LOD	
peroxide [CHOOH]	<LOD	<LOD	<LOD	<LOD	
methylene [CH_2]	13.03	12.81	12.99	12.69	12.88 ± 0.14
total – methylene [15 – CH_2]	1.97	2.19	2.01	2.31	2.12 ± 0.14
Elemental composition[1]					
O/C	0.25 (0.32)				
H/C	1.91 (2.20)				
N/C	0.056 (0.062)				

[1]The values were calculated from functional group composition analysis and the values in parentheses were calculated from elemental analysis.

and nitrate, consistent with expectations based on the reaction mechanism (Figure 3.1) and previous measurements of gas-phase products (Reisen et al. 2005). Concentrations of ester, carboxyl, and peroxide groups were below detection limits. Alkyl hydroperoxides peroxides are not expected to form in the presence of NO_x (Atkinson and Arey 2003) and carboxylic acids would be possible second- and third-generation products formed via very minor decomposition pathways (Tuazon et al. 1998; Aschmann et al. 2010) and thus present in low concentrations and almost entirely in the gas phase. As shown in Figure 3.2, carbonylesters can be formed via the heterogeneous/multiphase cyclization of 1,4-hydroxycarbonyls to cyclic hemiacetals followed by dehydration to dihydrofurans that then evaporate and react with OH radicals. All this must occur within the 1 min of light exposure. Nonetheless, the *m/z* 239, 241, and 286 peaks observed in the SOA mass spectrum (Figure 3.4), which are associated with cyclic hydroxynitrates that are carbonylester co-products (Figure 3.2) indicate that some carbonylesters are formed. On the basis of a gas-particle partitioning calculation similar to those described above using an estimated carbonylester vapor pressure of 5×10^{-3} Pa [Pankow and Asher 2008] and average OA mass concentration of 300 μg m^{-3} during the filter sampling period, ~30% of the carbonylester is expected to be present in the collected particles. Considering, however, that no alkyl nitrate was detected in the particles by TPTD analysis, and that alkyl nitrates have a much higher yield and similar vapor pressure to carbonylesters, it is probably reasonable that ester groups were not detected. It should also be noted that under the conditions used in the carbonyl group analysis cyclic hemiacetals and cyclic hemiacetal dimers with be hydrolyzed to 1,4-hydroxycarbonyls and thus the original

carbonyl groups will be detected, whereas this is not the case under the conditions used in the hydroxyl group analysis. Although cyclic hemiacetals will be analyzed as 1,4-hydroxycarbonyls since both have a single hydroxyl group, cyclic hemiacetal dimers will not be detected.

The average number of nitrate, hydroxyl, carbonyl, and methylene groups per C_{15} molecule in the SOA were 0.83 ± 0.04, 1.03 ± 0.13, 0.26 ± 0.02, and 12.88 ± 0.14. This corresponds to an average of 2.12 non-methylene groups per C_{15} molecule. The O/C, N/C, and H/C ratios calculated from these values are 0.25, 0.056, and 1.91, in good agreement with values of 0.32, 0.062, and 2.20 measured by elemental analysis. If all the alkyl nitrates, 1,4-hydroxynitrates, and 1,4-hydroxycarbonyls formed in the reaction with yields of 0.3, 0.1, and 0.6 and then condensed to form SOA, the functional group composition should instead be 0.4, 0.7, 0.6, and 13.3. Comparing these values it is apparent that the SOA is enriched with respect to nitrate, hydroxyl, and methylene groups and depleted with respect to carbonyl groups, presumably because of differences in gas-particle partitioning. As shown in Figure 3.3A, the maximum SOA yield is only 0.42 in the first few minutes of the reaction and then decreases to 0.12 over 225 min due to evaporation of products. As noted in the discussion above, mass spectra indicate loss of cyclic hemiacetals and cyclic hydroxynitrates from the particles due to dehydration and evaporation, whereas evaporation of 1,4-hydroxynitrates is possibly due to re-partitioning in response to the reduction of SOA mass from loss of other compounds and/or because of loss of gases to the chamber walls [Matsunaga and Ziemann 2010].

60 minute irradiation. In the experiments described here the lights were turned on for 60 min at 50% light intensity (corresponding to a NO_2 photolysis rate constant of 0.37 min^{-1}) and then turned off. Results for the three experiments conducted were similar, so representative results from one experiment are discussed.

SMPS analysis. The OA mass concentrations measured over the course of Experiment 6 are shown in Figure 3.10. The concentrations have been corrected for loss of aerosol to the chamber walls by using the decay in the DOS signal. The initial mass concentration was 230 μg m^{-3} from DOS seed particles, and in 60 min of irradiation 5740 μg m^{-3} of SOA was formed. The concentration of *n*-pentadecane reacted in this 60 min period was 7010 μg m^{-3} (0.871 ppmv), corresponding to an SOA yield of 0.75. Unlike the 1 min irradiation experiments, there was no significant decrease in the SOA mass concentration after the lights were turned off.

RTMS and TPTD analysis. The total ion RTMS signal (*m/z* 40–500) measured during Experiment 6 and corrected for wall loss using the decay in the DOS signal is shown in Figure 3.10B, where it is plotted normalized to the maximum value and compared with the similarly normalized OA mass concentrations. The two profiles track each other well, as expected if the total ion signal is proportional to the OA mass concentration [Harrison et al. 1966; Sauter et al. 1986; Allan et al. 2003].

The real-time mass spectrum of SOA obtained 30 min after the start of the reaction is shown in Figure 3.11 with the signals from DOS removed and the mass spectrum corrected for particle loss to the walls using the DOS signal. The spectrum is similar to those from the reaction with 1 min of irradiation (Figure 3.4), except that the relative

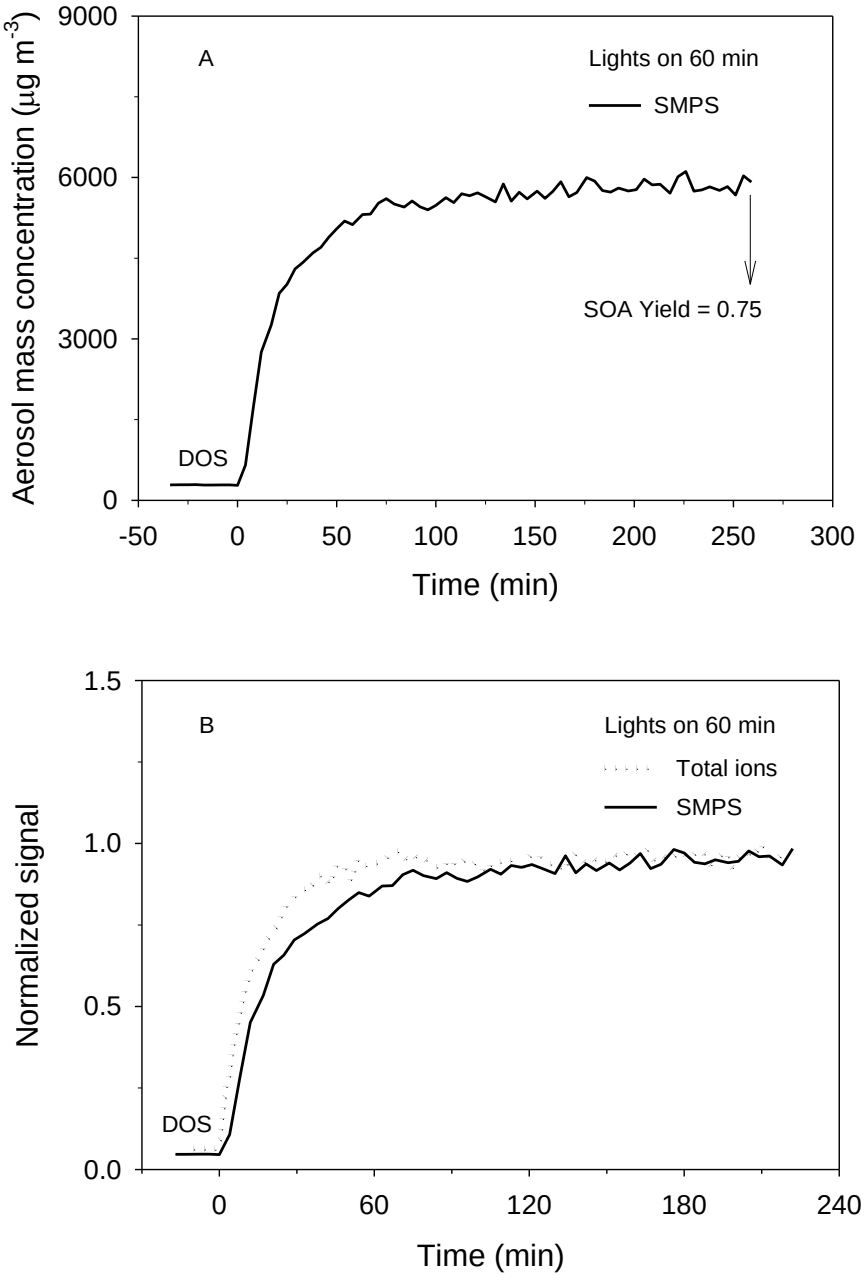

Figure 3.10. (A) Aerosol mass concentrations and SOA yields measured during the 60 min irradiation experiment using the SMPS, and (B) aerosol mass concentrations and total ion signals measured during the 60 min irradiation experiment using the SMPS and TDPBMS. SMPS and TDPBMS measurements were corrected for loss of aerosol to the chamber walls by using the decay in the DOS mass spectral signal, and in Figure (B) the profiles were normalized to the maximum values.

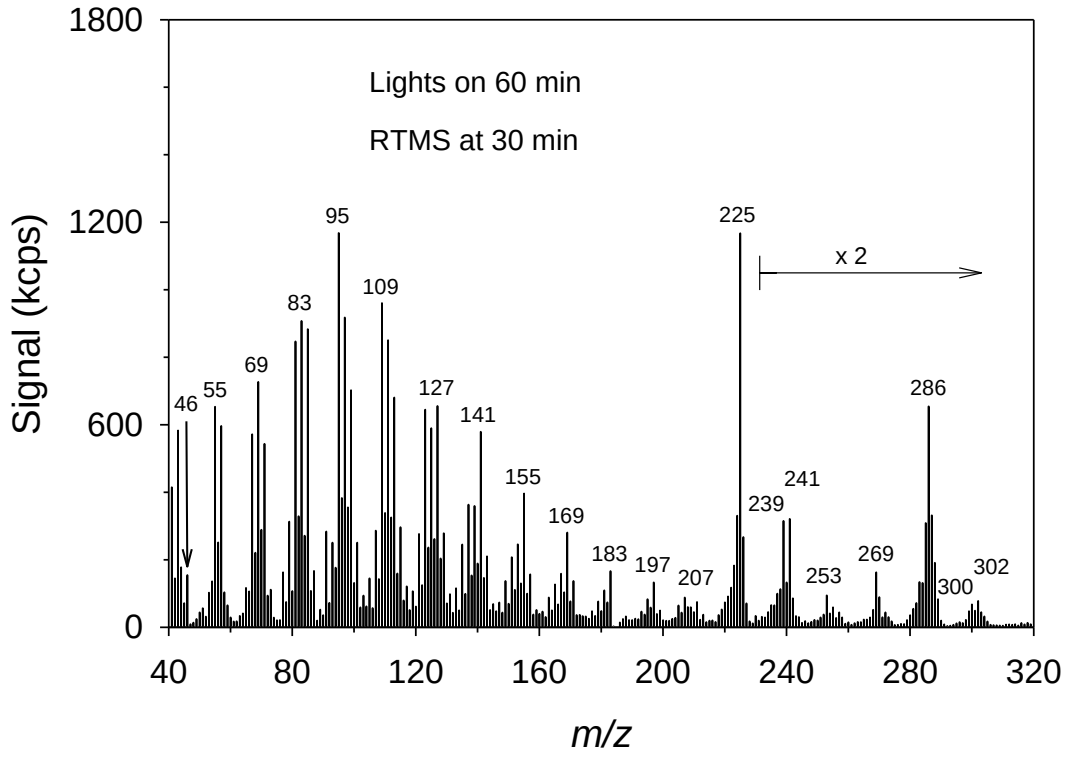

Figure 3.11. Real-time mass spectra of SOA formed during the 60 min irradiation experiment, measured 30 min after turning on the lights. The signals from DOS were removed from the mass spectrum and the mass spectrum was corrected for particle loss to the walls using the decay in the DOS mass spectral signal.

intensities of peaks with *m/z* > 225 such as *m/z* 239, 241, 253, 269, 286, 300, and 302 (there is also a peak at *m/z* 347 that is not shown), compared to those with *m/z* ≤ 225, are larger in the reaction with 60 min of irradiation. This is reasonable, considering that the peaks with *m/z* > 225 are associated with second- and higher-generation products that will increase in concentration relative to first-generation products at higher OH radical exposures. The products likely associated with *m/z* 215, 225, 239, 241, and 286 have been discussed above and probably correspond primarily to 1,4-hydroxynitrates [**2**] (*m/z* 215), cyclic hemiacetals [**4**] (*m/z* 225), and cyclic hydroxynitrates [**6**,**7**] (*m/z* 239, 241, and 286). The peaks at *m/z* 269, 300, 302, and 347 are likely due to reactions of OH radicals with alkyl nitrates, which are first-generation products formed in high yield that are almost entirely in the gas phase, to form 1,4-hydroxydinitrates and cyclic hydroxynitrates with an additional nitrate group. Loss of $HNO_3 + H_2O$ from the acyclic hydroxydinitrates (M = 350) will lead to a peak at *m/z* 269 $(M–81)^+$, whereas fragmentation of the cyclic hydroxydinitrates by the same pathways described above for the cyclic hydroxynitrates (M =364) involving loss of $NO_2 + H_2O$, NO_3, and OH, will lead to peaks at *m/z* 300, 302, and 347, since adding a nitrate group simply shifts the peaks at *m/z* 239, 241, and 286 by 61 mass units. We have already suggested above that reactions of alkyl nitrates that lead to the formation of cyclic hemiacetals with an additional nitrate group and dinitrates may contribute slightly to peaks at *m/z* 241 and 286 in the SOA formed from 1 min of irradiation.

TPTD profiles of the total ions and *m/z* 215, 225, 239, 241, and 286 are shown in Figure 3.12 for comparison with those shown in Figures 3.5–3.7 and 3.9 for the reaction

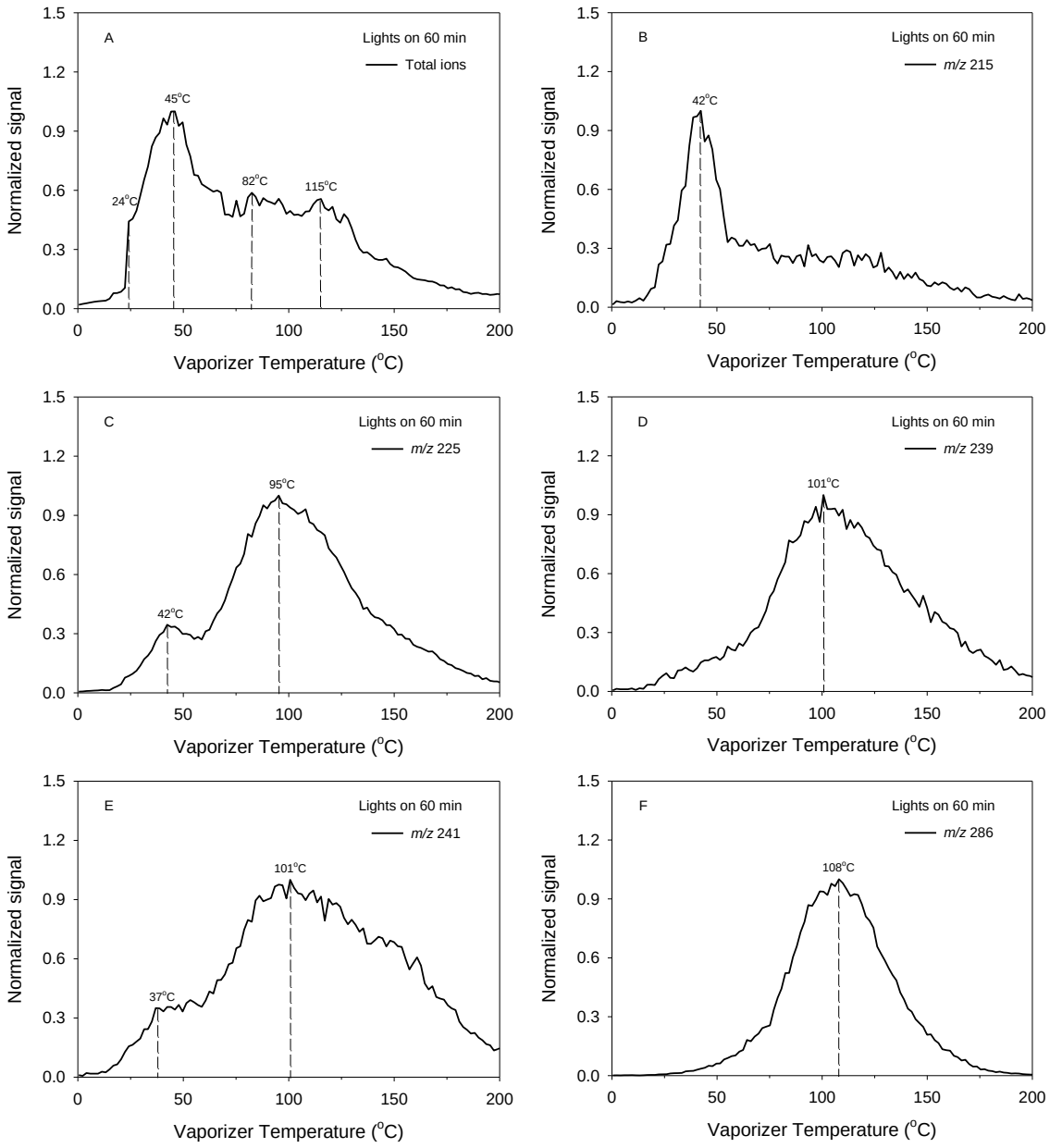

Figure 3.12. TPTD profiles of (A) the total ions, (B) *m/z* 215, (C) *m/z* 225, and (D) *m/z* 239, (E) *m/z* 241, and (F) *m/z* 286 for SOA formed during the 60 min irradiation experiment and collected at the end of the experiment. The signals from DOS were removed from the profile and the signal was normalized to the maximum value.

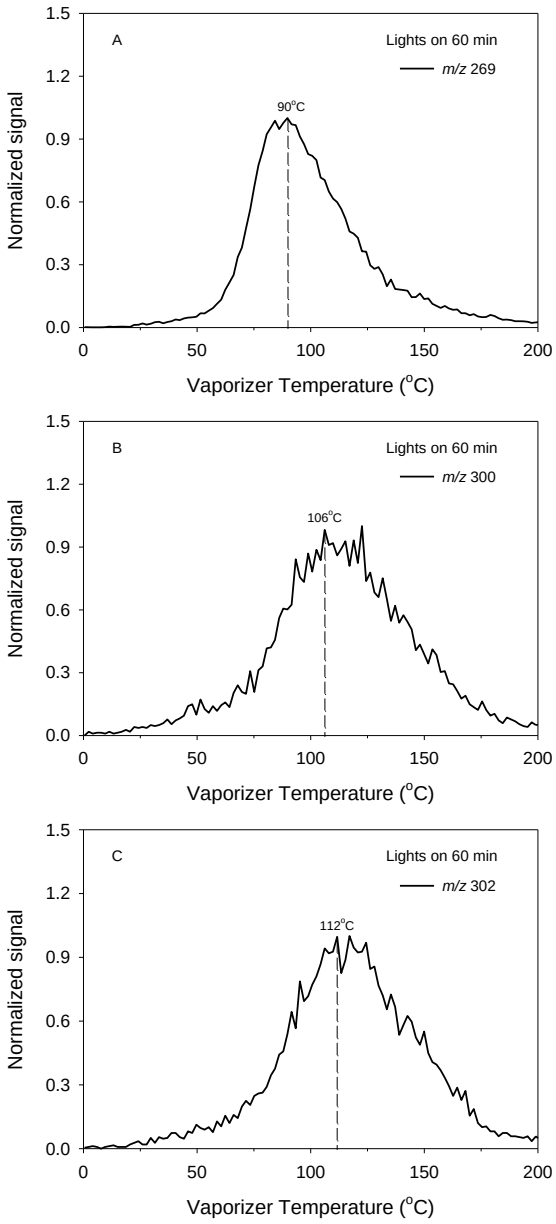

Figure 3.13. TPTD profiles of (A) *m/z* 269, (B) *m/z* 300, and (C) *m/z* 302 for SOA formed during the 60 min irradiation experiment and collected at the end of the experiment. The signals from DOS were removed from the profile and the signal was normalized to the maximum value.

with 1 min of irradiation. Assuming our assignment of products is correct, the changes in the profiles, which in general shift to higher desorption temperatures, indicate a relative increase in 1,4-hydroxynitrates, dinitrates, cyclic hemiacetal dimers, and cyclic hydroxynitrate dimers (similar in structure to cyclic hemiacetal dimers) or possibly associated with carbonylesters in the form of hemiacetals. The profiles of *m/z* 269, 300, and 302 are shown in Figure 3.13, and indicate similarly low volatility compounds that probably exist either as dimers or as hemiacetals formed according to the reaction

$$ROH + R'CHO \rightarrow ROCH(OH)R'$$

The time profiles for all these ions are similar to the total ion profile (Figure 3.10), although some decay slightly with time as observed previously (Lim and Ziemann 2009a).

Functional group analysis. The results of the functional group analysis of the SOA are shown in Table 3.3, with experiments 5 and 6 being conducted in dry air (< 0.1% RH) and experiment 7 being conducted in humid air (75% RH). The functional groups detected were carbonyl, hydroxyl, and nitrate, as in the reaction with 1 min of irradiation, but also ester, carboxyl, and peroxide groups. The average number of nitrate, hydroxyl, carbonyl, and methylene groups per C_{15} molecule in the SOA formed in dry air were 1.25 ± 0.16, 0.69 ± 0.12, 0.32 ± 0.03, and 12.27 ± 0.21. Comparing these values with the corresponding values of 0.83, 1.03, 0.26, and 12.88 in the reaction with 1 min of irradiation indicates an increase in nitrate and carbonyl groups and decrease in hydroxyl

Table 3.3. Functional group composition of SOA products formed from the reaction of *n*-pentadecane with OH radicals in the presence of NO_x for 60 min light exposure.

Functional group	Functional group/C_{15} molecule			
	exp. 5	exp. 6	average ± SD	exp. 7
nitrate [$CHONO_2$]	1.13	1.36	1.25 ± 0.16	1.18
hydroxyl [CH_2OH]	0.77	0.60	0.69 ± 0.12	0.72
carbonyl [C(O)]	0.29	0.34	0.32 ± 0.03	0.28
ester [C(O)O]-R	0.34	0.33	0.33 ± 0.01	0.18
carboxyl [C(O)OH]	0.08	0.13	0.11 ± 0.04	0.07
peroxide [CHOOH]	NA	0.09	0.09 ± 0.00	0.04
methylene [CH_2]	12.38	12.15	12.27 ± 0.21	12.53
total – methylene [15 – CH_2]	2.62	2.85	2.74 ± 0.21	2.47
Elemental composition[1]				
O/C	0.38 (0.31)			
H/C	1.82 (1.86)			
N/C	0.083 (0.061)			

[1]The values were calculated from functional group composition analysis and the values in parentheses were calculated from elemental analysis.

groups. The average number of ester, carboxyl, and peroxide groups per C_{15} molecule in the SOA formed in dry air were 0.33 ± 0.01, 0.11 ± 0.04, and 0.09 (only one analysis), whereas these functional groups were all below the detection limits in the reactions conducted with 1 min of irradiation. The average number of non-methylene groups increased from 2.12 to 2.74. The O/C, N/C, and H/C ratios calculated from these values are 0.38, 0.083, and 1.82, in good agreement with values of 0.31, 0.061, and 1.86 measured by elemental analysis.

The increase in the average number of nitrate groups is consistent with the enhanced formation of higher-generation products via OH reactions with alkyl nitrates, as is also indicated by the mass spectra. The appearance of ester groups is also expected, since carbonyl esters are second-generation products formed as shown in Figure 3.2. As noted above, these compounds are probably too volatile to partition significantly into particles, so the ester groups detected in the SOA are probably associated with third-generation products formed from reactions of carbonylesters with OH groups. A major product of that reaction should be acyl peroxynitrates formed as shown in Figure 2. The aldehyde group on carbonylesters is the preferred site for H-atom abstraction by OH radicals, with structure-activity calculations [Kwok and Atkinson 1995] indicating that ~40% of the reaction occurs at that site. Concentrations of NO_2 should be sufficiently high to compete with NO in the reaction with acyl peroxy radicals, thus forming acyl peroxynitrates. The formation of acyl peroxynitrates also explains the detection of carboxyl and peroxide groups in the SOA, which as discussed above is unlikely for the reactions conducted with 1 min of irradiation. The peroxide group in an acyl

peroxynitrate should be detected the same as any other organic peroxide, since the method employed is completely general for all peroxide compounds [Banerjee and Budke 1964; Docherty et al. 2005]. It is also well established that the method employed for carboxyl group analysis detects acyl (RC(O)OOR) and diacyl RC(O)OO(O)CR hydroperoxides the same as monocarboxylic and dicarboxylic acids, respectively [Chapter 2 and references therein], so acyl peroxynitrates are likely to be detected as if they were monocarboxylic acids. This explanation is also consistent with the approximately equal measured amounts of carboxyl and peroxide groups, and with the results of the functional group analysis of SOA formed at 75% RH. The average number of nitrate, hydroxyl, carbonyl, and methylene groups per C_{15} molecule in the SOA formed at high humidity were 1.18, 0.72, and 0.28, similar to the values of 1.25, 0.69, and 0.32 for SOA formed in dry air, whereas values for ester, carboxyl, and peroxide groups decreased from 0.33, 0.11, and 0.09 in dry air to 0.18, 0.07, and 0.04 in humid air. This decrease is likely due to the reduced rate of dehydration of cyclic hemiacetals to dihydrofurans at higher humidity because of the lower concentration of acid catalyst, and to a shift in the reaction equilibrium from dihydrofurans to cyclic hemiacetals (Figure 3.2), both of which reduce carbonylester yields and acyl peroxynitrate yields. If for example, one assumes that the SOA is composed of acyl peroxynitrate esters, carbonylesters, cyclic hemiacetals, hydroxynitrates, and dinitrates, then from the functional group analysis of SOA formed in dry air the mole fractions of each would be 0.1, 0.23, 0.09, 0.59, and 0.33.

3.4 Conclusions

In this chapter the functional group analysis methods described in Chapter 2 were used to investigate the chemical composition of secondary organic aerosol formed from the OH radical-initiated reaction of *n*-pentadecane in the presence of NO_x for 1 min and 60 min of irradiation. Results of functional group analysis indicate the presence of carbonyl, hydroxyl, and nitrate groups in SOA formed from 1 min of irradiation, consistent with expectations based on the well-established reaction mechanism and product vapor pressures, with the major SOA products appearing to be first-generation 1,4-hydroxynitrates, cyclic hemiacetals, and their dimers, and second-generation cyclic hydroxynitrates. SOA formed from 60 min of irradiation contained carbonyl, hydroxyl, and nitrate groups as well as ester and peroxide groups associated with second- and third-generation carbonylesters and acyl peroxynitrate esters, and possibly hemiacetals. The cyclic hydroxynitrates, carbonylesters, and acyl peroxynitrate esters were formed via heterogeneous/multiphase cyclization and dehydration of 1,4-hydroxycarbonyls to form dihydrofurans, followed by further OH radical reactions. Based on the reaction mechanism, if one assumes that the SOA formed in the 60 min irradiation experiment in dry air is composed of acyl peroxynitrate esters, carbonylesters, cyclic hemiacetals, hydroxynitrates, and dinitrates, then from the functional group analysis the mole fractions of each would be 0.1, 0.23, 0.09, 0.59, and 0.33. The effects of increased exposure to OH radicals on functional group composition, real-time mass spectra, and thermal desorption profiles is consistent with an expected increase in the oxidation of reaction products and enhanced heterogeneous/multiphase reactions, and the effects of relative humidity on the

functional group composition is also consistent with the reaction mechanism. The results of functional group analysis were also in good agreement with the results of elemental CHON analysis. The results demonstrate the value of these functional group analysis methods for SOA studies and lend additional support for the currently accepted mechanism of SOA formation from reactions of alkanes with OH radicals in the presence of NO_x, including the role of heterogeneous/multiphase reactions.

3.5 References

Allan, J. D., Jimenez, J. L., Williams, P. I., Alfarra, M. R., Bower, K. N., Jayne, J. T., Coe, H., and Worsnop, D. R. Quantitative Sampling Using an Aerodyne Aerosol Mass Spectrometer 1. Techniques of Data Interpretation and Error Analysis. *J. Geophys. Res.*, 108(D3), 4090, DOI: 10.1029/2002JD002358 (2003).

Andreae, M. O., and Rosenfeld, D. Aerosol-Cloud-Precipitation Interactions. Part 1. The Nature and Sources of Cloud-Active Aerosols. *Earth-Sci. Rev.*, 89, 13-41 (2008).

Arey, J., Aschmann, S. M., Kwok, E. S. C., and Atkinson, R. Alkyl Nitrate, Hydroxyalkyl Nitrate, and Hydroxycarbonyl Formation from the NO_x-Air Photooxidations of C_5-C_8 *n*-alkanes. *J. Phys. Chem. A*, 105, 1020-1027 (2001).

Aschmann, S. M., Tuazon, E. C., Arey, J., and Atkinson, R. Products and Mechanisms of the Gas Phase Reactions of OH Radicals with 1-Octene and 7-Tetradecene in the Presence of NO. *Environ. Sci. Technol.*, 44, 3825-3831 (2010).

Atkinson, R., Carter, W. P. L., Winer, A. M., and Pitts, J. N., Jr. An Experimental Protocol for the Determination of OH Radical Rate Constants with Organics Using Methyl Nitrite Photolysis as an OH Radical Source. *J. Air Pollut. Control Assoc*., 31, 1090-1092 (1981).

Atkinson, R., and Arey, J. Atmospheric Degradation of Volatile Organic Compounds. *Chem. Rev*., 103, 4605-4638 (2003).

Atkinson, R., Arey, J., and Aschmann, S. M. Atmospheric Chemistry of Alkanes: Review and Recent Developments. *Atmos. Environ.*, 42, 5859-5871 (2008).

Banerjee, D. K., and Budke, C. C. Spectrophotometric Determination of Traces of Peroxides in Organic Solvents. *Anal. Chem.*, 36, 792-796 (1964).

Calvert, J. G., Atkinson, R., Kerr, J. A., Madronich, S., Moortgat, G. K., Wallington, T. J., and Yarwood, G. *The Mechanisms of Atmospheric Oxidation of the Alkenes,* Oxford University Press, New York. (2000).

Chattopadhyay, S., and Ziemann, P. J. Vapor Pressures of Unsubstituted and Substituted Monocarboxylic and Dicarboxylic Acids Measured Using an Improved Thermal Desorption Particle Beam Mass Spectrometry Method. *Aerosol Sci. Technol.*, 39, 1085-1100 (2005).

Davidson, C. I., Phalen, R. F., and Solomon, P. A. Airborne Particulate Matter and Human Health: A Review. *Aerosol. Sci. Technol.*, 39, 737-749 (2005).

de Gouw, J., and Jimenez, J. L. Organic Aerosols in the Earth's Atmosphere. *Environ. Sci. Technol*., 43, 7614-7618 (2009).

Docherty, K. S., Wu, W., Lim, Y. B., and Ziemann, P. J. Contributions of Organic Peroxides to Secondary Aerosol formed from Reactions of Monoterpenes with O_3. *Environ. Sci. Technol.*, 39, 4049-4059 (2005).

Guenther, A., Hewitt, C. N., Erickson, D., Fall, R., Geron, C., Graedel, T., Harley, P., Klinger, L., Lerdau, M., McKay, W. A., Pierce, T., Scholes, B., Steinbrecher R., Tallamraju, R., Taylor, J., and Zimmerman, P. A Global Model of Natural Volatile Organic Compound Emissions. *J. Geophys. Res.*, 100, 8873-8892 (1995).

Harrison, A. G., Jones, E. G., Gupta, S. K., and Nagy, G. P. Total Cross Sections for Ionization by Electron Impact. *Can. J. Chem*., 44, 1967-1973 (1966).

Haywood, J., and Boucher, O. Estimates of the Direct and Indirect Radiative Forcing due to Tropospheric Aerosols: A Review. *Rev. Geophys*., 38, 513-543 (2000).

Kroll, J. H., and Seinfeld, J. H. Chemistry of Secondary Organic Aerosol: Formation and Evolution of Low-Volatility Organics in the Atmosphere. *Atmos. Environ*. 42, 3593-3624 (2008).

Kwok, E. S. C., and Atkinson, R. Estimation of Hydroxyl Radical Reaction Rate Constants for Gas Phase Organic Compounds Using a Structure-Reactivity Relationship: An Update. *Atmos Environ*. 29, 1685-1695 (1995).

Lim, Y. B., and Ziemann, P. J. Chemistry of Secondary Organic Aerosol Formation from OH Radical-Initiated Reactions of Linear, Branched, and Cyclic Alkanes in the Presence of NO_x. *Aerosol Sci. Technol*., 43, 604-619 (2009a).

Lim, Y. B., and Ziemann, P. J. Kinetics of the Heterogeneous Conversion of 1,4-Hydroxycarbonyls to Cyclic Hemiacetals and Dihydrofurans on Organic Aerosol Particles. *Phys. Chem. Chem. Phys*., 11, 8029-8039 (2009b).

Lim, Y. B., and Ziemann, P. J. Effects of Molecular Structure on Aerosol Yields from OH Radical-Initiated Reactions of Linear, Branched, and Cyclic Alkanes in the Presence of NO. *Environ. Sci. Technol.*, 43, 2328-2334 (2009c).

Lohmann, U., and Feichter, J. Global Indirect Aerosol Effects: a Review. *Atmos. Chem. Phys*. 5, 715-737 (2005).

Martin, P., Tuazon, E. C., Aschmann, S. M., Arey, J., and Atkinson, R. Formation and Atmospheric Reactions of 4,5-Dihydro-2-Methylfuran. *J. Phys. Chem. A*, 106, 11492-11501 (2002).

McLafferty F. W., and Turecek, F. *Interpretation of Mass Spectra*, Fourth Edition, University Science Books, Sausalito, CA. (1993).

Matsunaga, A., and Ziemann, P. J. Yields of β-Hydroxynitrates and Dihydroxynitrates in Aerosol formed from the OH Radical-Initiated Reactions of Linear Alkenes in the Presence of NO_x. *J. Phys. Chem. A*, 113, 599-606 (2009).

Matsunaga, A., and Ziemann, P. J. Yields of β-Hydroxynitrates, Dihydroxynitrates, and Trihydroxynitrates formed from OH Radical-Initiated Reactions of 2-Methyl-1-Alkenes. *Proc. Natl. Acad. Sci. USA*, 107, 6664-6669 (2010).

Pankow, J. F. An Absorption Model of Gas/Particle Partitioning of Organic Compounds in the Atmosphere. *Atmos. Environ*., 28, 185-188 (1994).

Pankow, J. F., and Asher, W. E. SIMPOL.1: A Simple Group Contribution Method for Predicting Vapor Pressures and Enthalpies of Vaporization of Multifunctional Organic Compounds, *Atmos. Chem. Phys*., 8, 2773-2796 (2008).

Presto, A. A., Miracolo, M. A., Donahue, N. M., and Robinson, A. L. Secondary Organic Aerosol Formation from High-NO_x Photo-Oxidation of Low Volatility Precursors: *n*-Alkanes. *Environ. Sci. Technol*., 44, 2029-2034 (2010).

Ramanathan, V., Crutzen, P. J., Kiehl, J. T., and Rosenfeld, D. Aerosols, Climate, and the Hydrological Cycle. *Science*, 294, 2119-2124 (2001).

Ravishankara, A. R. Heterogeneous and Multiphase Chemistry in the Troposphere. *Science*, 276, 1058-1065 (1997).

Reisen, F., Aschmann, S. M., Atkinson, R., and Arey, J. 1,4-Hydroxycarbonyl Products of the OH Radical Initiated Reactions of C_5-C_8 *n*-Alkanes in the Presence of NO. *Environ. Sci. Technol*., 39, 4447-4453 (2005).

Sauter, A. D., Down, J. J., Buchner, J. D., Ringo, N. T., Shaw, D. L., and Dulak, J. G. Model for the Estimation of Electron Impact Gas Chromatography/Mass Spectrometry Response Factors Quadrupole Mass Spectrometers. *Anal. Chem*., 58, 1665-1670 (1986).

Seinfeld, J. H., and Pandis, S. N. *Atmospheric Chemistry and Physics*, First Edition, Wiley-Interscience, New York. (1998).

Taylor, W. D., Allston, T. D., Moscato, M. J., Fazekas, G. B., Kozlowski, R., and Takacs, G. A. Atmospheric Photodissociation Lifetimes for Nitromethane, Methyl Nitrite, and Methyl Nitrate. *Int. J. Chem. Kinet.*, 12, 231-240 (1980).

Tobias, H. J., and Ziemann, P. J. Compound Identification in Organic Aerosols Using Temperature-Programmed Thermal Desorption Particle Beam Mass Spectrometry. *Anal. Chem*., 71, 3428-3435 (1999).

Tobias, H. J., Kooiman, P. M., Docherty, K. S., and Ziemann, P. J. Real-Time Chemical Analysis of Organic Aerosols Using a Thermal Desorption Particle Beam Mass Spectrometer. *Aerosol Sci. Technol*., 33, 170-190 (2000).

Tuazon, E. C., Aschmann, S. M., Atkinson, R., and Carter, W. P. L. The Reactions of Selected Acetates with the OH Radical in the Presence of NO: Novel Rearrangement of Alkoxy Radicals of Structure RC(O)OCH(O•)R'. *J. Phys. Chem. A*, 102, 2316-2321 (1998).

van Dam, H. E., Kieboom, A. P. G., and van Bekkum, H. The Conversion of Fructose and Glucose in Acidic Media: Formation of Hydroxymethylfurfural. *Starch*, 38, 95-101 (1986).

Ziemann, P. J. Effects of Molecular Structure on the Chemistry of Aerosol Formation from the OH-Radical-Initiated Oxidation of Alkanes and Alkenes. *Int. Rev. Phys. Chem*., 30, 161-195 (2011).

CHAPTER 4

Composition in Secondary Organic Aerosol Formed from the Environmental Chamber Reaction of *n*-Pentadecane with OH Radicals in the Absence of NO_x

Abstract

In this chapter the functional group analysis methods described in Chapter 2 were used to investigate the chemical composition of secondary organic aerosol formed from the OH radical-initiated reaction of *n*-pentadecane in the absence of NO_x. Experiments were conducted in an environmental chamber with OH radicals formed by reaction of tetramethylethylene with O_3 and by photolysis of H_2O_2. The effect of adding HNO_3 to catalyze heterogeneous/multiphase reactions was also investigated. Real-time and offline thermal desorption particle mass spectrometry and SOA yield measurements were used in addition to functional group analysis to characterize the SOA. Results of functional group analysis indicate the presence of carbonyl, hydroxyl, peroxide, and carboxyl groups in SOA formed in all reactions, and ester groups were also present in reactions with HNO_3 present. The major SOA products appear to be first-generation *n*-ketones, *n*-alcohols, *n*-hydroperoxides, and cyclic hemiacetals, second-generation carbonyl and hydroxy cyclic hemiacetals, and acetals formed from heterogeneous/multiphase reactions of these various cyclic hemiacetals with each other and with *n*-alcohols. The results demonstrate the value of these functional group analysis methods for SOA studies and lend additional support for the currently accepted mechanism of SOA formation from reactions of

alkanes with OH radicals in the absence of NO_x, including the role of heterogeneous/multiphase reactions.

4.1 Introduction

Volatile organic compounds (VOC) consisting primarily of alkanes, alkenes, and aromatics hydrocarbons are emitted to the atmosphere from anthropogenic and biogenic sources. Alkanes and aromatic hydrocarbons are most abundant in urban areas [Calvert et al. 2000] whereas alkenes dominate biogenic emissions and represent ~90% of global VOC emissions [Guenther et al. 1995]. In the atmosphere VOCs react primarily with OH radicals, O_3, and NO_3 radicals to form oxidized products [Atkinson and Arey 2003], some of which have sufficiently low vapor pressures to partition into aerosol particles and form secondary organic aerosol (SOA) [Kroll and Seinfeld 2008]. A large fraction of the mass of atmospheric fine particulate matter (diameter ≤ 2.5 μm) is comprised of organic matter, and most of this is SOA [de Gouw and Jimenez 2009]. There is currently much interest in fine particles (especially SOA) because of their effects on atmospheric processes such as light scattering and absorption [Seinfeld and Pandis 1998; Haywood and Boucher 2000], cloud formation [Andreae and Rosenfeld 2008; Lohmann and Feichter 2005], the hydrologic cycle [Ramanathan et al. 2001], and atmospheric chemistry [Ravishankara 1997] and human health [Davidson et al. 2005].

The chemical composition of the products of VOC oxidation and thus SOA depends on the identity of the VOC and oxidant, NO_x concentrations, and particle properties such as acidity and water content that can affect heterogeneous/multiphase reactions that can

occur on/in particles and potentially lead to the formation of oligomers [Atkinson and Arey 2003; Kroll and Seinfeld 2008]. Most studies of alkane oxidation have focused on reactions that occur in the presence of NO_x, conditions that are representative of polluted air. Few studies have investigated the reactions in the absence of NO_x, conditions that are representative of remote atmospheres including those sufficiently far downwind of urban areas where alkane and NO_x concentrations are high. In the clean atmosphere OH radical-initiated reactions of alkanes are expected to lead to the formation of mostly hydroperoxides, whereas at the higher VOC concentrations typically used in laboratory studies the reactions can form a much larger array of first-generation products including carbonyls, alcohols, hydroperoxides, and 1,4-hydroxycarbonyls that can undergo heterogeneous/multiphase reactions [Atkinson et al. 2008; Lim and Ziemann 2009a; Ziemann 2011] that lead to highly reactive dihydrofurans [Martin et al. 2002]. Subsequent reactions of products with OH radicals or O_3 (in the case of dihydrofurans) can form higher-generation multifunctional products containing additional carbonyl, hydroxyl, and hydroperoxy groups as well as ester, carboxyl, and peroxycarboxyl groups. Whereas the mechanisms and products of the OH radical-initiated reactions of alkanes in the presence of NO_x are reasonably well understood and the yields of many gas-phase products and SOA have been quantified [Arey et al. 2001; Martin et al. 2002; Reisen et al. 2005; Lim and Ziemann 2009a,b; Presto et al. 2010], the mechanisms of reactions in the absence of NO_x are less well understood and there have been few studies of gas-phase product yields [Atkinson and Arey 2003; Atkinson et al. 2008] and (to our knowledge) no studies of SOA products or yields. Because of the very different products expected to be

formed from the OH radical-initiated reactions of alkanes in the absence of NO_x, compared to in the presence of NO_x, and the lack of prior SOA studies, an investigation of SOA formation from these reactions provides a good alternative to the high NO_x reactions investigated in Chapter 3 for the application of the functional group analysis methods described in Chapter 2. This chapter describes the results of environmental chamber experiments conducted on the reaction of OH radicals with *n*-pentadecane, the linear C_{15} alkane, in the absence of NO_x and in the absence and presence of HNO_3, which can catalyze heterogeneous/multiphase reactions. The study employs two different methods for generating OH radicals, and functional group analysis, elemental analysis, particle mass spectrometry, and measurements of SOA yields are employed to investigate the chemistry of SOA formation.

4.2 Experimental Section

Chemicals. The following chemicals, with purities or grades and suppliers, were used: *n*-pentadecane (99%), tetramethylethylene (TME) (99%), tridecanoic acid (98%), benzoyl peroxide (97%), and 1,2-tetradecanediol (90%) [Sigma-Aldrich]; bis(2-ethylhexyl)-decanedioate (DOS) (97%) and hydrogen peroxide (30% in water) [Fisher Chemicals]; 3-hexadecanone (99%) [Alfa Aesar]. Ozone was generated using a Welsbach T-408 ozone generator. See Chapter 2 for a description of the chemicals used for functional group analysis.

Environmental chamber method. Reactions were conducted in a 8300 L FEP Teflon environmental chamber filled with clean, dry air (< 5ppbv hydrocarbon and < 1%

RH) at about 20^{o}C and atmospheric pressure. UV lamps cover two walls outside the chamber and act as a light source for photolysis. All chemicals were added to the chamber in a flow of N_2. Measured amounts of *n*-pentadecane, TME, O_3, and HNO_3 were added separately from a glass bulb, H_2O_2 was added by atomization from a Collison atomizer, and dioctyl sebacate (DOS) seed particles were generated using an evaporation-condensation apparatus. In the TME + O_3 reactions, TME was added last in ~2 min to initiate the reaction. TME reacts rapidly with O_3 (rate constant = 1.1×10^{-15} cm^3 molecule^{-1} s^{-1}) to form OH radicals with a yield of ~1 [Atkinson 1997], so OH reactions are complete within ~2 min. This was apparent from the observation that the O_3 concentration stopped decreasing after ~ 2 min. Using the rate constant for reaction of OH radicals with *n*-pentadecane of 1.8×10^{-11} cm^3 molecule^{-1} s^{-1} [Kwok and Atkinson 1995] and the fraction of *n*-pentadecane reacted, the average concentration of OH radicals during the 2 min reactions was ~1.5×10^8 molecules cm^{-3}. In the H_2O_2 reaction, the reaction was initiated by turning on the lights at 100% intensity (corresponding to a NO_2 photolysis rate constant of 0.61 min^{-1}), which formed OH radicals by photolyzing H_2O_2. The lights remained on for 80 min. In this experiment the average concentration of OH radicals was ~ 3×10^6 molecules cm^{-3}. The experimental conditions for all reactions are listed in Table 4.1.

Particle and gas analysis. A thermal desorption particle beam mass spectrometer (TDPBMS) was used to analyze particle composition in real-time [Tobias et al. 2000] and by temperature-programmed thermal desorption (TPTD) [Tobias and Ziemann 1999]. Air was sampled into the TDPBMS and particles were formed into a beam and impacted on a

Table 4.1. Experimental conditions of the reaction of *n*-pentadecane with OH radicals in the absence of NO_x.

Experiment		*n*-Pentadecane (ppmv)	O_3 (ppmv)	TME (ppmv)	HNO_3 (ppmv)	H_2O_2[3] (ppmv)	OA[1] ($\mu g\ m^{-3}$)	SOA[2] corrected ($\mu g\ m^{-3}$)	SOA yield
1	Initial	4.88	10.6	2	-	-	240		
	Final	3.79	9.43				3930	3940	0.411
2	Initial	2.93	10.9	2	-	-	220		
	Final	1.84	8.3				3870	3910	0.405
3	Initial	4.88	1.6	3	-	-	280		
	Final	3.58	0.0				3320	3250	0.292
4	Initial	4.88	11.2	2	5	-	270		
	Final	3.42	8.9				8850	8630	0.672
5	Initial	2.93	10.8	2	5	-	200		
	Final	1.98	8.1				6720	6660	0.794
6	Initial	2.93	2.6	3	5	-	250		
	Final	2.10	0.0				6810	6650	0.910
7	Initial	2.93	-	-	-	7	170		
	Final	2.24					1230	1170	0.191

[1]Initial OA is DOS seed.
[2]Corrected for loss to walls using decay in DOS *m/z* 185 signal.
[3]H_2O_2 was photolyzed at 100 % light intensity for 80 min.

polymer-coated metal vaporizer [Chattopadhyay and Ziemann 2005]. For real-time analysis, the rod was resistively heated to 160^{o}C. Particles vaporized upon impact and the vapor was ionized by 70 eV electrons and analyzed in a quadrupole mass spectrometer. For TPTD analysis, the rod was cooled to -40^{o}C and particles were collected for 30 min. The rod was allowed to warm to -5^{o}C and then heated to 200^{o}C using a 2^{o}C min^{-1} ramp to desorb and separate compounds by volatility prior to mass analysis.

Aerosol volume concentrations were measured using a scanning mobility particle sizer (SMPS). SOA mass concentration was calculated by subtracting the initial particle volume concentration from the maximum corrected aerosol volume concentration and then multiplying by an assumed particle density of 1.0 g cm^{-3}. *n*-Pentadecane was collected on Tenax TA and analyzed by GC-FID [Docherty et al. 2005] to determine the mass of *n*-pentadecane reacted. SOA yields were calculated as SOA mass/reacted *n*-pentadecane mass. Ozone was measured using a Thermo Electron Corporation model 49i O_3 analyzer.

Filter sampling and sample preparation for functional group analysis. Duplicate particle samples were collected after each experiment on previously weighed Millipore filters (0.45 μm pore size, Fluoropore FHLP, 47 mm). Sample air volumes were ~0.6 m^3 collected over ~40 min through stainless steel tubing for the O_3 + TME experiments and ~1 m^3 collected over ~70 min for the H_2O_2 photolysis experiment. Immediately after sampling, each filter was weighed to calculate the mass of sample collected, and then extracted twice in 4 ml of ethyl acetate at room temperature for >10 min. For each filter, extracts were combined into a 4-ml brown vial that was previously

weighed, and then dried in a stream of N_2. The vial was weighed again to determine the mass of sample. The aerosol mass collected was approximately 2, 4, and 6 mg for the H_2O_2 photolysis, O_3 + TME, and O_3 + TME + HNO_3 experiments. Dried samples were dissolved in an appropriate volume of ethyl acetate to achieve a sample concentration of at least ~1 mg mL^{-1}. Separate aliquots were taken for analysis of each functional group and dried in a stream of N_2 to remove ethyl acetate, and then dissolved in an appropriate solvent for each analysis of each functional group as described in Chapter 2. A clean blank filter was also prepared and analyzed similarly. The method used for peroxide analysis was described previously [Matsunaga and Ziemann 2009, Docherty and Ziemann 2005]. Because these experiments were conducted in the absence of NO_x, samples were not analyzed for nitrate. The standard curves used for quantification of each functional group were prepared using 3-hexadecanone for carbonyl groups, 5-hydroxy-2-pentanone for hydroxyl groups, tridecanoic acid for carboxyl groups, benzoyl peroxide for peroxide groups, and bis(2-ethylhexyl)-decanedioate for ester groups.

Elemental analysis. Dried filter extracts were also analyzed for C and N using a high temperature combustion elemental analyzer (Costech ECS 4010 CHNSO) and for O and H using a temperature conversion elemental analyzer (Thermo TC/EA) interfaced to an isotope ratio mass spectrometer (Thermo Delta V).

4.3 Results and Discussion

Reaction mechanism and potential products. The mechanism and potential products of the reaction of *n*-pentadecane with OH radicals in the absence of NO_x is

shown in Figure 4.1 [Atkinson and Arey, 2003; Atkinson et al., 2008; Lim and Ziemann, 2009]. The reaction is initiated by abstraction of an H atom to form H_2O and an alkyl radical. Structure-reactivity calculations [Kwok and Atkinson 1995] indicate that this abstraction occurs 98% at secondary H atoms (C_2–C_{14}) and 2% at primary H atoms (C_1 and C_{15}), thus leading to the formation of 8 alkyl radical isomers since the molecule is symmetric. In air, alkyl radicals immediately add O_2 to form alkylperoxy (RO_2•) radicals, which in the absence of NO_x then react either with HO_2 to form hydroperoxides [**1**] or with alkylperoxy radicals ($R'O_2$•) to form alcohols [**2**], carbonyls [**3**], or alkoxy radicals (RO•). Alkoxy radicals then isomerize through a 1,5-H-atom shift to form 1,4-hydroxyalkyl radicals, which then add O_2 and react either with HO_2 to form 1,4-hydroxyhydroperoxides [**4**] or with alkylperoxy radicals to form 1,4-diols [**5**], 1,4-hydroxycarbonyls [**6**], or 1,4-hydroxyalkoxy radicals. The 1,4-hydroxyalkoxy radicals undergo a reverse isomerization and then react with O_2 to form a 1,4-hydroxycarbonyl [**6**] and HO_2. It is worth noting that although alkoxy radicals can also react with O_2 to form carbonyls and decompose to form pairs of carbonyls and alkyl radicals, for *n*-alkanes > C_6 these reactions are too slow to compete with isomerization and so are not shown in the mechanism figure. Yields of hydroperoxides from reactions of alkylperoxy radicals with HO_2 are 1, whereas yields of alcohols, carbonyls, and alkoxy radical products from self- and cross-reactions are not well established, although usually all three pathways are significant [Atkinson 1997; Tyndall et al. 2001; Atkinson et al 2008]. The amounts of products formed in a reaction depends on the relative concentrations of HO_2 and RO_2• radicals and the RO_2• + HO_2 and RO_2• + $R'O_2$• rate constants.

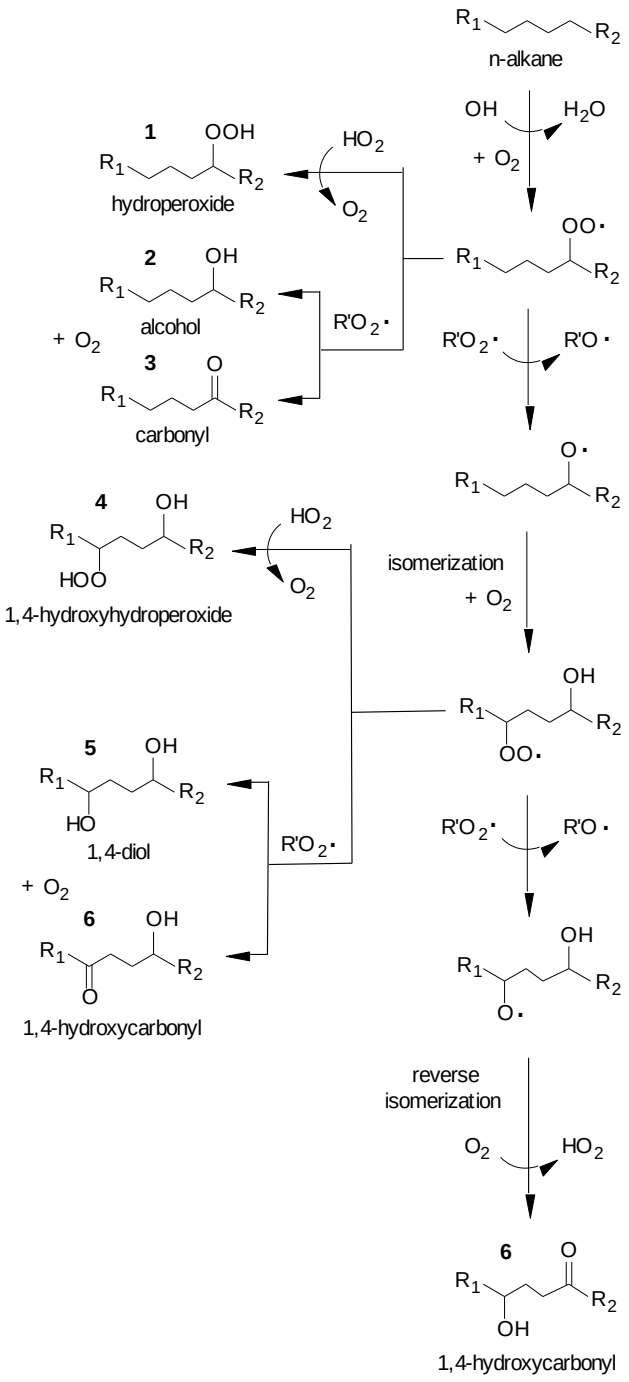

Figure 4.1. Mechanism of reaction of OH radicals with *n*-alkanes in the absence of NO_x.

The 1,4-hydroxycarbonyls formed in this reaction can react on/in particles or the walls of the environmental chamber, as shown in Figure 4.2. The reactions are catalyzed by acid and involve first cyclization to form cyclic hemiacetals [**7**] and then dehydration to form dihydrofurans [**8**] [Martin et al. 2002; Atkinson et al. 2008; Lim and Ziemann, 2009a]. Measurements and modeling indicate that for reactions conducted in the presence of NO_x and therefore HNO_3 the probability that a 1,4-hydroxycarbonyl will cyclize upon collision with a particle (i.e., the reactive uptake coefficient) is ≥ 0.5, and that the timescale for dehydration is ~15 min [Lim and Ziemann, 2009b]. Dihydrofurans formed via this process evaporate from the particles and will react rapidly with OH radicals, O_3, or NO_3 radicals (if present) [Martin et al. 2002]. The mechanism and potential products of reactions of dihydrofurans with OH radicals and O_3 in the absence of NO_x (the conditions of these experiments) are shown in Figure 4.2. Using an average OH radical concentration of $\sim 1.5 \times 10^8$ and average O_3 concentrations of $\sim 2.5 \times 10^{14}$ and $\sim 2.5 \times 10^{13}$ molecules cm^{-3} for the excess O_3 and excess TME reactions, and the corresponding rate constants for reactions with dihydrofurans of 2.2×10^{-10} and 3.5×10^{-15} cm^3 $molecule^{-1}$ s^{-1} [Martin et al. 2002], the fraction of dihydrofurans that react with OH radicals and O_3 are approximately 0.04 and 0.96 and 0.27 and 0.73, respectively. Furthermore, the lifetime for reaction of dihydrofurans with O_3 is ~1 s. The reaction of a dihydrofuran with an OH radical (Figure 4.2) is initiated by addition of the OH radical to the C=C bond to form a pair of 1,2-hydroxyalkyl radical isomers, which then add O_2 and react either with HO_2 to form cyclic 1,2-hydroxyhydroperoxides [**9**,**10**] or with $R'O_2$• radicals to form cyclic 1,2-diols [**11**,**12**], cyclic 1,2-hydroxycarbonyls [**13**], or cyclic 1,2-hydroxyalkoxy radicals.

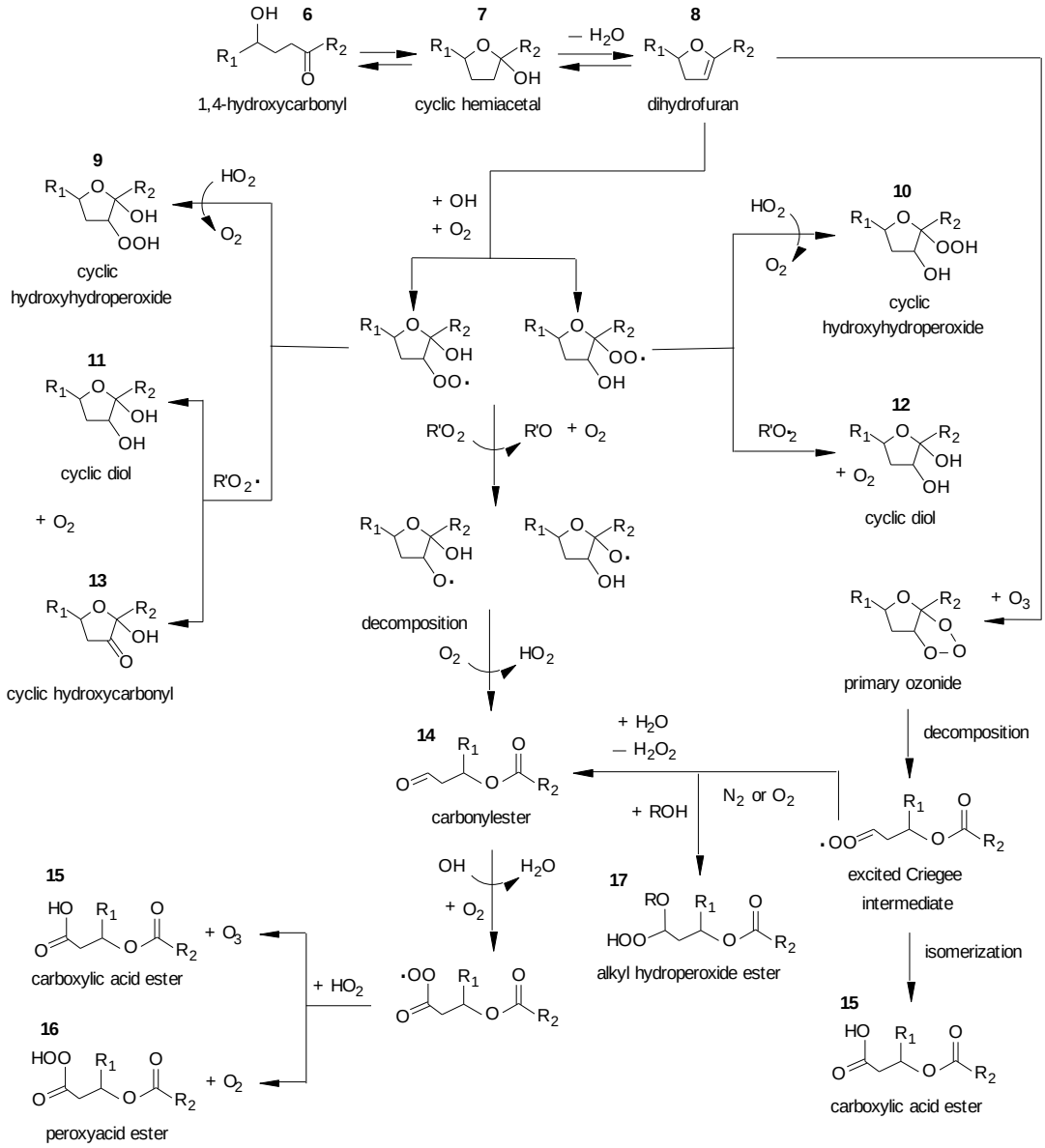

Figure 4.2. Mechanism of heterogeneous/multiphase reactions of 1,4-hydroxycarbonyls to form cyclic hemiacetals and dihydrofurans, and subsequent reactions with OH radicals and O_3 in the absence of NO_x.

Cyclic 1,2-hydroxyalkoxy radicals are expected to rapidly decompose via ring opening and then react with O_2 to form carbonylesters [**14**] and HO_2. All of these products can react further with OH radicals to form higher generation products. Reactions that occur via H-atom abstraction should mostly be similar to those shown in Figure 4.1 and thus add one or two hydroperoxy, hydroxyl, or carbonyl groups to the parent compound. In the case of carbonylesters, however, H-atom abstraction occurs preferentially from the aldehyde group to form an acyl radical that then adds O_2 to form an acylperoxy radical (Figure 4.2). Acylperoxy radicals either react with HO_2 to form carboxylic acid esters [**15**] or peroxyacid esters [**16**], or with $R'O_2$• radicals to form carboxylic acid esters [**15**] or acyloxy radicals that decompose to alkyl radicals and CO_2 (not shown) [Tyndall et al. 2001].

The reaction of a dihydrofuran with O_3 (Figure 4.2) is initiated by addition of O_3 to the C=C bond to form a primary ozonide, which rapidly decomposes to form a pair of bifunctional excited Criegee intermediates containing a carbonyl oxide group on one end and either a carbonyl or ester group on the other. Only the latter is shown in Figure 4.2 since the reactions of this type of carbonyl oxide are better understood. The subsequent reactions of large excited Criegee intemediates such as these are complex and can lead to numerous products, many of which have not been determined. The excited Criegee intermediate shown in Figure 4.2 can be stabilized by collisions with air and react with an alcohol to form an alkyl hydroperoxide ester [**17**], or react with H_2O and then decompose by loss of H_2O_2 for form a carbonylester [**14**] [Martin et al. 2002], or it can isomerize to form a carboxylic acid ester **[15]** [Orzechowska et al. 2005].

Reactions with OH radicals formed from the reaction of TME + O_3.

The SOA formed in environmental chamber reactions was analyzed as described above to obtain the following information: aerosol mass concentrations (SMPS), real-time (RTMS) and temperature-programmed thermal desorption (TPTD) mass spectra, and functional group composition (FG). In the experiments described here reactions were initiated by adding TME to the chamber, which created OH radicals for a period of ~2 min. Experiments were conducted with excess O_3 (O_3/TME ~ 5) and excess TME (TME/O_3 ~ 2 and 1.2) without and with 5 ppmv of added HNO_3. The experimental conditions are shown given in Table 4.1. Results of replicate experiments were similar, so representative results are discussed below. Specifically, results are shown for reactions with excess TME without and with HNO_3 (Experiments 3 and 6) and with excess O_3 without and with HNO_3 (Experiments 2 and 5).

SOA yields. The organic aerosol (OA) mass concentrations measured over the course of reactions with excess TME and excess O_3 are shown in Figure 4.3. The concentrations have been corrected for loss of aerosol to the chamber walls by using the decay in the DOS mass spectral signal at *m/z* 185, which is possible because DOS is effectively non-volatile and essentially all the *m/z* 185 signal comes from DOS (shown from similar experiments conducted without DOS seed particles). The typical wall loss rate was ~10–15% hr^{-1}. The initial OA mass concentrations were ~200–300 μg m^{-3} from DOS seed particles, and within a few minutes of adding TME increased to maximum values of 3000–4000 μg m^{-3} and ~7000 μg m^{-3} for reactions without and with HNO_3, respectively. After reaching the maximum values, corrected OA mass concentrations

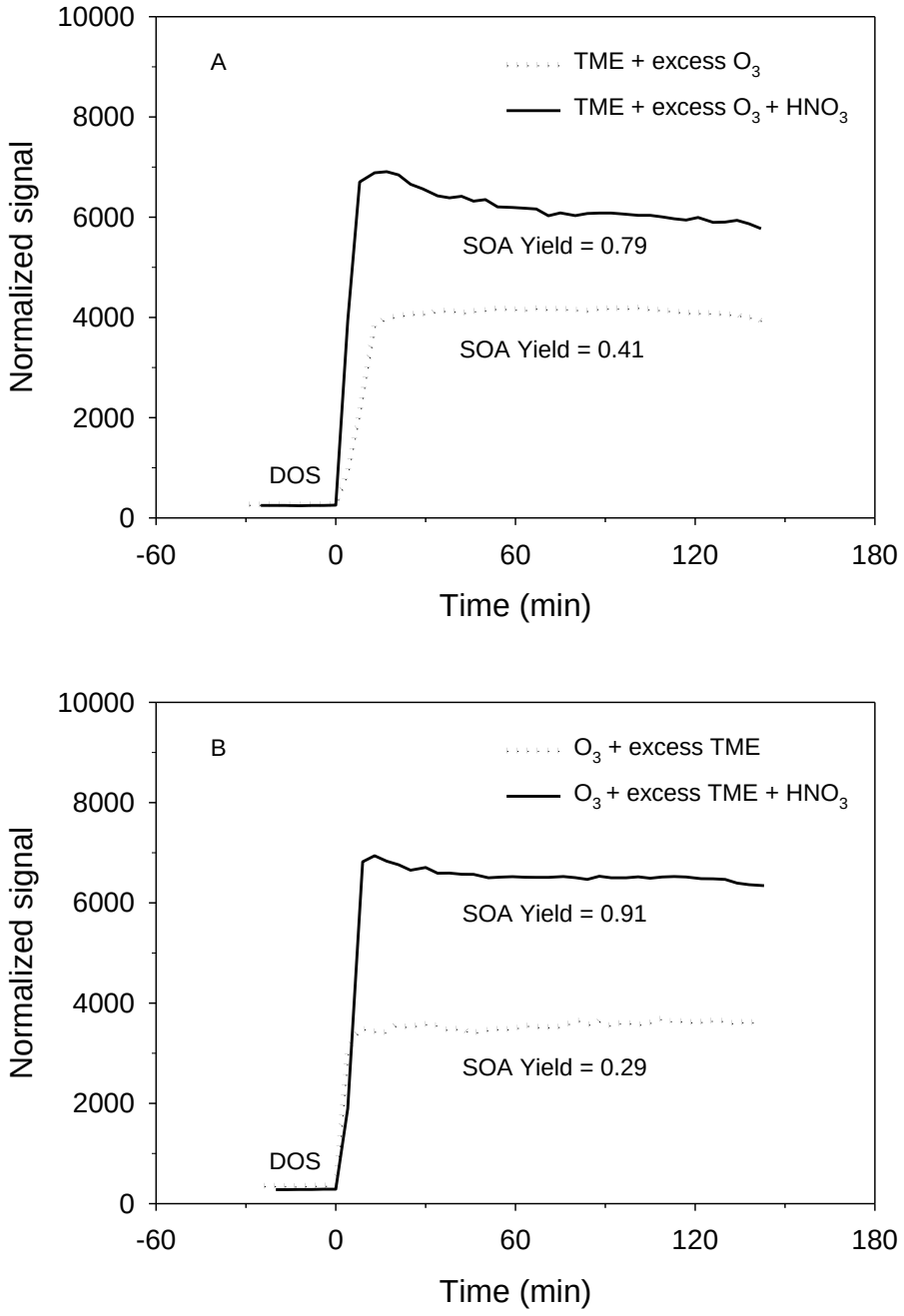

Figure 4.3. Aerosol mass concentrations and SOA yields measured using the SMPS during reactions of *n*-pentadecane with OH radicals formed in (A) reactions of TME with excess O_3 and (B) reactions of O_3 with excess TME without and with HNO_3. Aerosol mass concentrations and SOA yields were corrected for loss of aerosol to the chamber walls by using the decay in the DOS mass spectral signal.

remained constant in the reactions without HNO_3, but in the reactions with HNO_3 they decreased slowly over ~30–60 min and then essentially leveled off. SOA yields were much higher for reactions with HNO_3: 0.79 compared to 0.41 for the excess O_3 reactions and 0.91 compared to 0.29 for the excess TME reactions. This occurred even though the amounts of *n*-pentadecane reacted were somewhat higher in the reactions without HNO_3: 1.1 ppmv compared to 0.95 ppmv for the excess O_3 reactions and 1.3 compared to 0.83 for the excess TME reactions, which for similar reactions would be expected to increase yields due to enhanced gas-to-particle partitioning because of higher SOA mass concentrations [Odum et al. 1996].

RTMS and TPTD analysis. As was the case in the experiments described in Chapter 3, the total ion RTMS signal (*m/z* 40–500) measured during these experiments (not shown) track the OA mass concentrations. This is expected if the total ion signal is proportional to the OA mass concentration and the proportionality factor does not change significantly during the experiment due to changes in composition that can potentially change compound ionization behavior. Changes tend to be small for compounds with large carbon numbers and similar structures [Harrison et al. 1966; Sauter et al. 1986; Allan et al. 2003], which is the case here.

Real-time mass spectra obtained 10 min and 120 min after the start of the reactions with excess O_3 are shown in Figure 4.4. The spectra for reactions with excess TME are similar and so are not shown. The signals from DOS have been removed and the mass spectrum at 120 min corrected for particle loss to the walls using the DOS signal. The spectra for reactions without HNO_3 are similar at 10 and 120 min, indicating no

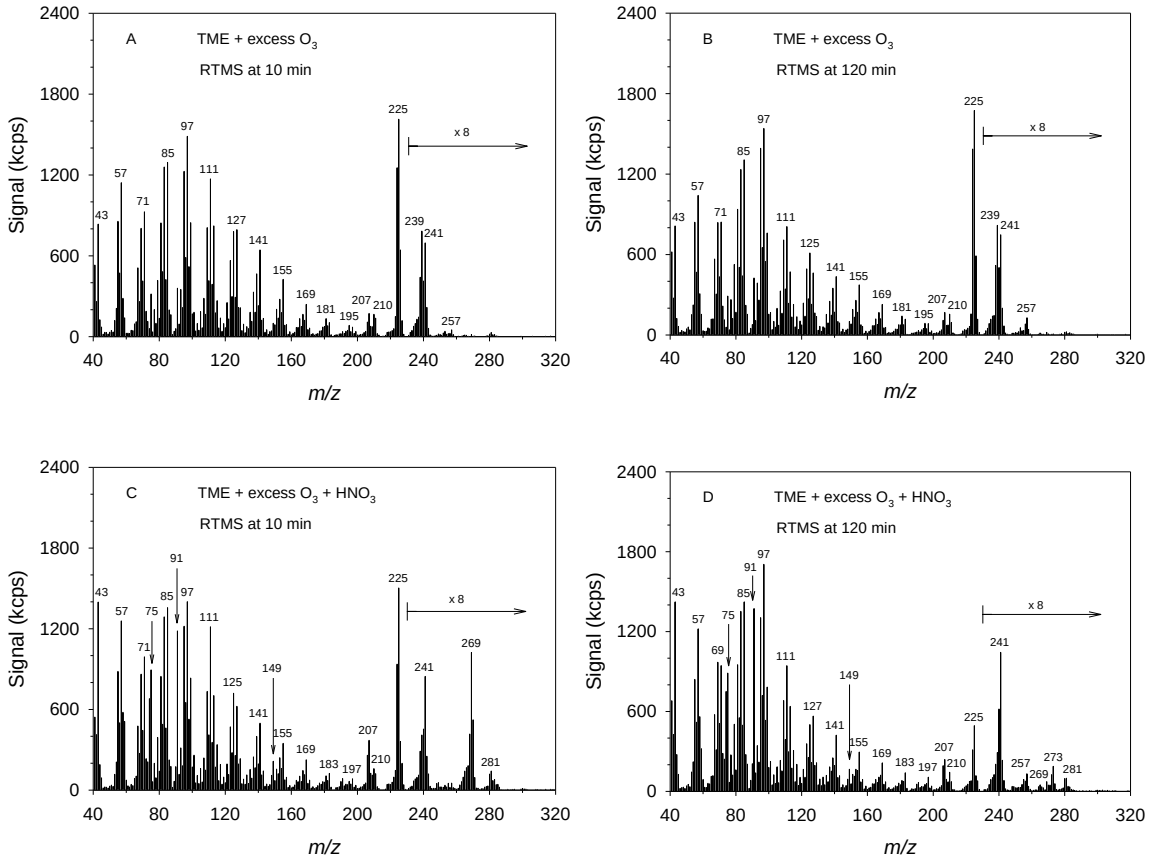

Figure 4.4. Real-time mass spectra of SOA formed in reactions of *n*-pentadecane with OH radicals formed in reactions of TME with excess O_3 (A, B) without and (C, D) with HNO_3, 10 min and 120 min after the start of the reaction. The signals from DOS were removed from the mass spectra and the mass spectrum at 120 min was corrected for particle loss to the walls using the decay in the DOS mass spectral signal.

significant change in composition. The spectra for reactions with HNO_3 are similar in most respects to those obtained for reactions without HNO_3, but contain a number of additional peaks with significant intensities, and the relative intensities of most peaks > *m/z* 200 change significantly between 10 and 120 min, indicating significant changes in composition. TPTD profiles of the total ion signal (with the contribution for DOS removed) for OA collected at the end of the experiments with excess TME and excess O_3 is shown in Figure 4.5. Because of the proportionality between total ion signal and OA mass this profile represents a quantitative distribution of SOA volatility. The SOA desorbs between ~0–150 ^{o}C, which by comparison with the desorption temperatures of compounds with known vapor pressures [Lim and Ziemann 2009a] corresponds to a very large range of compound vapor pressures of ~10^{-1}–10^{-13} Pa. Most of the various distinctive, high mass peaks (and a few low mass peaks) observed in the SOA mass spectra can be explained based on products expected to be formed in these reactions (Figures 4.1– 4.2), TPTD profiles and mass spectra, RTMS time profiles, and known electron ionization fragmentation pathways.

The most volatile products expected in these reactions, in order of decreasing vapor pressure and thus increasing desorption temperature are C_{15} *n*-ketones [**3**], *n*-alcohols [**2**], and *n*-hydroperoxides [**1**]. The vapor pressures of these compounds calculated using the structure-activity relationship of Pankow and Asher (2008) are 2×10^{-1}, 1×10^{-2}, and 5×10^{-3} Pa, and using the calibration curve $\log P(Pa) = -0.55 - [0.079 \times T_{des}(^{o}C)]$ reported previously [Lim and Ziemann 2009a], their estimated desorption temperatures are 2, 18, and 22 ^{o}C. Although no single ion TPTD profiles exhibit a peak which is indicative of

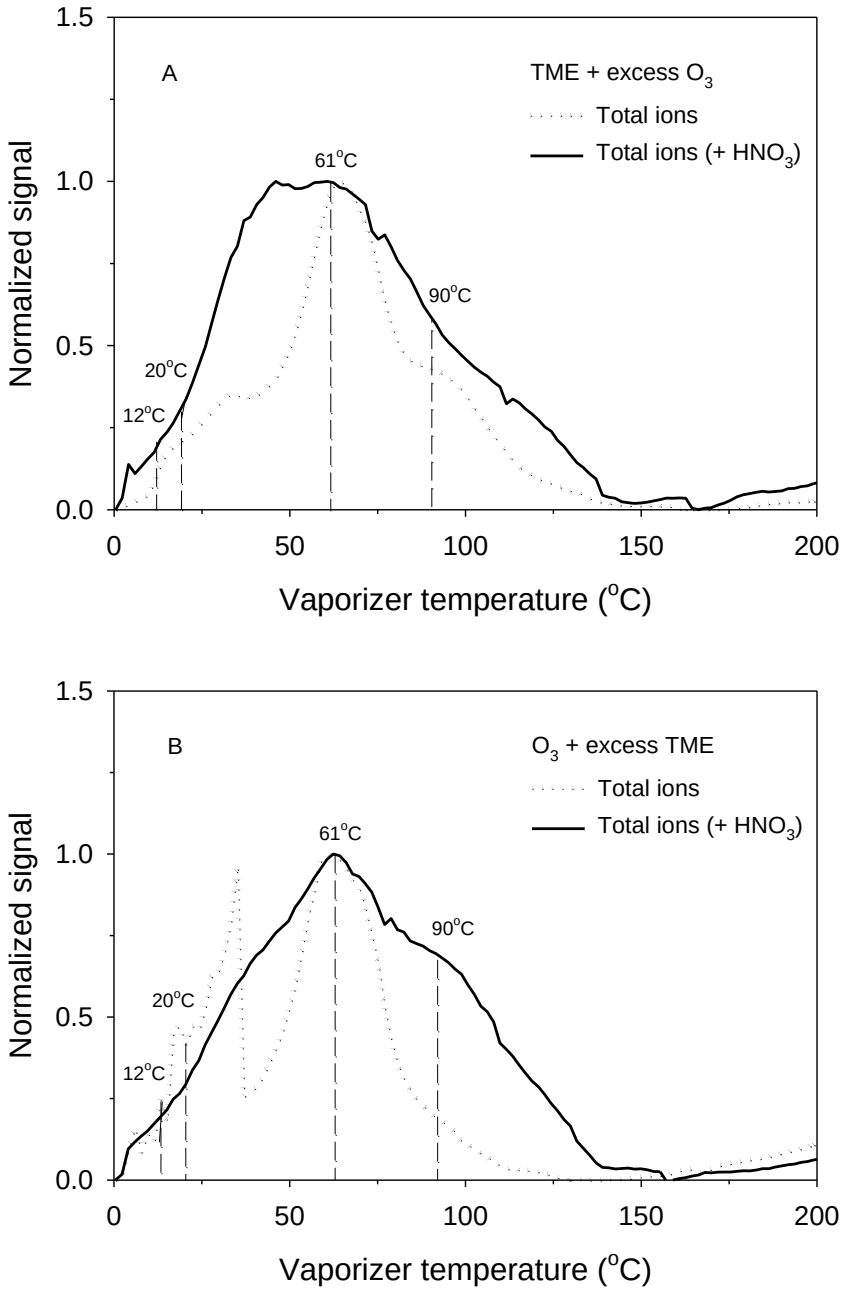

Figure 4.5. TPTD profiles of the total ions for SOA formed in reactions of *n*-pentadecane with OH radicals formed in reactions of (A) TME with excess O_3 and (B) O_3 with excess TME, without and with HNO_3. The signals from DOS were removed from the profiles and the signal was normalized to the maximum value.

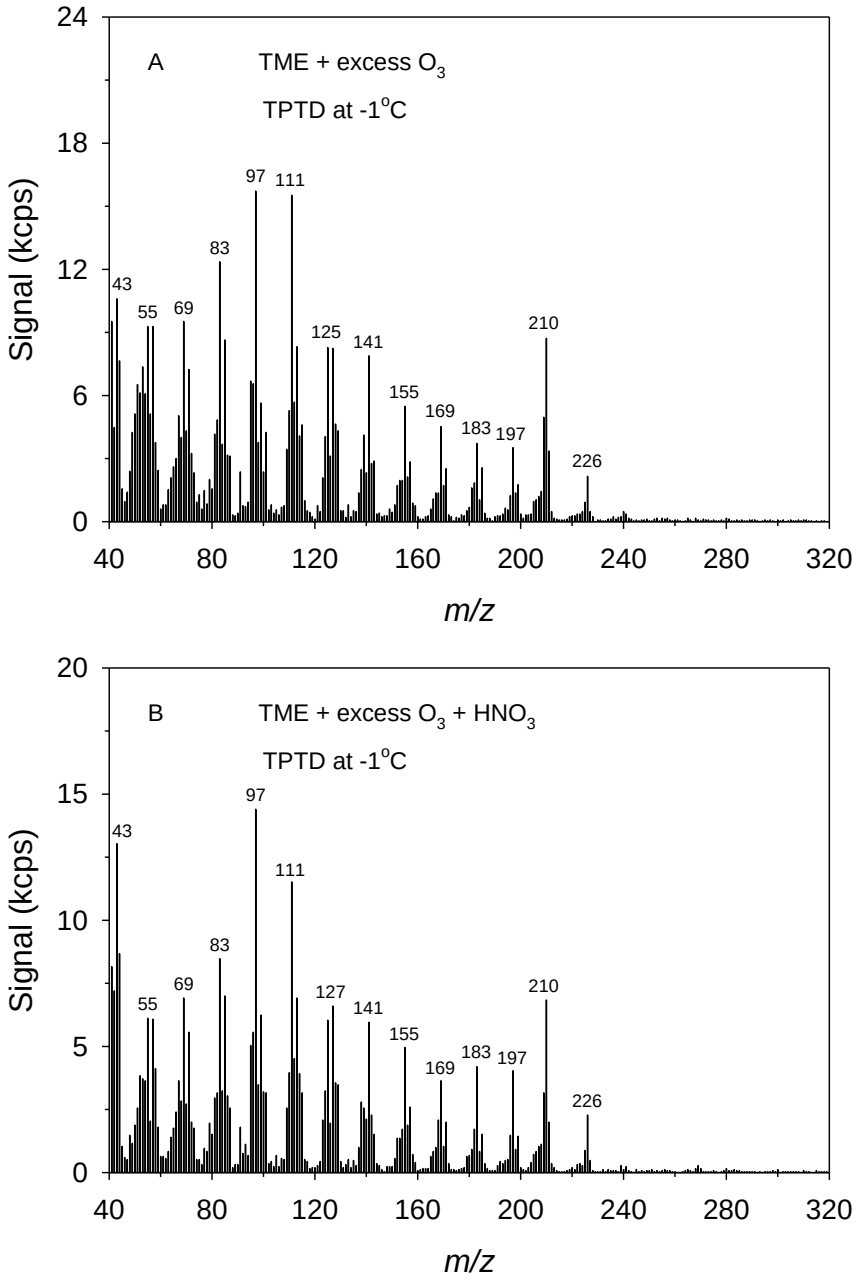

Figure 4.6. TPTD mass spectra measured at –1 ^{o}C for SOA formed in reactions of *n*-pentadecane with OH radicals formed in reactions of TME with excess O_3 (A) without and (B) with HNO_3. The signals from DOS were removed from the mass spectra.

the desorption of a single compound (or isomers) at temperatures close to 2 ^{o}C, the mass spectrum at low temperatures is characteristic of a series of *n*-ketone isomers (M = 226). For example, the TPTD mass spectra measured at –1 ^{o}C for reactions with excess O_3 are shown in Figure 4.6. The peak at *m/z* 226 is the molecular ion $(M)^+$ of *n*-ketones and the peaks at *m/z* 211, 197, 183… are due to loss of an alkyl group (CH_3, C_2H_5, C_3H_7…) that depends on the particular isomer via α-cleavage at the carbonyl group [McLafferty and Turecek 1993]. This was the lowest temperature TPTD mass spectrum obtained and at higher temperatures the *m/z* 226 signal decreased, indicating that the peak in the *n*-ketone desorption profile was ≤ –1 ^{o}C. The peak in the mass spectrum at *m/z* 210 is not associated with *n*-ketones, but with *n*-alcohols that desorb at higher temperatures. Similar results are obtained for SOA formed from reactions with excess TME.

The TPTD profiles of *m/z* 210 for reactions with excess TME and excess O_3 are shown in Figure 4.7. The lowest temperature peak occurs at ~12 ^{o}C, higher than the region where *n*-ketones desorb and reasonably close to the estimated desorption temperature for *n*-alcohols of ~18 ^{o}C. TPTD mass spectra at 12 ^{o}C for the reactions with excess O_3 are shown in Figure 4.8. The dominant peaks in the mass spectrum for *m/z* ≤ 210 are characteristic of a series of *n*-alcohol isomers (M = 228). Molecular ions are usually not observed, and the largest high mass peak is instead the $(M–18)^+$ ion due to loss of H_2O. The peaks at *m/z* 213, 199, 185, … are due to loss of an alkyl group (CH_3, C_2H_5, C_3H_7…) that depends on the particular isomer via α-cleavage at the hydroxyl group [McLaffery and Turecek 1993]. The peaks in the mass spectrum with *m/z* > 210 (except for the small *m/z* 213 peak) are not associated with *n*-alcohols, but compounds

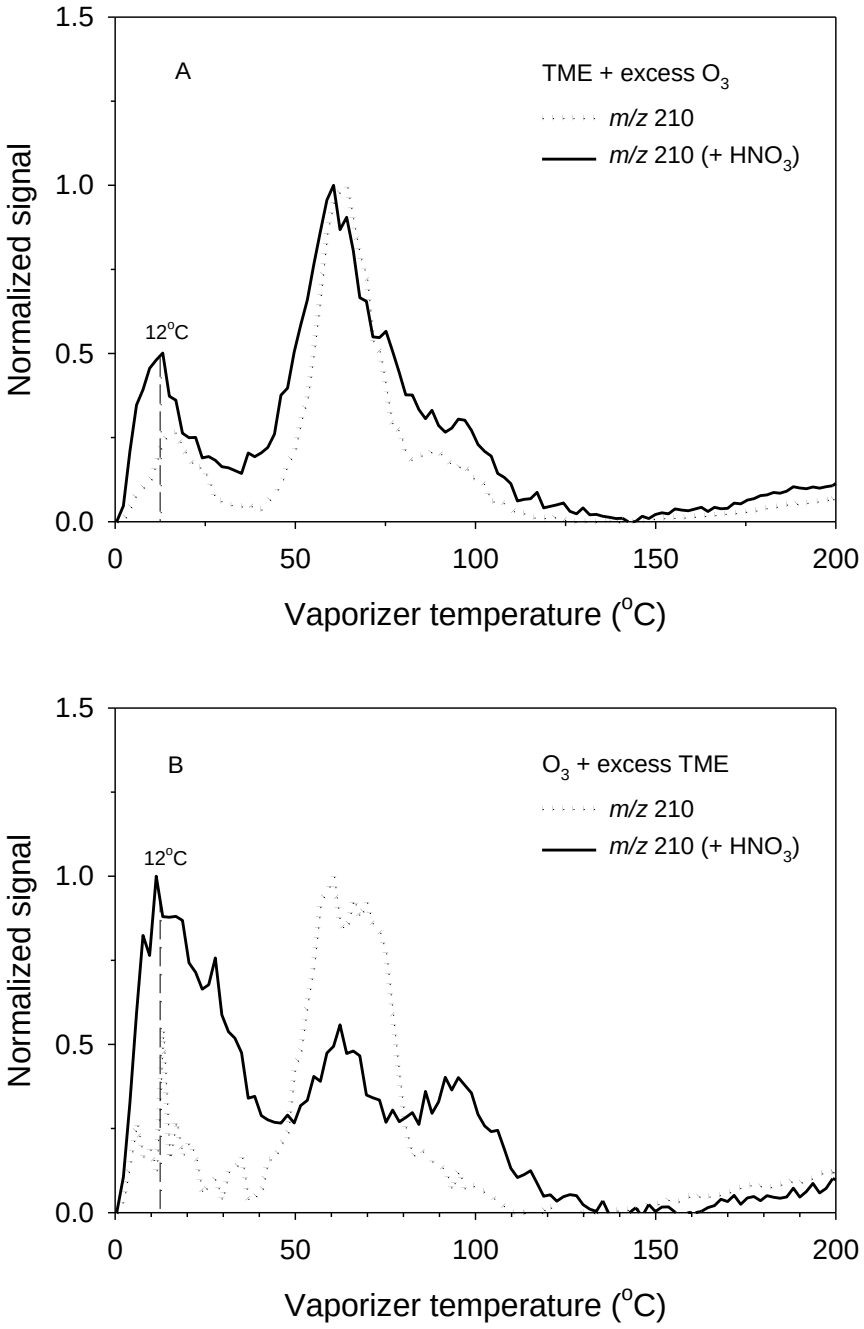

Figure 4.7. TPTD profiles of *m/z* 210 measured for SOA formed in reactions of *n*-pentadecane with OH radicals formed in reactions of (A) TME with excess O_3 and (B) O_3 with excess TME, without and with HNO_3. The signals from DOS were removed from the profiles and the signal was normalized to the maximum value.

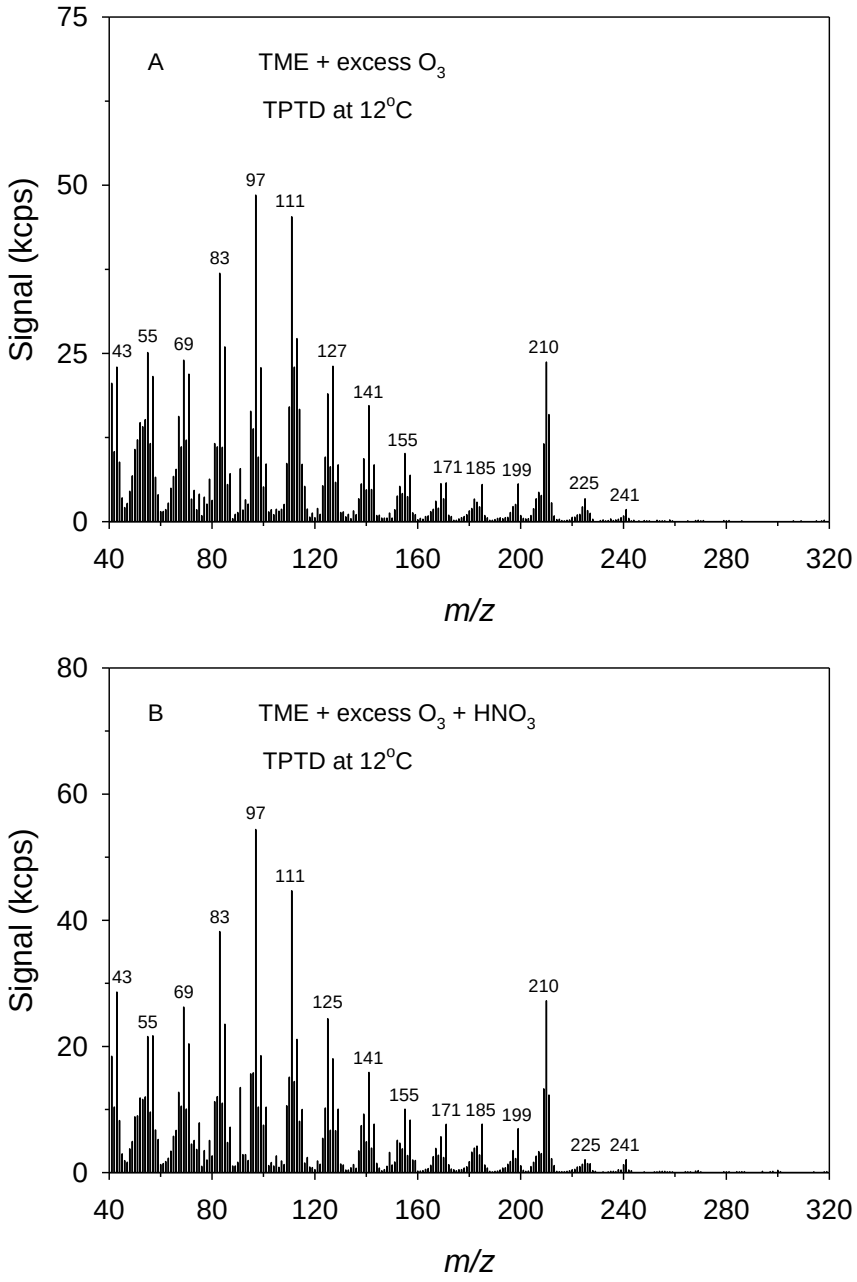

Figure 4.8. TPTD mass spectra measured at 12 ^{o}C for SOA formed in reactions of *n*-pentadecane with OH radicals formed in reactions of TME with excess O_3 (A) without and (B) with HNO_3. The signals from DOS were removed from the mass spectra.

that desorb at higher temperatures. Similar results are obtained for SOA formed from reactions with excess TME.

Mass spectra of *n*-hydroperoxides, which are expected to be the next reaction products to desorb after *n*-alcohols, do not contain molecular ion peaks. The dominant high-mass peak is instead due to loss of HO_2 [Burgess et al. 1969; Tobias and Ziemann 2000], which for *n*-hydroperoxides (M = 244) gives a peak at *m/z* 211. TPTD profiles of *m/z* 211 for reactions with excess O_3 and excess TME are shown in Figure 4.9. The lowest temperature peak occurs at ~20 ^{o}C, higher than the region where *n*-alcohols desorb and close to the estimated desorption temperature for *n*-hydroperoxides of ~22 ^{o}C. TPTD mass spectra at 20 ^{o}C for reactions with excess O_3 are shown in Figure 4.10. The peak at *m/z* 210 is due to loss of H_2O_2 [Burgess et al. 1969] and possibly to some *n*-alcohols, and the dominant peaks in the mass spectrum for *m/z* ≤ 211 at *m/z* 197, 183, 169… are due to loss of H_2O + an alkyl group (C_2H_5, C_3H_7, C_4H_9…; loss of H_2O + CH_3 overlaps with *m/z* 211 formed from HO_2 loss) that depends on the particular isomer via α-cleavage from the 4-member ring formed by loss of H_2O [Burgess et al. 1969]. The peaks in the mass spectrum with *m/z* > 211 are not associated with *n*-hydroperoxides, but compounds that desorb at higher temperatures. Similar results are obtained for reactions with excess TME.

The partitioning of C_{15} *n*-ketones, *n*-alcohols, and *n*-hydroperoxides between the gas and particle phases can be calculated using the theory developed by Pankow (1994), the vapor pressures estimated from TPTD desorption temperatures of -1, 12, and 20 ^{o}C and the calibration equation given above, an average OA mass concentration of 5000 µg

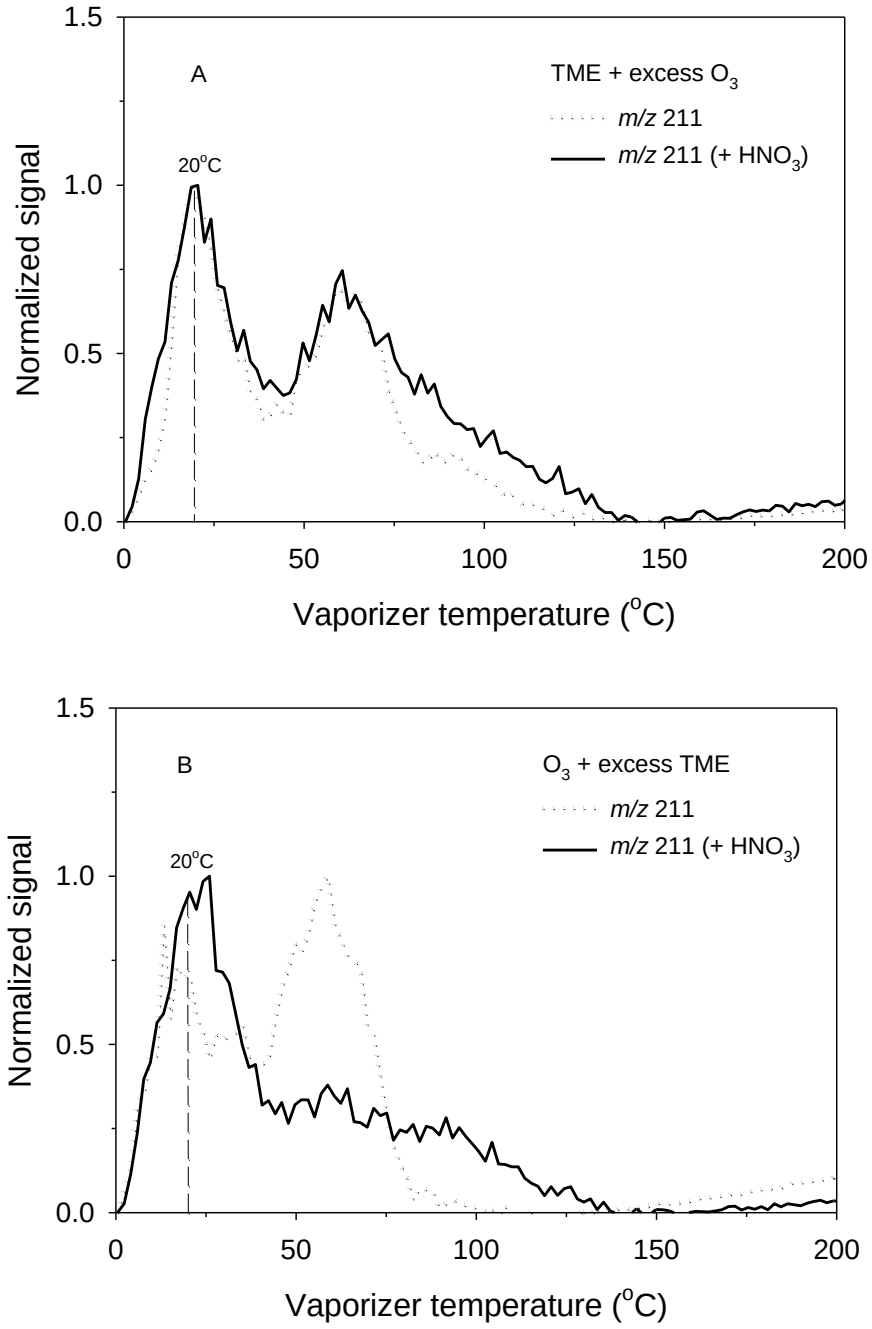

Figure 4.9. TPTD profiles of *m/z* 211 measured for SOA formed in reactions of *n*-pentadecane with OH radicals formed in reactions of (A) TME with excess O_3 and (B) O_3 with excess TME, without and with HNO_3. The signals from DOS were removed from the profiles and the signal was normalized to the maximum value.

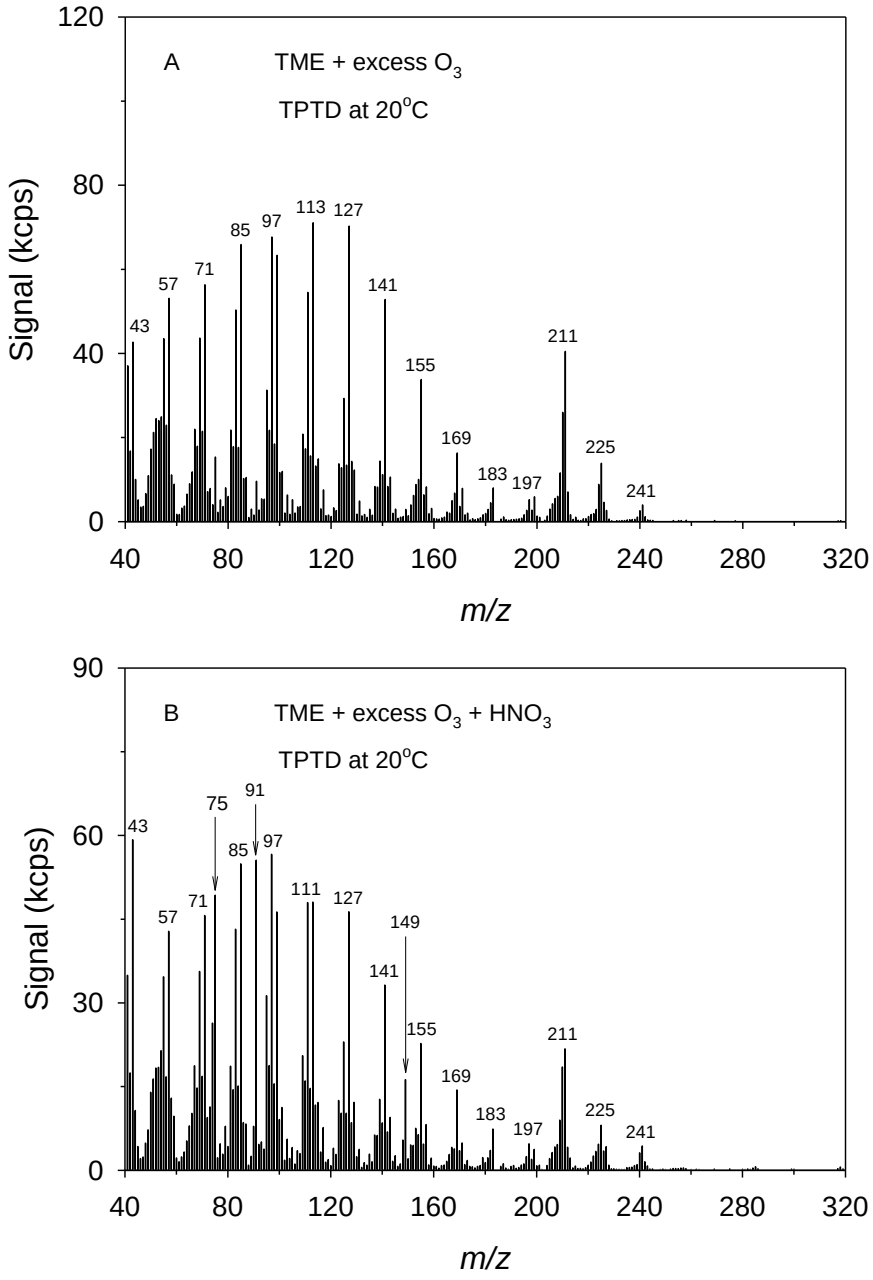

Figure 4.10. TPTD mass spectra measured at 20 ^{o}C for SOA formed in reactions of *n*-pentadecane with OH radicals formed in reactions of TME with excess O_3 (A) without and (B) with HNO_3. The signals from DOS were removed from the mass spectra.

m^{-3}, and an assumed mean molecular weight of OA of 300 g mol^{-1} and activity coefficient of unity. The calculated vapor pressures for the *n*-ketones, *n*-alcohols, and *n*-hydroperoxides are 3×10^{-1}, 3×10^{-2}, and 7×10^{-3} Pa and the calculated fractions in particles are approximately 0.1, 0.6, and 0.9. It is thus reasonable that all these products were detected in the particles.

The next highest mass peak in the spectra after *m/z* 211 is *m/z* 225, which is the largest peak in most of the real-time mass spectra shown in Figure 4.4. TPTD profiles of *m/z* 225 for reactions with excess O_3 and excess TME are shown in Figure 4.11 and TPTD mass spectra obtained at 61 ^{o}C for reactions with excess O_3 are shown in Figure 4.12. The large peak at *m/z* 225 is consistent with loss of OH from cyclic hemiacetals [**8**] (M = 242) and the desorption temperature of 61 ^{o}C is the same as that observed for the cyclic hemiacetals formed from reactions involving NO. A series of peaks at *m/z* 195, 181, 167… that are characteristic of the different isomers was also observed in the reaction with NO, but this series of peaks is smaller here especially at the higher masses. One possibility is that the distribution of isomers present in the particles is different for the two reactions due to effects of isomer structure on the branching ratios for reactions of 1,4-hydroxyperoxy radical reactions with NO and $R'O_2$• radicals, and also the dehydration of cyclic hemiacetals to dihydrofurans. The time profiles of *m/z* 225 for reactions with excess O_3 and excess TME (corrected for loss of aerosol to the chamber walls by using the decay in the DOS mass spectral signal at *m/z* 185) are shown in Figure 4.13. Both reactions without HNO_3 show rapid formation of cyclic hemiacetals within the first few minutes, when OH radicals are present, with no subsequent decay during the

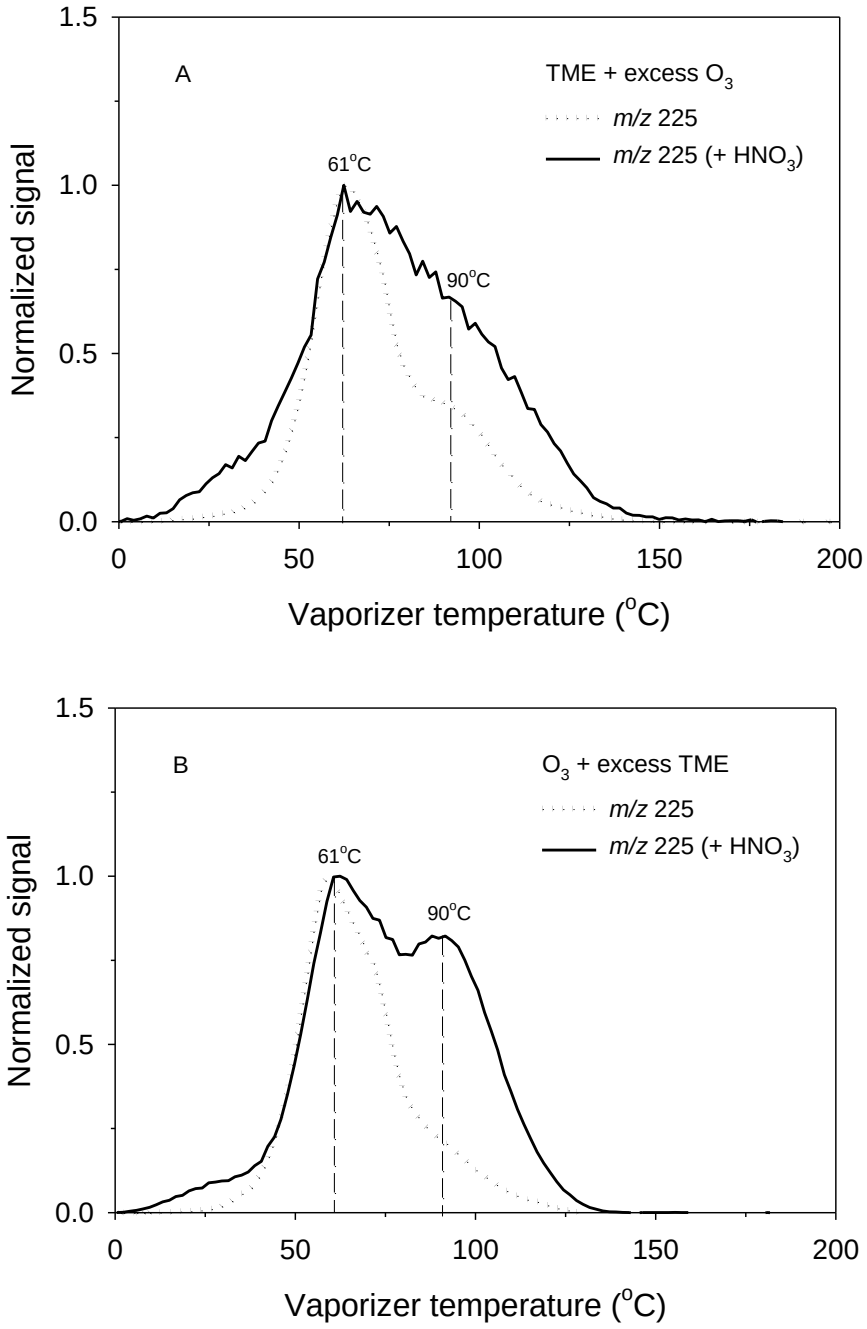

Figure 4.11. TPTD profiles of *m/z* 225 measured for SOA formed in reactions of *n*-pentadecane with OH radicals formed in reactions of (A) TME with excess O_3 and (B) O_3 with excess TME, without and with HNO_3. The signals from DOS were removed from the profiles and the signal was normalized to the maximum value.

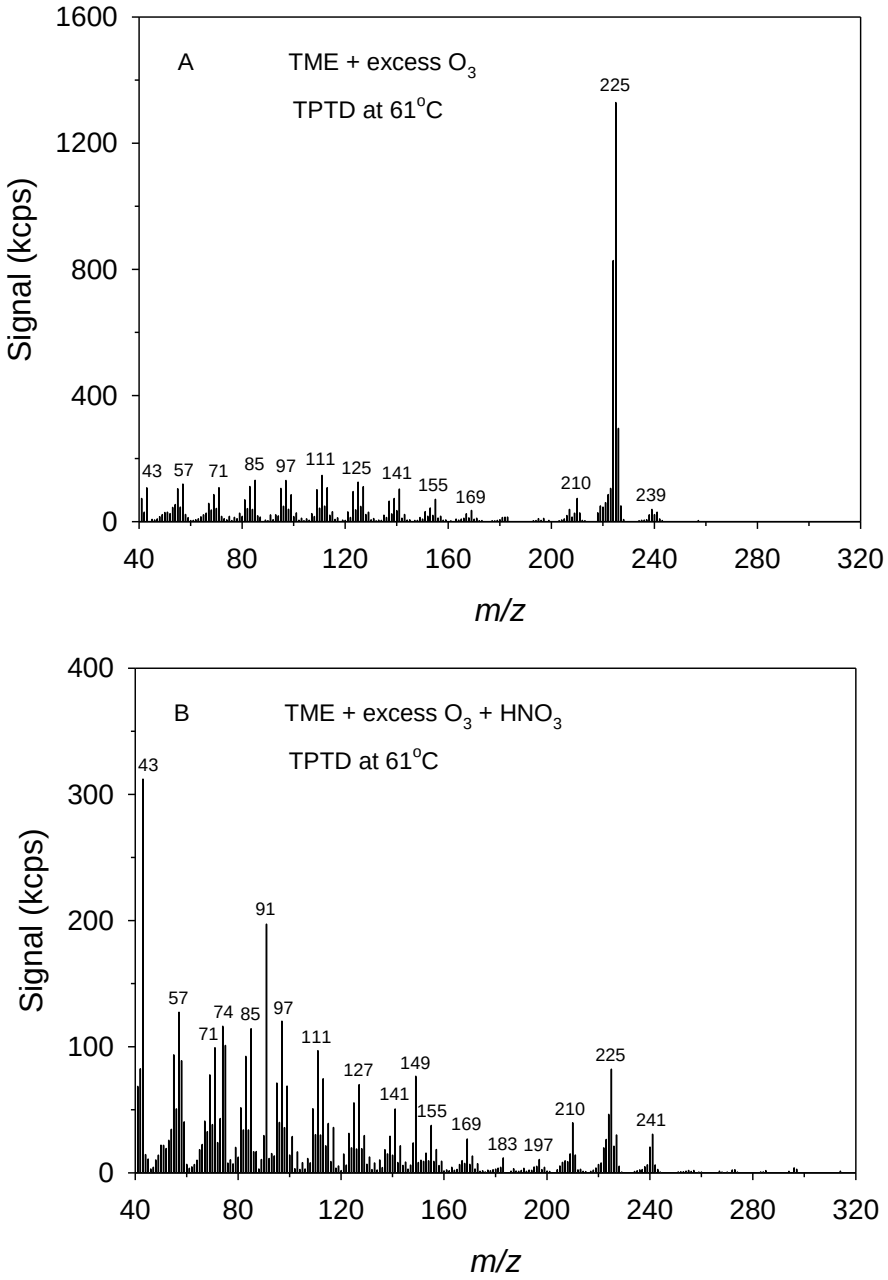

Figure 4.12. TPTD mass spectra measured at 61 °C for SOA formed in reactions of *n*-pentadecane with OH radicals formed in reactions of TME with excess O_3 (A) without and (B) with HNO_3. The signals from DOS were removed from the mass spectra.

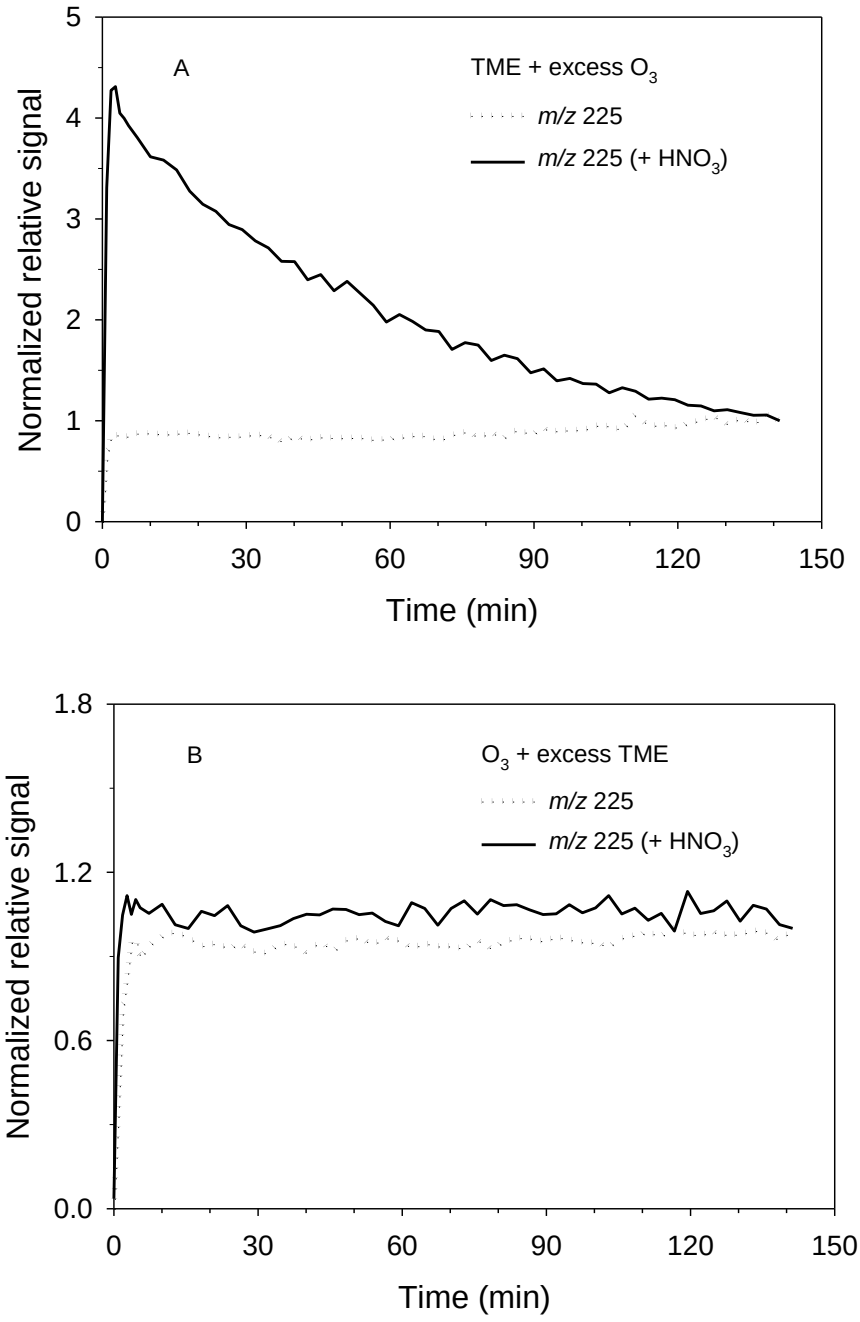

Figure 4.13. Real-time profiles of *m/z* 225 for SOA formed in reactions of *n*-pentadecane with OH radicals formed in reactions of (A) TME with excess O_3 and (B) O_3 with excess TME, without and with HNO_3. The *m/z* 225 signal was corrected for particle loss to the walls using the decay in the DOS mass spectral signal and the signal was normalized to the value at 140 min.

next 140 min. This indicates that cyclization of 1,4-hydroxycarbonyls to cyclic hemiacetals does not require strong acid such as HNO_3, consistent with solution studies on sugars [Swain and Brown 1952] which indicate that cyclization occurs via a concerted mechanism involving general acid-base catalysis with one step of the reaction catalyzed by weak acid and another step by weak base. Subsequent dehydration of cyclic hemiacetals to form dihydrofurans involves catalysis by H^+, as do other alcohols [Morrison and Boyd 1973], and thus requires HNO_3 (or another strong acid). The time profile for the reaction with excess TME and HNO_3 is similar to those without HNO_3, whereas time profile for the reaction with excess O_3 and HNO_3 decays continuously for 140 min after the initial rapid formation of cyclic hemiacetals. The dehydration rate constant, k_d, determined by fitting a first-order decay curve to this time profile is 0.02 min^{-1}, equivalent to a time scale of 50 min. This is the same value measured in Chapter 2 in the experiment with 1 min of irradiation, when HNO_3 formed by the reaction of OH radicals with NO_2 was present.

The next highest mass peaks in the spectra after *m/z* 225 are *m/z* 239 and 241, which are present in all the real-time mass spectra shown in Figure 4.4 although the relative intensity of *m/z* 239 is lower in the reactions with HNO_3. The peaks at *m/z* 239 and 241 can be explained as coming from the loss of OH from second-generation carbonyl cyclic hemiacetals (M = 256) and hydroxy cyclic hemiacetals (M = 258) formed from *n*-ketones and *n*-alcohols by the same radical initiated reactions that lead to cyclic hemiacetals (Figure 1). Loss of HO_2 from hydroperoxy cyclic hemiacetals (M = 274) formed from similar reactions of *n*-hydroperoxides could also contribute to the *m/z* 241 peak. The

TPTD profiles of *m/z* 239 and 241 for reactions with excess O_3 and excess TME are shown in Figures 4.14 and 4.15, respectively, and both exhibit peaks at ~70 ºC, which is consistent with them being slightly less volatile than cyclic hemiacetals due to the additional carbonyl and hydroxy groups.

The TPTD profiles of *m/z* 210, 211, 225, 239, and 241 (Figures 4.7, 4.9, 4.11, 4.14, and 4.15) all have interesting similarities with regards to the effects of excess O_3, excess TME, and HNO_3. In general, for a particular *m/z* value the profiles for reactions with excess O_3 without and with HNO_3 are similar above ~50 ^{o}C with a peak at ~60–70 ^{o}C and a shoulder centered at ~90–100 ^{o}C. The profiles for reactions with excess TME without HNO_3 are similar to those with excess O_3, but for reactions with HNO_3 the shoulder at ~90–100 ^{o}C is significantly larger. Furthermore, TPTD mass spectra at 61 ^{o}C (Figure 4.12) for reactions with excess O_3 are similar to those at 90 ^{o}C (Figure 4.16), indicating that the SOA composition is similar. These observations can be explained by considering the two potential effects of HNO_3 on the reactions: catalysis of the dehydration of cyclic hemiacetals (including the carbonyl and hydroxy substituted compounds) to form dihydrofurans, and catalysis of acetal formation from reactions of cyclic hemiacetals and *n*-alcohols according to the reaction

$$ROH + R'OH \rightarrow ROR' + H_2O$$

where ROH and R'OH are not both *n*-alcohols. For the cyclic hemiacetals this reaction is similar to the acid-catalyzed reversion reaction that occurs with sugars such as glucose

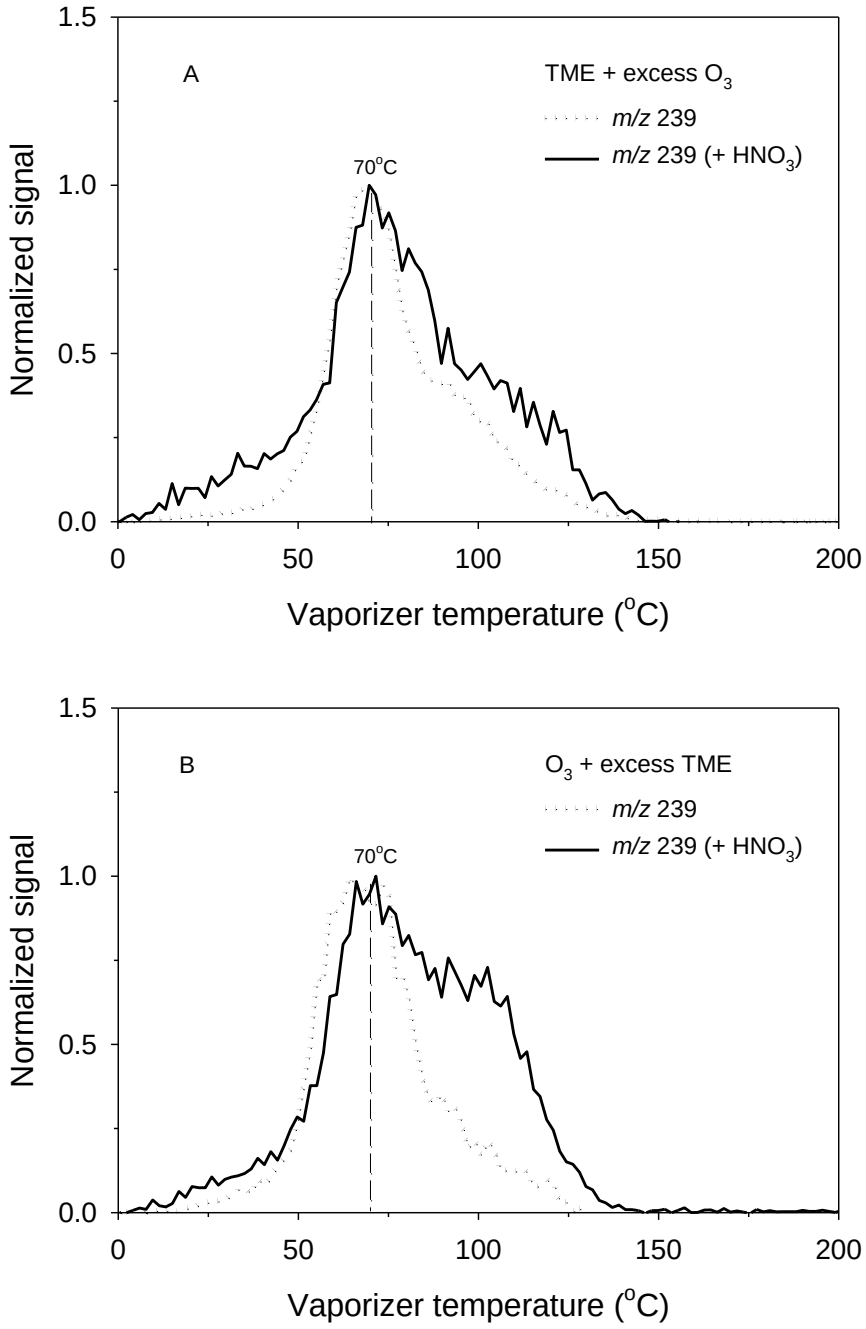

Figure 4.14. TPTD profiles of *m/z* 239 measured for SOA formed in reactions of *n*-pentadecane with OH radicals formed in reactions of (A) TME with excess O_3 and (B) O_3 with excess TME, without and with HNO_3. The signals from DOS were removed from the profiles and the signal was normalized to the maximum value.

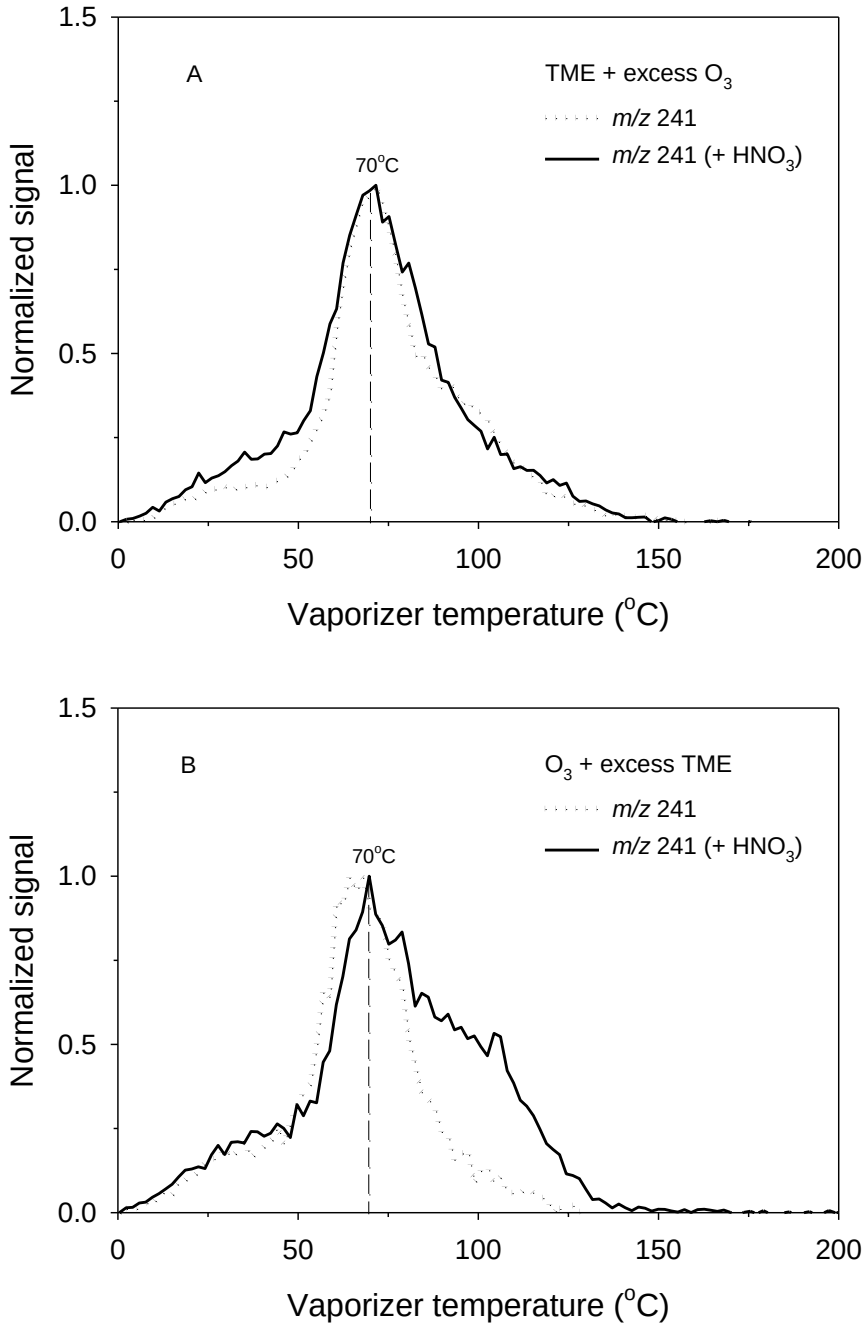

Figure 4.15. TPTD profiles of *m/z* 241 measured for SOA formed in reactions of *n*-pentadecane with OH radicals formed in reactions of (A) TME with excess O_3 and (B) O_3 with excess TME, without and with HNO_3. The signals from DOS were removed from the profiles and the signal was normalized to the maximum value.

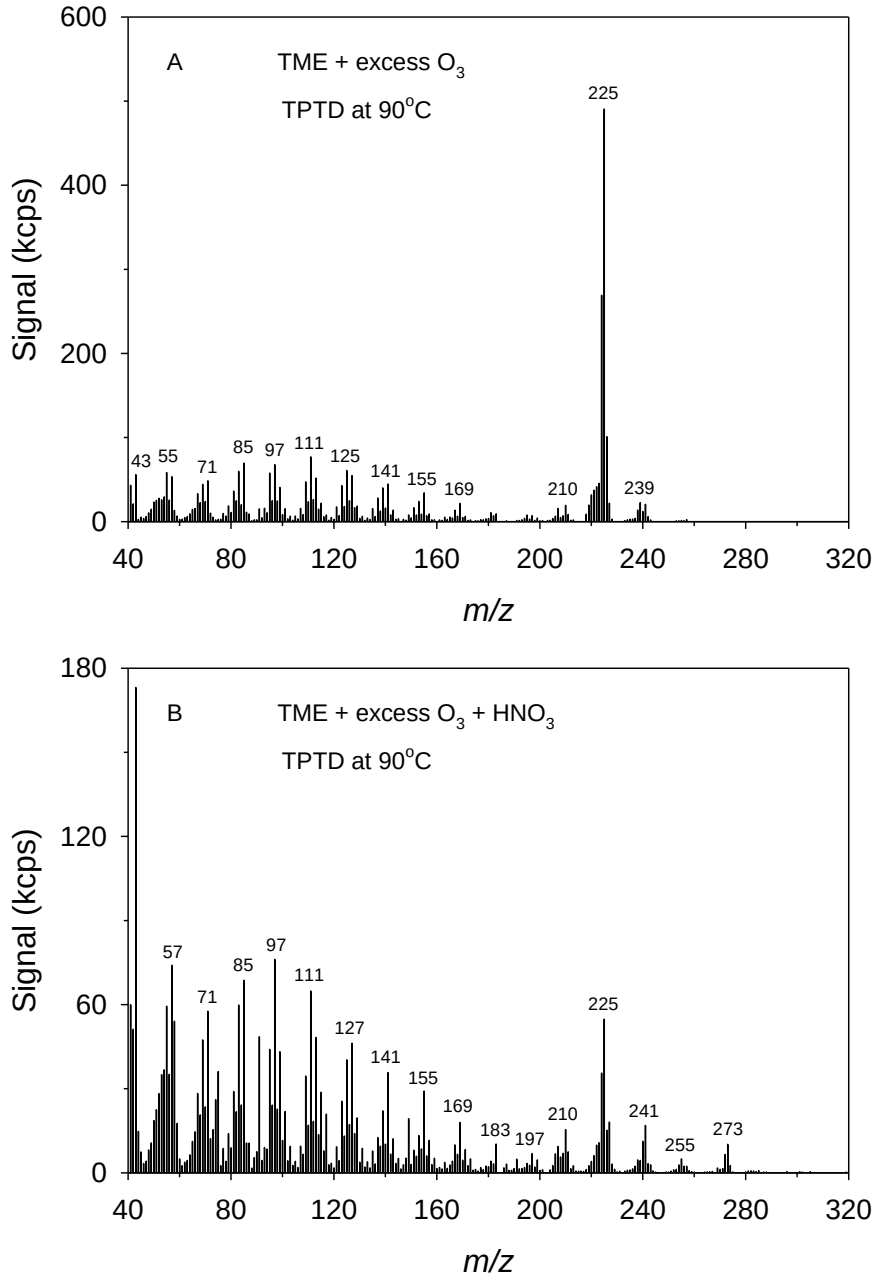

Figure 4.16. TPTD mass spectra measured at 90 ^{o}C for SOA formed in reactions of *n*-pentadecane with OH radicals formed in reactions of TME with excess O_3 (A) without and (B) with HNO_3. The signals from DOS were removed from the mass spectra.

and fructose [van Dam et al. 1986]. These acetal products should desorb at higher temperatures than the cyclic hemiacetals, but their mass spectra should be similar since α-cleavage following ionization of the O atoms in the furan ring will generate the same ions. The snaller effect of HNO_3 on acetal formation in reactions with excess O_3 compared to excess TME is probably caused by rapid reaction of O_3 with dihydrofurans formed by dehydration of cyclic hemiacetals in the presence of HNO_3, which shifts the equilibrium towards dihydrofurans such that dehydration competes with acetal formation (Figure 4.2).

The peaks at *m/z* 210 and 211 in the mass spectra at 61 and 90 ^{o}C can be explained as being due to acetals formed by reactions of cyclic hemiacetals with *n*-alcohols. These compounds should desorb in this temperature range and their mass spectra should contain the same peaks as the cyclic hemiacetals and the *n*-alcohols. H-atom transfer from the 2-carbon on the cyclic furan ring to the O atom that links the two monomers followed by decomposition will lead to an *n*-alcohol ion + dihydrofuran. Subsequent loss of H_2O and further fragmentation of the *n*-alcohol ion will lead to peaks at *m/z* 210 and at *m/z* 213, 199, 185, … as discussed above. The peak at *m/z* 211 is likely due to α-cleavage at the O atom that links the two monomers [McLafferty and Turecek 1993].

Ionization of acetals should also lead to peaks other those observed in the cyclic hemiacetal mass spectra. In particular, α-cleavage at the O atom that links the two monomers [McLafferty and Turecek 1993] will add an O atom to the ions responsible for the peaks at *m/z* 225, 239, and 241 in the acetal mass spectra resulting in *m/z* 241, 255, and 257 ions. These effects are apparent in the real-time mass spectra for reactions with

excess O_3 (excess TME mass spectra were similar) shown in Figure 4.4. Note that for the reactions without HNO_3 the peak at *m/z* 239 is larger than the peak at *m/z* 241, but that for the reactions with HNO_3 the peak at *m/z* 239 is much smaller. The likely reason for this is that when the cyclic hemiacetals dehydrate or react to form acetals, their contributions to the peaks at *m/z* 225, 239, and 241 decrease. Ionization of the acetals also leads to *m/z* 225, 239, and 241 ions, thus compensating to some extent for this loss, and by other pathways *m/z* 241, 255, and 257 ions. The m/z 241 ions formed by these latter pathways therefore leads to a relative increase in the *m/z* 241 peak compared to *m/z* 225 and 239.

Another noteworthy feature of the real-time mass spectra shown in Figure 4.4 is the appearance of a peak at *m/z* 269 in the reactions with HNO_3, and which decreases significantly between 10 and 120 min. The time profiles of *m/z* 269 for reactions with excess O_3 and excess TME (corrected for loss of aerosol to the chamber walls by using the decay in the DOS mass spectral signal at *m/z* 185) are shown in Figure 4.17. In the absence of HNO_3 the *m/z* 269 signal increases immediately and rapidly after the reaction is initiated and then remains nearly constant for ~5–10 min before decaying continuously until the experiment ends at 140 min. The rate constant for decay, k_d, determined by fitting a first-order decay curve to this time profile is 0.04 min^{-1}, equivalent to a time scale of 25 min. This is rate constant is twice the value measured for the dehydrations of cyclic hemiacetals. The compound associated with *m/z* 269 is probably also undergoing acid-catalyzed dehydration, given the similarities in the time scales and the lack of reasonable alternative explanations.

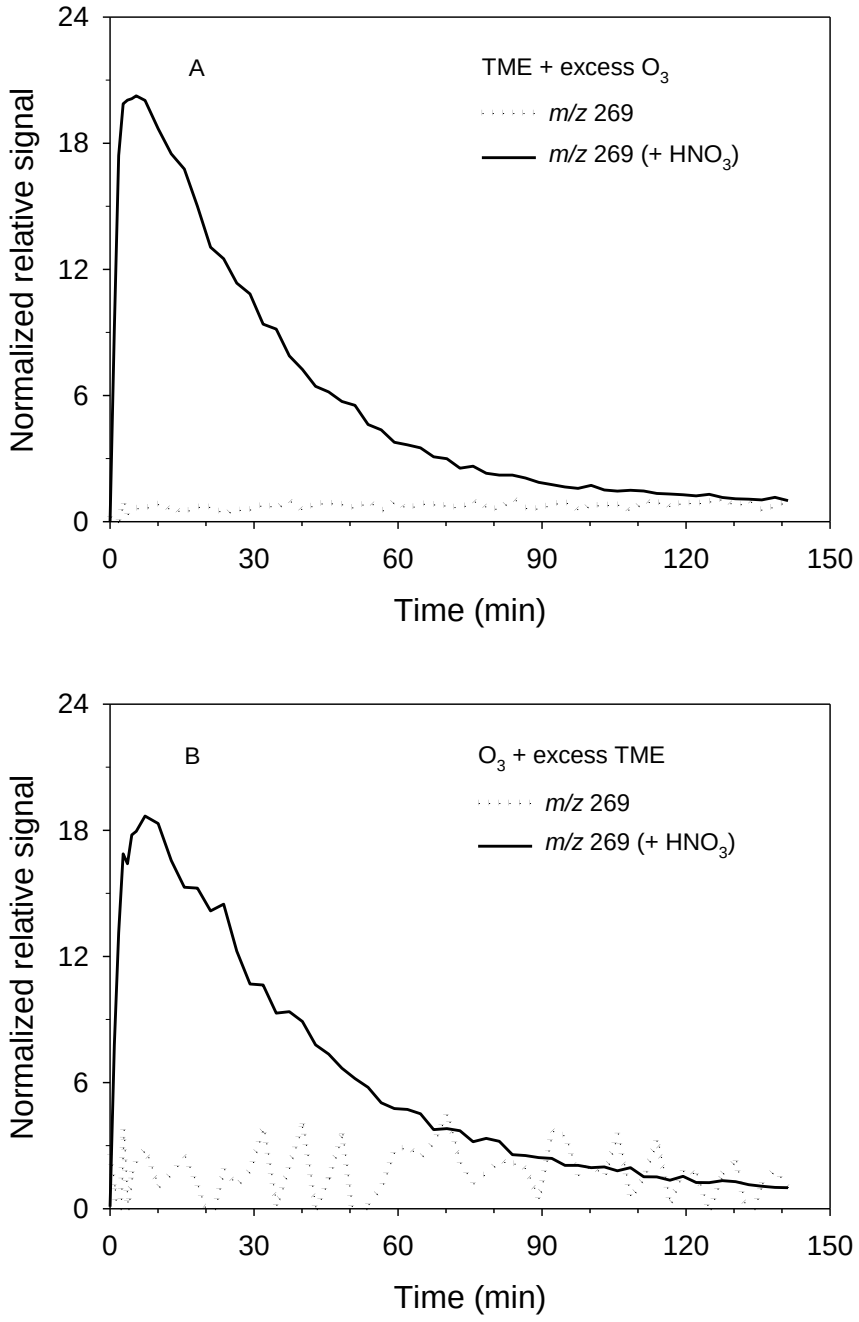

Figure 4.17. Real-time profiles of *m/z* 269 for SOA formed in reactions of *n*-pentadecane with OH radicals formed in reactions of (A) TME with excess O_3 and (B) O_3 with excess TME, without and with HNO_3. The *m/z* 269 signal was corrected for particle loss to the walls using the decay in the DOS mass spectral signal and the signal was normalized to the value at 140 min.

The identity of the compound associated with *m/z* 269 is not obvious, since none of the first- or second-generation cyclic hemiacetals discussed thus far should give this peak. The observation that the compound forms only when HNO_3 is present indicates that its formation involves dehydration of cyclic hemiacetals, since these reactions require the acid catalyst whereas acetal formation appears to be enhanced in the presence of HNO_3 but not require it. Furthermore, the observation that the compound decays rapidly beginning 5–10 min after formation indicates that it is a substituted cyclic hemiacetal. A compound with these properties could be formed by reaction of OH radicals with 1,4-hydroxycarbonyls to for products containing two 1,4-hydroxycarbonyl groups. Cyclization of one of these groups, followed by dehydration and reaction with either O_3 or OH radicals would lead to the formation of (among other products) 1,4-hydroxycarbonyl carbonylesters, with molecular weight 286. Cyclization of the 1,4-hydroxycarbonyl group would lead to a cyclic hemiacetal carbonylester, which, like other cyclic hemiacetals is expected form predominantly *m/z* 269 ions via loss of OH when ionized. The formation of second-generation 1,4-hydroxycarbonyl cyclic hemiacetals is certainly plausible, since the second-generation carbonyl and hydroxy cyclic hemiacetals were observed. Subsequent dehydration and reaction with OH radicals or O_3 during the two minute period when OH radicals are present is also plausible, since in the high NO_x reactions of *n*-pentadecane discussed in Chapter 3 cyclic hemiacetal nitrates were formed in 1 min of exposure to OH radicals from reactions of dihydrofurans.

Although we have focused here on interpreting the high mass peaks in the mass spectrum, since these tend to be the most characteristic of particular compounds and

therefore of the most use for identification, there are a few peaks that appear at *m/z* < 150 that deserve comment. In particular, in the real-time mass spectra shown in Figure 4 there are unusually large peaks at *m/z* 75, 91, and 149. These are not due to reactions involving *n*-pentadecane, but are instead fragments of hemiacetal oligomers formed from hydroxyacetone, $CH_3C(O)CH_2OH$, which is a major product of the reaction of TME with O_3 with a molecular weight of 74. The oligomers are formed via the reaction

$$n\ CH_3C(O)CH_2OH \rightarrow CH_3C(O)CH_2\text{-}O\text{-}[C(CH_3)(OH)CH_2]_{n\text{-}2}\text{-}O\text{-}C(CH_3)(OH)CH_2OH$$

Hemiacetals oligomers formed from glycolaldehyde ($HCOCH_2OH$) and other small multifunctional compounds have been observed in high-resolution mass spectra of SOA formed from the reaction of isoprene with OH radicals [Nguyen et al. 2011]. The conclusion that hydroxyacetone does not participate otherwise in SOA formation in these reactions is supported by the observation that the results of experiments conducted by forming OH radicals by photolysis of H_2O_2 rather than by the reaction of TME with O_3 are similar. These results are discussed below.

Reactions with OH radicals formed from H_2O_2 photolysis.

SOA yields. The organic aerosol (OA) mass concentrations measured over the course of a reaction with OH formation by H_2O_2 photolysis are shown in Figure 4.18. The concentrations have been corrected for loss of aerosol to the chamber walls by using the decay in the DOS mass spectral signal at *m/z* 185. The initial OA mass concentration was ~200 μg m^{-3} from DOS seed particles, and over the course of 80 min of OH exposure

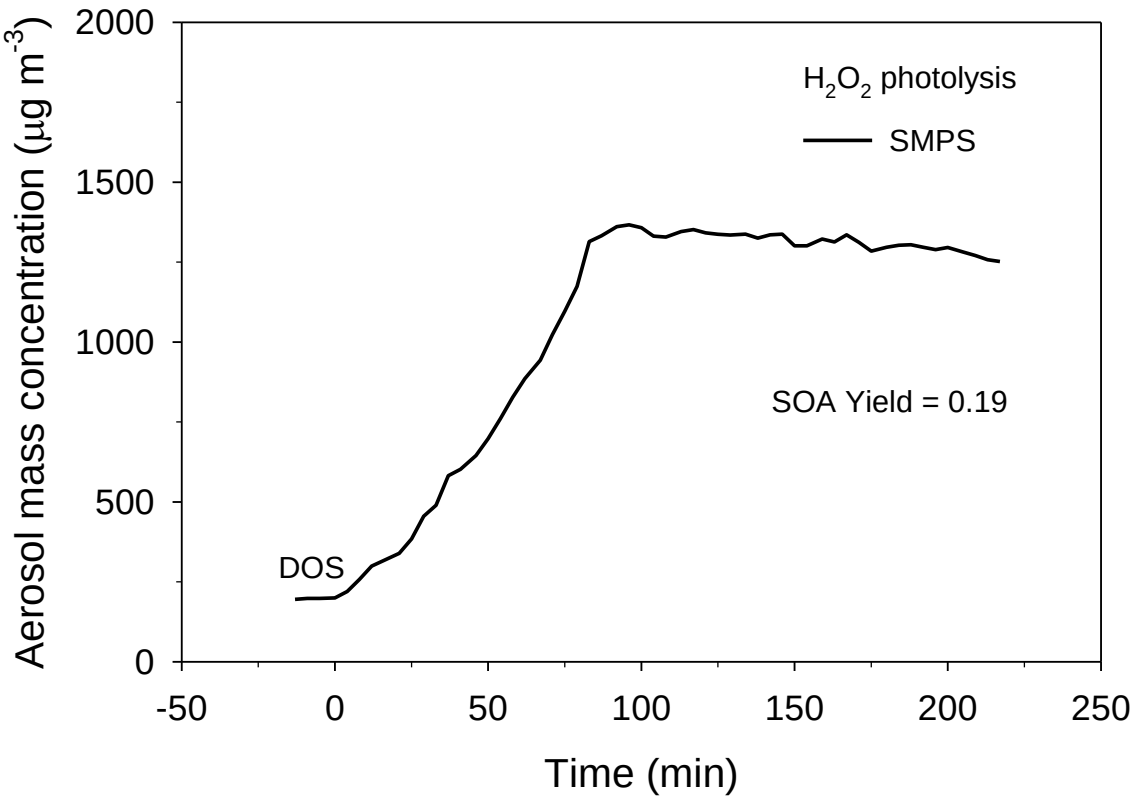

Figure 4.18. Aerosol mass concentrations and SOA yield measured using the SMPS during reactions of *n*-pentadecane with OH radicals formed by photolysis of H_2O_2. Aerosol mass concentrations and SOA yields were corrected for loss of aerosol to the chamber walls by using the decay in the DOS mass spectral signal.

increased to a corrected maximum value of ~1350 μg m^{-3}. After the lights were turned off the corrected OA mass concentrations decreased slowly to ~1250 μg m^{-3}. The SOA yield was 0.19, about one-half the yield in the O_3 + TME experiments without HNO_3. The amount of *n*-petadecane reacted was 0.69 ppmv, significantly less than in the other experiments, but probably not responsible for the much lower SOA yield. More likely, the lower yield is due to loss of semi-volatile products to the chamber walls, as is indicated by the apparent evaporation of particles after the lights were turned off [Matsunaga and Ziemann 2010]. The time profiles of single ions (not shown) are similar to the SMPS profile, except for *m/z* 211, which peaks at 80 min and then decays by ~30% in ~20 min and the decays similar to the SMPS profile.

RTMS and TPTD analysis. A real-time mass spectrum obtained 100 min after the start (20 min after turning off the lights) of the reaction with OH formation by H_2O_2 photolysis is shown in Figure 4.19. The signals from DOS have been removed and the mass spectrum corrected for particle loss to the walls using the DOS signal. The spectrum is similar to the ones shown in Figure 4.4 for reactions with TME and excess O_3 without HNO_3, indicating similar SOA chemical compositions. TPTD profiles of the total ions and *m/z* 210, 211, 225, 239, and 241 (with the contribution for DOS removed) are shown in Figure 4.20. The SOA desorbs between ~0–125 ^{o}C and the profile is more similar to the one measured for the excess O_3 reactions than for the excess TME reactions, without HNO_3 (Figure 4.5), although it has a significantly larger peak at 90 ^{o}C than either of those. There are peaks at ~10 ^{o}C in the *m/z* 210 and 211 profiles and in all profiles there

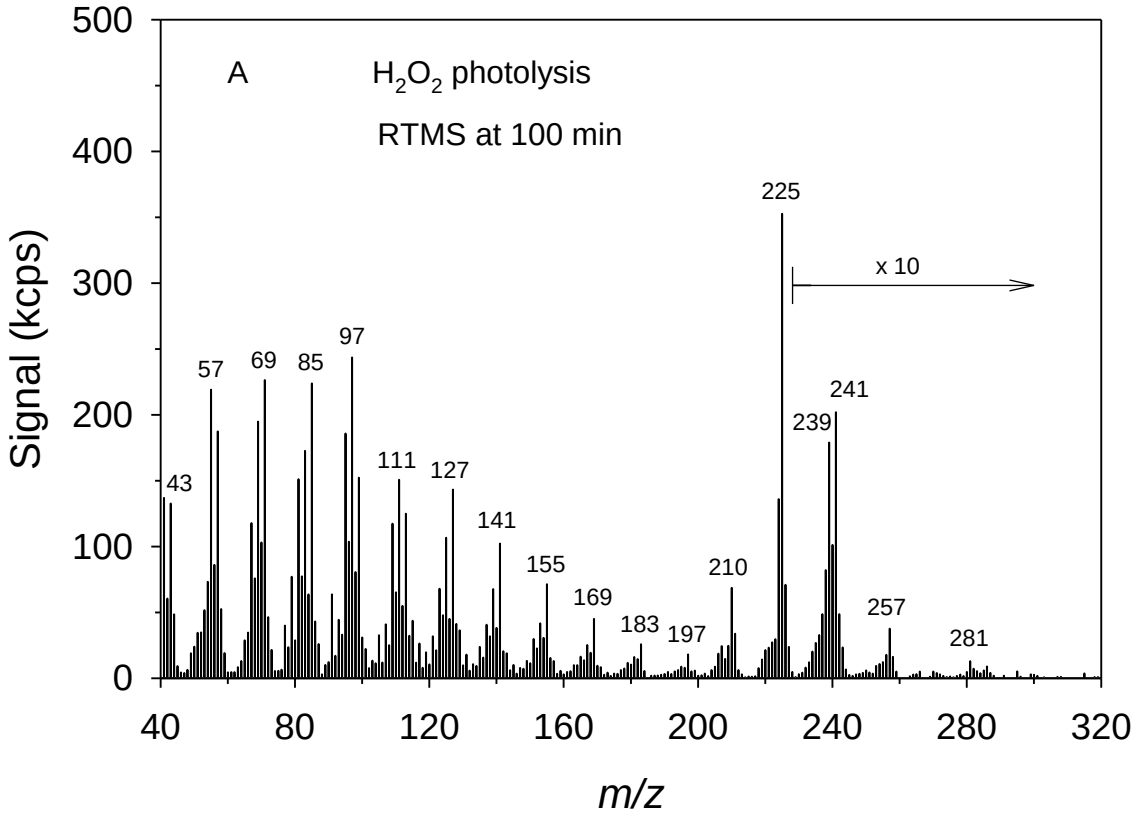

Figure 4.19. Real-time mass spectra of SOA formed in reactions of *n*-pentadecane with OH radicals formed from photolysis of H_2O_2. The signals from DOS were removed from the mass spectra and the mass spectrum at 100 min was corrected for particle loss to the walls using the decay in the DOS mass spectral signal.

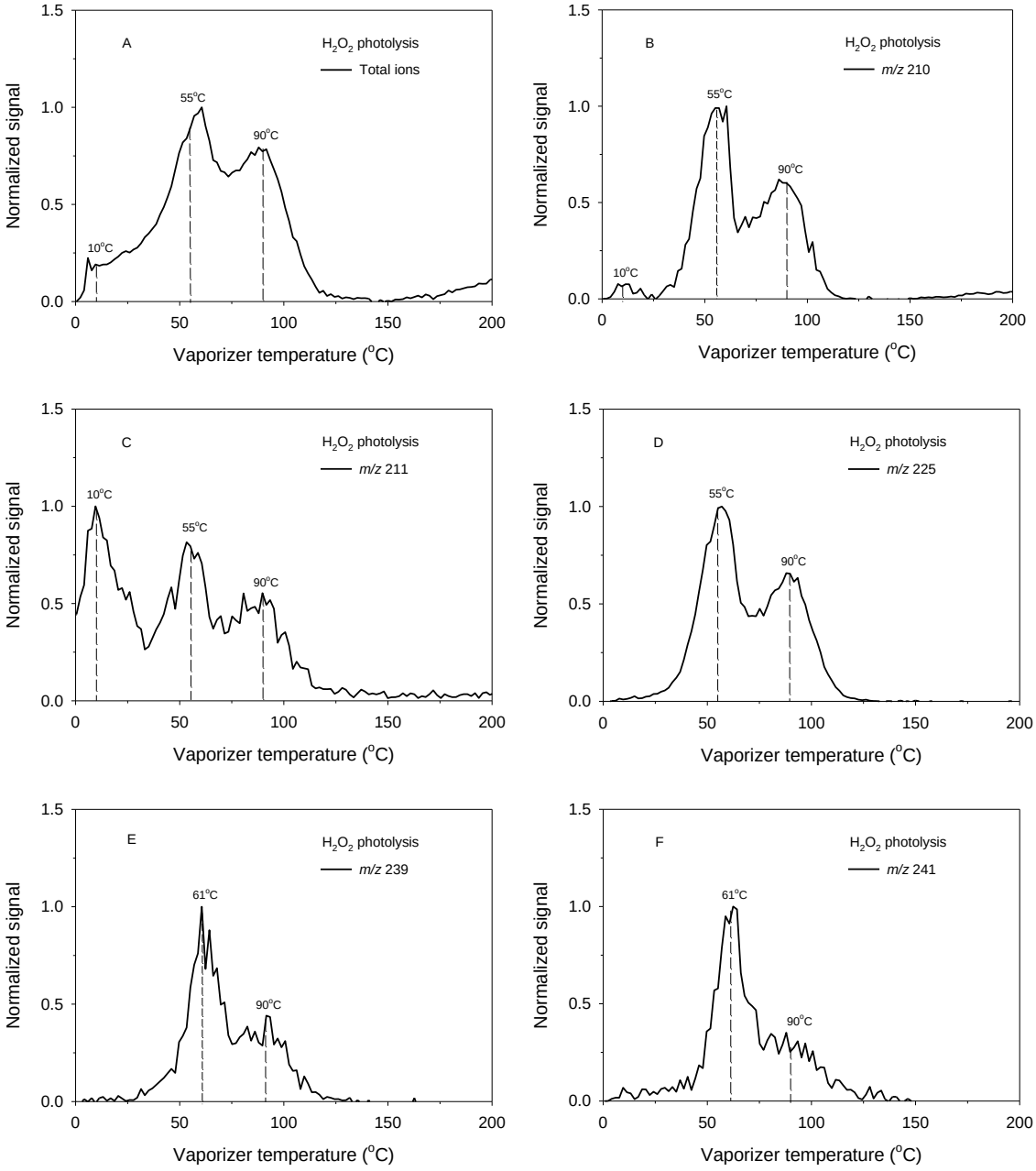

Figure 4.20. TPTD profiles of (A) total ions, (B) *m/z* 210, (C) *m/z* 211, (D), *m/z* 225, (E) *m/z* 239, and (F) *m/z* 241 measured for SOA formed in reactions of *n*-pentadecane with OH radicals formed by photolysis of H_2O_2. The signals from DOS were removed from the profiles and the signal was normalized to the maximum value.

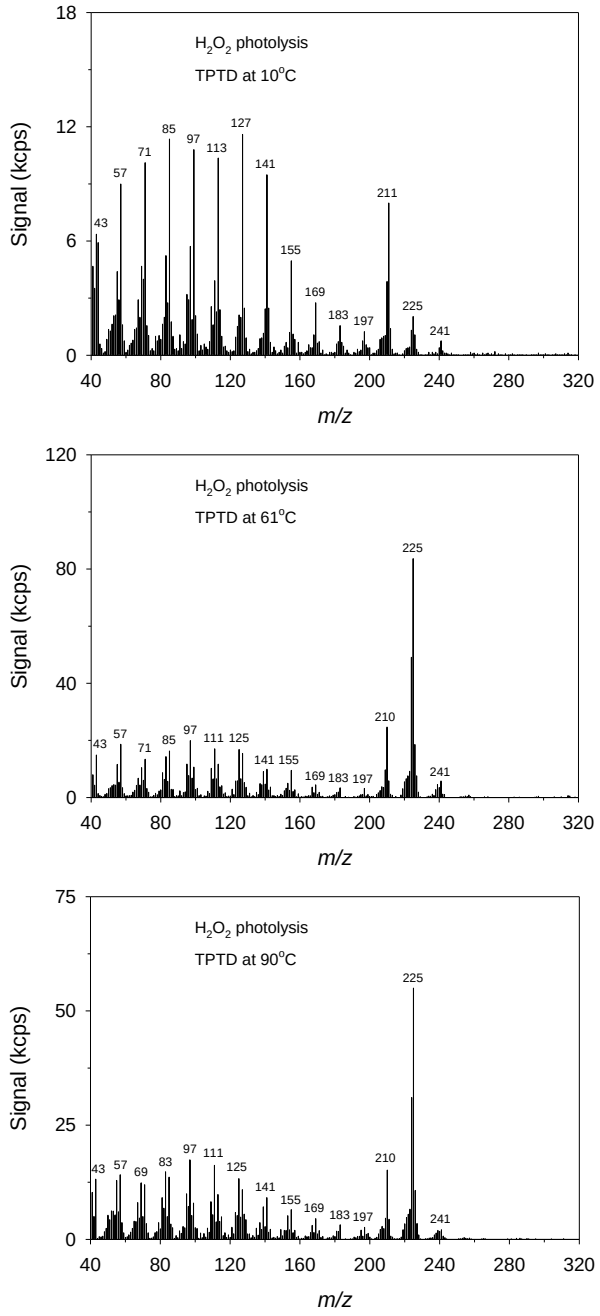

Figure 4.21. TPTD mass spectra measured at 10, 61, and 90 ^{o}C for SOA formed in reactions of *n*-pentadecane with OH radicals formed by photolysis of H_2O_2. The signals from DOS were removed from the mass spectra.

are peaks ~60 and 90 ^{o}C, similar to those measured for the TME + O_3 reactions without HNO_3 although some of the peak temperatures are slightly different.

TPTD mass spectra measured at 10, 61, and 90 ^{o}C for reactions with OH formation by H_2O_2 photolysis are shown in Figure 4.21. The mass spectrum at 10 ^{o}C is the same at that shown in Figure 4.9 for reactions with excess O_3 and excess TME at 20 ^{o}C and is characteristic of *n*-hydroperoxides. There is no evidence for *n*-alcohols, which were observed in the reactions with excess O_3 and TME and desorbed at ~10 ^{o}C (Figure 4.7). Gas-particle partitioning calculations for an *n*-hydroperoxide with a vapor pressure of 3×10^{-2} obtained from the calibration equation given above and a desorption temperature of 10 ^{o}C, and an average OA mass concentration during the 80 reaction of 600 μg m^{-3} gives an average fraction of compound in the particles of ~0.1. This value is ~ 6× lower than in the excess O_3 and excess TME experiments because of the much lower OA mass concentration, as is likely responsible for the absence of *n*-ketones and *n*-alcohols in the SOA formed in this experiment since they are more volatile than n-hydroperoxides. The TPTD mass spectra measured at 61 and 90 ^{o}C are similar to those measured at those temperatures for the excess O_3 and excess TME reactions, indicating the presence of cyclic hemiacetals, carbonyl and hydroxy hemiacetals, and acetals formed from these compounds and *n*-alcohols.

Functional group analysis.

The results of functional group analysis of the SOA formed in reactions with OH radicals formed from reactions of TME + O_3 without and with HNO_3 and from H_2O_2

Table 4.2. Functional group composition of SOA products formed from the reaction of *n*-pentadecane with OH radicals in the absence of NO_x.

Functional group	Functional group/C_{15} molecule								
	exp. 1	exp. 2	exp. 3	exp. 4	exp. 5	exp. 6	exp. 7	Average Exp. 1-3	Average Exp. 4-6
hydroxyl [CH_2OH]	0.48	0.56	0.57	0.52	0.64	0.71	0.41	0.54 ± 0.05	0.62 ± 0.10
carbonyl [C(O)]	0.40	0.39	0.30	0.82	1.09	0.90	0.25	0.36 ± 0.06	0.94 ± 0.14
ester [C(O)O]-R	0.00	0.02	0.01	0.13	0.21	0.07	0.00	0.01 ± 0.01	0.14 ± 0.07
carboxyl [C(O)OH]	0.26	0.14	0.26	0.37	0.19	0.19	0.12	0.22 ± 0.07	0.25 ± 0.10
peroxide [CHOOH]	0.27	0.20	0.27	0.34	0.45	0.67	0.19	0.25 ± 0.04	0.49 ± 0.17
methylene [CH_2]	13.59	13.69	13.59	12.82	12.42	12.46	14.02	13.62 ± 0.11	12.57 ± 0.27
total – methylene [15 – CH_2]	1.41	1.31	1.41	2.18	2.58	2.54	0.98	1.38 ± 0.11	2.43 ± 0.27
Elemental composition[1]									
O/C	0.13 (0.17)		0.13 (0.15)	0.20 (0.16)				0.13 ± 0.00 (0.16 ± 0.01)	0.20 (0.16)
H/C	1.94 (2.53)		1.93 (2.10)	1.94 (1.72)				1.94 ± 0.01 (2.32 ± 0.30)	1.94 (1.72)

[1]The values were calculated from functional group composition analysis and the values in parentheses were calculated from elemental analysis.

photolysis are shown in Table 4.2. Carbonyl, hydroxyl, peroxide, and carboxyl groups were detected in all experiments, and in the experiments with HNO_3 ester groups were also detected. The composition of SOA formed from reactions with excess O_3 (Exps. 1 and 2) and excess TME (Exp. 3) without HNO_3 were similar, as were those performed with excess O_3 (Exps. 4 and 5) and excess TME (Exp. 6) with HNO_3. The results for reactions without HNO_3 (Exps. 1–3) and with HNO_3 (Exps. 4–6), respectively, were therefore averaged for ease of comparison with each other and the results for the H_2O_2 photolysis reaction (Exp. 7). There are a number of interesting observations to be made from these results. First, however, it is necessary to note that to properly interpret the results for carbonyl and hydroxyl groups one must be aware that analysis of carbonyls is conducted under acidic conditions in which cyclic hemiacetals and acetals (including carbonyl and hydroxyl substituted versions) will hydrolyze and be quantified as 1,4-hydroxycarbonyls, whereas analysis of hydroxyl groups is conducted under basic conditions in which hydrolysis does not occur. Thus, cyclic hemiacetals will be quantified as 1,4-hydroxycarbonyls since both have a hydroxyl group whereas the two hydroxyl groups lost when acetals are formed will not be detected. For example, for an unsubstituted cyclic hemiacetal formed from a 1,4-hydroxycarbonyl one carbonyl and one hydroxyl group will be measured, whereas for an acetal formed from two of these cyclic hemiacetals two carbonyl groups will be measured but no hydroxyl groups.

In the reactions without HNO_3 (including TME + O_3 and H_2O_2 photolysis reactions) the number of hydroxyl, carbonyl, ester, carboxyl, and peroxide groups per C_{15} molecule are similar, and are approximately 0.50, 0.30, 0.00, 0.17, and 0.22. The significant excess

of hydroxyl groups compared to carbonyl groups can be interpreted based on the reaction mechanisms shown in Figures 4.1 and 4.2 in which the major products are *n*-ketones, *n*-alcohols, *n*-hydroperoxides, cyclic hemiacetals, and acetals (not shown in the figures), and the cyclic hemiacetals do not dehydrate and react further because of the absence of HNO_3. Other products can include 1,4-diols and 1,4-hydroxyhydroperoxides and second-generation products of reactions of *n*-ketones and *n*-alcohols. In general, carbonyl and hydroxyl groups are formed in pairs, such as *n*-ketone [**3**] + *n*-alcohol [**2**] or a 1,4-hydroxycarbonyl [**6**,**7**]. An excess of hydroxyl groups in SOA can result from reactions that involve isomerization, such as those that form 1,4-hydroxyhydroperoxides and 1,4-diols, or because *n*-ketones are much more volatile than *n*-alcohols and so do not partition as much to the particle phase. It is apparent from the SOA mass spectral analysis that *n*-ketones were barely detectable or absent, whereas *n*-alcohols were clearly present at least in the TME + O_3 reactions. No peaks were identified in mass spectra that were obviously characteristic of 1,4-hydroxyhydroperoxides or 1,4-diols, so their presence in the SOA is uncertain. Overall, it appears that the excess of hydroxyl groups from the pathways described above more than compensate for the hydroxyl groups not detected (compared to carbonyls) because of acetal formation. The similar concentrations of peroxide groups compared to carbonyl and hydroxyl groups indicates that both $RO_2\bullet$ + $RO_2\bullet$ and $RO_2\bullet$ + HO_2 reactions are significant under these reaction conditions. The presence of carboxyl groups is surprising, since formation of carboxylic acids is not predicted to occur in the absence of HNO_3. It is possible to propose a plausible mechanism for their formation

involving the reaction of OH radicals with cyclic hemiacetals, but the source of these carboxylic acids will be investigated in the future.

The most obvious difference in functional group composition is between reactions conducted without and with HNO_3, and these differences are also consistent with the reaction mechanisms shown in Figures 4.1 and 4.2. The reason that esters are only present in SOA formed from reactions with HNO_3 is because they are formed from reactions of OH radicals or O_3 with dihydrofurans, which are formed by acid-catalyzed dehydration of cyclic hemiacetals. The higher concentrations of carbonyl, peroxide, and carboxyl groups in the HNO_3 reactions is also reasonable, since reactions of dihydrofurans with O_3 (the dominant reaction, as discussed above) lead to a variety of products that contain these functional groups, some of which are shown in Figure 2.

4.4 Conclusions

In this chapter the functional group analysis methods described in Chapter 2 were used with thermal desorption particle beam mass spectrometry to investigate the chemical composition of secondary organic aerosol formed from the OH radical-initiated reaction of *n*-pentadecane in the absence of NO_x. The OH radicals were generated by two different methods in the presence and absence of O_3 and HNO_3. Results of functional group analysis indicate the presence of carbonyl, hydroxyl, peroxide, and carboxyl groups in SOA formed in all reactions, and ester groups were also present in reactions with HNO_3. The major SOA products appear to be first-generation *n*-ketones, *n*-alcohols, *n*-hydroperoxides, and cyclic hemiacetals, second-generation carbonyl and hydroxy

cyclic hemiacetals, and acetals formed from heterogeneous/multiphase reactions of these various cyclic hemiacetals with each other and with *n*-alcohols. In was shown that cyclization of 1,4-hydroxycarbonyls to cyclic hemiacetals occurs rapidly on/in particles in the absence of HNO_3, but that dehydration to form dihydrofurans requires HNO_3 to catalyze the reaction, which occurred on the same time scale here (~50 min) as in reactions conducted in the presence of NO_x that are described in Chapter 3. The heterogeneous/multiphase formation of acetals also appears to be catalyzed by HNO_3. The formation of dihydrofurans results in the subsequent formation of a number of additional products via reaction with (primarily) O_3, including carbonylesters and other products containing ester groups. The results of functional group analysis were also in good agreement with the results of elemental CHON analysis. These results demonstrate the value of these functional group analysis methods for SOA studies and lend additional support for the currently accepted mechanism of SOA formation from reactions of alkanes with OH radicals in the absence of NO_x, including the role of heterogeneous/multiphase reactions.

4.5 References

Allan, J. D., Jimenez, J. L., Williams, P. I., Alfarra, M. R., Bower, K. N., Jayne, J. T., Coe, H., and Worsnop, D. R. Quantitative Sampling Using an Aerodyne Aerosol Mass Spectrometer 1. Techniques of Data Interpretation and Error Analysis. *J. Geophys. Res.*, 108(D3), 4090, DOI: 10.1029/2002JD002358 (2003).

Andreae, M.O., and Rosenfeld, D. Aerosol-Cloud-Precipitation Interactions. Part 1. The Nature and Sources of Cloud-Active Aerosols. *Earth-Sci. Rev.*, 89, 13-41 (2008).

Arey, J., Aschmann, S. M., Kwok, E. S. C., and Atkinson, R. Alkyl Nitrate, Hydroxyalkyl Nitrate, and Hydroxycarbonyl Formation from the NO_x-Air Photooxidations of C_5-C_8 *n*-alkanes. *J. Phys. Chem. A*, 105, 1020-1027 (2001).

Atkinson, R. Gas-Phase Tropospheric Chemistry of Volatile Organic Compounds: 1. Alkanes and Alkenes. *J. Phys. Chem. Ref. Data*, 26, 215-290 (1997).

Atkinson, R., and Arey, J. Atmospheric Degradation of Volatile Organic Compounds. *Chem. Rev.*, 103, 4605-4638 (2003).

Atkinson, R., Arey, J., and Aschmann, S. M. Atmospheric Chemistry of Alkanes: Review and Recent Developments. *Atmos. Environ.*, 42, 5859-5871 (2008).

Banerjee, D. K., and Budke, C. C. Spectrophotometric Determination of Traces of Peroxides in Organic Solvents. *Anal. Chem.*, 36, 792-796 (1964).

Burgess, A. R., Lane, R.D. G., and Sen Sharma, D. K. Mass Spectrometric Study of Some Alkyl Hydroperoxides. *J. Chem. Soc. B.*, 341-347 (1969).

Calvert, J. G., Atkinson, R., Kerr, J. A., Madronich, S., Moortgat, G. K., Wallington, T. J., and Yarwood, G. *The Mechanisms of Atmospheric Oxidation of the Alkenes,* Oxford University Press, New York. (2000).

Chattopadhyay, S., and Ziemann, P. J. Vapor Pressures of Unsubstituted and Substituted Monocarboxylic and Dicarboxylic Acids Measured Using an Improved Thermal Desorption Particle Beam Mass Spectrometry Method. *Aerosol Sci. Technol.*, 39, 1085-1100 (2005).

Davidson, C. I., Phalen, R. F., and Solomon, P.A. Airborne Particulate Matter and Human Health: A Review. *Aerosol. Sci. Technol.*, 39, 737-749 (2005).

de Gouw, J., and Jimenez, J. L. Organic Aerosols in the Earth's Atmosphere. *Environ. Sci. Technol.*, 43, 7614-7618 (2009).

Docherty, K. S., Wu, W., Lim, Y. B., and Ziemann, P. J. Contributions of Organic Peroxides to Secondary Aerosol formed from Reactions of Monoterpenes with O_3. *Environ. Sci. Technol.*, 39, 4049-4059 (2005).

Guenther, A., Hewitt, C. N., Erickson, D., Fall, R., Geron, C., Graedel, T., Harley, P., Klinger, L., Lerdau, M., McKay, W. A., Pierce, T., Scholes, B., Steinbrecher R., Tallamraju, R., Taylor, J., and Zimmerman, P. A Global Model of Natural Volatile Organic Compound Emissions. *J. Geophys. Res.*, 100, 8873-8892 (1995).

Harrison, A. G., Jones, E. G., Gupta, S. K., and Nagy, G. P. Total Cross Sections for Ionization by Electron Impact. *Can. J. Chem*., 44, 1967-1973 (1966).

Haywood, J., and Boucher, O. Estimates of the Direct and Indirect Radiative Forcing due to Tropospheric Aerosols: A Review. *Rev. Geophys*., 38, 513-543 (2000).

Kroll, J. H., and Seinfeld, J. H. Chemistry of Secondary Organic Aerosol: Formation and Evolution of Low-Volatility Organics in the Atmosphere. *Atmos. Environ*., 42, 3593-3624 (2008).

Kwok, E. S. C., and Atkinson, R. Estimation of Hydroxyl Radical Reaction Rate Constants for Gas Phase Organic Compounds Using a Structure-Reactivity Relationship: An Update. *Atmos Environ*., 29, 1685-1695 (1995).

Lim, Y. B., and Ziemann, P. J. Chemistry of Secondary Organic Aerosol Formation from OH Radical-Initiated Reactions of Linear, Branched, and Cyclic Alkanes in the Presence of NO_x. *Aerosol Sci. Technol*., 43, 604-619 (2009a).

Lim, Y. B., and Ziemann, P. J. Kinetics of the Heterogeneous Conversion of 1,4-Hydroxycarbonyls to Cyclic Hemiacetals and Dihydrofurans on Organic Aerosol Particles. *Phys. Chem. Chem. Phys*., 11, 8029-8039 (2009b).

Lohmann, U., and Feichter, J. Global Indirect Aerosol Effects: a Review. *Atmos. Chem. Phys*., 5, 715-737 (2005).

Martin, P., Tuazon, E. C., Aschmann, S. M., Arey, J., and Atkinson, R. Formation and Atmospheric Reactions of 4,5-Dihydro-2-Methylfuran. *J. Phys. Chem. A*, 106, 11492-11501 (2002).

McLafferty F. W., and Turecek, F. *Interpretation of Mass Spectra*, Fourth Edition, University Science Books, Sausalito, CA. (1993).

Matsunaga, A., and Ziemann, P. J. Yields of β-Hydroxynitrates and Dihydroxynitrates in Aerosol formed from the OH Radical-Initiated Reactions of Linear Alkenes in the Presence of NO_x. *J. Phys. Chem. A*., 113, 599-606 (2009).

Matsunaga, A., Ziemann, P. J. Gas-Wall Partitioning of Organic Compounds in a Teflon Film Chamber and Potential Effects of Reaction Product and Aerosol Yield Measurements. *Aerosol Sci. Technol.*, 44, 881-892 (2010).

Matsunaga, A., and Ziemann, P. J. Yields of β-Hydroxynitrates, Dihydroxynitrates, and Trihydroxynitrates formed from OH Radical-Initiated Reactions of 2-Methyl-1-Alkenes. *Proc. Natl. Acad. Sci. USA*, 107, 6664-6669 (2010).

Morrison, R. T., and Boyd, R. N. *Organic Chemistry*, Third Edition, Allyn and Bacon, Boston (1973).

Nguyen, T. B., Roach, P. J., Laskin J., Laskin A., and Nizkorodov S. A. Effect of Humidity on the Composition of Isoprene Photooxidation Secondary Organic Aerosol. *Atmos. Chem. Phys*., 11, 6931-6944 (2011).

Odum, J. R., Hoffmann, T., Bowman, F., Collins, D., Flagan, R. C., and Seinfeld, J. H. Gas/Particle Partitioning and Secondary Organic Aerosol Yields. *Environ. Sci. Technol*., 30, 2580-2585 (1996).

Orzechowska, G. E., Nguyen, H. T., and Paulson, S. E., Photochemical Sources of Organic Acids. 2. Formation of C_5-C_9 Carboxylic Acids from Alkene Ozonolysis under Dry and Humid Conditions. *J. Phys. Chem. A*, 109, 5366-5375 (2005).

Pankow, J. F. An Absorption Model of Gas/Particle Partitioning of Organic Compounds in the Atmosphere. *Atmos. Environ*., 28, 185-188 (1994).

Pankow, J. F., and Asher, W. E. SIMPOL.1: A Simple Group Contribution Method for Predicting Vapor Pressures and Enthalpies of Vaporization of Multifunctional Organic Compounds. *Atmos. Chem. Phys*., 8, 2773-2796 (2008).

Presto, A. A., Miracolo, M. A., Donahue, N. M., and Robinson, A. L. Secondary Organic Aerosol Formation from High-NO_x Photo-Oxidation of Low Volatility Precursors: *n*-Alkanes. *Environ. Sci. Technol*., 44, 2029-2034 (2010).

Ramanathan, V., Crutzen, P. J., Kiehl, J. T., and Rosenfeld, D. Aerosols, Climate, and the Hydrological Cycle. *Science*, 294, 2119-2124 (2001).

Ravishankara, A.R. Heterogeneous and Multiphase Chemistry in the Troposphere. *Science*, 276, 1058-1065 (1997).

Reisen, F., Aschmann, S. M., Atkinson, R., and Arey, J. 1,4-Hydroxycarbonyl Products of the OH Radical Initiated Reactions of C_5-C_8 *n*-Alkanes in the Presence of NO. *Environ. Sci. Technol*., 39, 4447-4453 (2005).

Sauter, A. D., Down, J. J., Buchner, J. D., Ringo, N. T., Shaw, D. L., and Dulak, J. G. Model for the Estimation of Electron Impact Gas Chromatography/Mass Spectrometry Response Factors Quadrupole Mass Spectrometers. *Anal. Chem*., 58, 1665-1670 (1986).

Seinfeld, J. H., and Pandis, S. N. *Atmospheric Chemistry and Physics*, First Edition, Wiley-Interscience, New York. (1998).

Swain C. G., and Brown, J. F. Jr. Concerted Displacement Reactions. VII. The Mechanism of Acid-Base Catalysis in Non-Aqueous Solvents. *J. Am. Chem. Soc.*, 74, 2534-2537 (1952).

Tobias, H. J., and Ziemann, P. J. Compound Identification in Organic Aerosols Using Temperature-Programmed Thermal Desorption Particle Beam Mass Spectrometry. *Anal. Chem*., 71, 3428-3435 (1999).

Tobias, H. J., Kooiman, P. M., Docherty, K. S., and Ziemann, P. J. Real-Time Chemical Analysis of Organic Aerosols Using a Thermal Desorption Particle Beam Mass Spectrometer. *Aerosol Sci. Technol*., 33, 170-190 (2000).

Tyndall, G. S., Cox R. A., Granier C., Lesclaux R., Moortgat G. K., Pilling M. J., Ravishankara A. R., and Wallington T. J. Atmospheric Chemistry of Small Organic Peroxy Radicals. *J. Geophys. Res*., 106, 12157–12182 (2001).

van Dam, H. E., Kieboom, A. P. G., and van Bekkum, H. The Conversion of Fructose and Glucose in Acidic Media: Formation of Hydroxymethylfurfural. *Starch*, 38, 95-101 (1986).

Ziemann, P. J. Effects of Molecular Structure on the Chemistry of Aerosol Formation from the OH-Radical-Initiated Oxidation of Alkanes and Alkenes. *Int. Rev. Phys. Chem*., 30, 161-195 (2011).

CHAPTER 5

Conclusions

Spectrophotometric methods were developed to quantify carbonyl, hydroxyl, carboxyl, and ester groups in samples with composition typical of oxidized atmospheric organic matter. The methods employ derivatizing agents to convert each functional group to a characteristic colored derivative that is then quantified by spectrophotometry. The effects of molecular structure on quantification were thoroughly evaluated by measuring calibration curves for a large variety of monofunctional and multifunctional compounds. In addition, potential interferences from other compounds containing non-target functional groups were determined and methods developed to eliminate these interferences. Detection limits are approximately 0.01, 0.02, 0.03, and 0.1 μmoles for carbonyl, hydroxyl, carboxyl, and ester groups.

The functional group analysis methods developed were used with nitrate and peroxide analysis methods to investigate the chemical composition of secondary organic aerosol (SOA) formed from the OH radical-initiated reactions of *n*-pentadecane in the presence of NO_x and in the absence of NO_x. Real-time and offline thermal desorption particle mass spectrometry and SOA yield measurements were used in addition to functional group analysis to characterize the SOA.

For the OH radical-initiated reaction of *n*-pentadecane in the presence of NO_x, experiments were conducted in an environmental chamber under low and high UV irradiation to vary OH radical exposure and thus evaluate the effects of the extent of

oxidation on the reaction products. Results of functional group analysis indicate the presence of carbonyl, hydroxyl, and nitrate groups in SOA formed from 1 min of irradiation, consistent with expectations based on the well established reaction mechanism and product vapor pressures, with the major SOA products appearing to be first-generation 1,4-hydroxynitrates, cyclic hemiacetals, and their dimers, and second-generation cyclic hydroxynitrates. SOA formed from 60 min of irradiation contained carbonyl, hydroxyl, and nitrate groups as well as ester and peroxide groups associated with second- and third-generation carbonylesters and acyl peroxynitrate esters, and possibly hemiacetals. The cyclic hydroxynitrates, carbonylesters, and acyl peroxynitrate esters were formed via heterogeneous/multiphase cyclization and dehydration of 1,4-hydroxycarbonyls to form dihydrofurans, followed by further OH radical reactions.

For the OH radical-initiated reaction of *n*-pentadecane in the absence of NO_x, experiments were conducted in an environmental chamber with OH radicals formed by reaction of tetramethylethylene with O_3 and by photolysis of H_2O_2. The effect of adding HNO_3 to catalyze heterogeneous/multiphase reactions was also investigated. Results of functional group analysis indicate the presence of carbonyl, hydroxyl, peroxide, and carboxyl groups in SOA formed in all reactions, and ester groups were also present in reactions with HNO_3 present. The major SOA products appear to be first-generation *n*-ketones, *n*-alcohols, *n*-hydroperoxides, and cyclic hemiacetals, second-generation carbonyl and hydroxy cyclic hemiacetals, and acetals formed from heterogeneous/multiphase reactions of these various cyclic hemiacetals with each other and with *n*-alcohols.

The results from these experiments demonstrate the value of these functional group analysis methods for SOA studies and lend additional support for the currently accepted mechanisms of SOA formation from reactions of alkanes with OH radicals in the presence and absence of NO_x, including the role of heterogeneous/multiphase reactions.

These results indicate that the functional group analysis methods developed here, when combined with nitrate and peroxide analysis methods are well suited for SOA studies. It would be worthwhile to apply these methods to studies of the relationships between functional group composition and SOA properties such as cloud condensation nucleating activity and toxicity to understand how SOA affects the environment and human heath, and also to apply these to gas phase analysis so that the complete gas and particle phase composition can be obtained.